RADC-TR-69-221
Technical Report
June 1969

MEASURED PERFORMANCE OF HF SUBSURFACE DIPOLES

John N. Entzminger, Jr.
Thomas F. Treadway
Stuart H. Talbot

Rome Air Development Center
Air Force Systems Command
Griffiss Air Force Base, New York

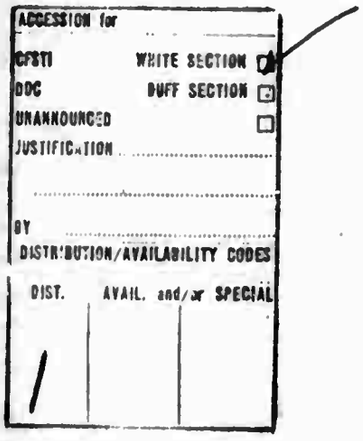

MEASURED PERFORMANCE OF HF SUBSURFACE DIPOLES

John N. Entzminger, Jr.
Thomas F. Treadway
Stuart H. Talbot

FOREWORD

This report is the result of an in-house study of subsurface HF dipole antennas between August 1968 and December 1969, under Project 6523.

The authors wish to acknowledge the technical assistance of G.R. Weatherup and S.J. Nasci and the excellent assistance in preparing the report by Mrs. Patricia Clinton. In addition, the pilots, navigators, and support personnel of the Flight Test Division, Mr. Ken Siarkiewicz (EMCVM-1), and the personnel at Sotckbridge, Ava, and Verona Test Sites are due a special note of thanks for their excellent support.

This report has been reviewed by the Office of Information (EMLS) and is releasable to the Clearing House for Federal Scientific and Technical Information.

This technical report has been reviewed and is approved.

Approved: For GEORGE E. BRUNETTE
Chief, Comm Appl Branch
Communications Division

Approved: RICHARD M. COSEL
Colonel, USAF
Chief, Communications Div

FOR THE COMMANDER: IRVING J. GABELMAN
Chief, Advanced Studies Group

ABSTRACT

Theoretical analysis and measured data are presented for determining the characteristics of High Frequency (HF) subsurface dipole antennas. The agreement between theory and experimental data is shown to be excellent. It is shown that HF subsurface dipoles radiate a surface wave having the same characteristics as that launched by an above ground vertical monopole and also radiate a space wave which has a pattern identical to that of a half wave horizontal dipole located a quarter wavelength or less above ground. The subsurface dipole length is shortened to about one-third to two-thirds of its above ground equivalent.

Engineering curves are presented which enable the system engineer to design a small, physically hard, relatively cheap HF antenna array having a gain of approximately -10 dB below that of simple above ground antennas, and having the radiation characteristics of both above ground whip and horizontal dipole antennas.

TABLE OF CONTENTS

LIST OF ILLUSTRATIONS

LIST OF TABLES

1. INTRODUCTION

Subsurface antennas have invoked considerable interest over the past 20 years because of their potential for providing communications to and from physically hard facilities and submerged submarines.

The theory is rather well developed and designs for subsurface antennas in soil can be engineered to meet most requirements depending primarily on conductivity of media, depth of burial and cost. The theory predicts that such antennas excite a normal surface and skywave mode similar except in gain to that excited by conventional above ground antennas. There is, however, a paucity of experimental measurements especially at the higher frequencies. Recently, some conflicting data was published (Ref. 1) which suggests that subsurface dipoles at frequencies of approximately 7 MHz radiated a trapped surface wave of extremely low attenuation and radiated little or no space wave which could propagate via the ionosphere. This represented a significant departure from known theory and had important ramifications to the use of such antennas. As a part of its overall program in survivable antennas and at the request of various government agencies, the Rome Air Development Center conducted a detailed measurement program to determine the radiation and electrical characteristics of subsurface dipoles in the HF band of 1 to 10 MHz. In Section 2, we summarize the pertinent theoretical work in order to be able to compare

with the measured performance and also to make available to system emgineers the expected performance of large arrays of subsurface dipoles. In Section 3, we present measured data taken on actual buried dipoles and Section 4 summarizes the results showing the close agreement between theory and measured data.

2. THEORETICAL PERFORMANCE

A. INTRODUCTION

Subsurface antennas have been the subject of a number of studies over the past twenty years and the reader is referred to several papers which contain extensive bibliographies (Ref. 2-5). The classic papers by Moore (Ref. 6, 7), Lein (Ref. 8), Baños & Wesley (Ref. 9), and Wait (Ref. 10) analyzed the surface wave fields of horizontal dipoles buried beneath the surface for the case of low frequencies and/or high conductivities. Practical subsurface antennas with these same restrictions were treated extensively in a series of reports by The Boeing Company (Ref. 11-14) and culminated in a design handbook for underground antenna systems (Ref. 15). These results have been extended recently (Ref. 16-20) to include the space wave and a broader range of frequencies and conductivities as well as the effects of tilting the dipoles.

The surface wave is the term used to describe the total wave which would exist along the surface of the earth if the ionosphere were absent. Over a plane, perfectly conducting earth, it attenuates at a rate equal to the inverse distance. At low conductivities and high frequencies it attenuates as the inverse distance squared. The space wave is that part of the total wave above the surface which attenuates at a rate equal to the inverse distance. If the ionosphere were present, the space wave might be reflected therefrom and appear at the surface as a skywave.

It can be shown (Ref. 7, 13, 18, and 20) that the optimum subsurface antenna is a simple insulated wire parallel to the interface, and for practical reasons, of an ungrounded or open-ended configuration at medium and high frequencies.

We shall present, in this section, a summary of the operation of such a simple dipole by comparing its gain to that of conventional above ground antennas and discussing the effect of paralleling a number of dipoles to achieve higher gain. The theory of the operation of subsurface antennas may be divided into two major categories. The first category involves the coupling of the energy of the antenna to the radiation or far zone fields. For this we shall depend primarily on the work by Biggs & Swarm (Ref. 16-18). The second category involves the fields immediately adjacent to the antenna which determine the current distribution, and self-impedance of a dipole and the mutual impedance between two neighboring dipoles. This category has been treated extensively by Guy and Hasserjian (Ref. 11, 14) and we shall use their results.

B. RADIATION FIELDS OF HORIZONTAL SUBSURFACE DIPOLES

The semi-infinite conducting medium is represented by a flat earth with a conductivity σ and a permittivity ε. Above this medium is nonconducting air with a dielectric constant ε_0. The permeability of both media is μ_0, which is the same as free space. The fields have a time dependence exp $(-i\omega t)$.

The coordinate system for the buried dipole is shown in Figure 2-1. The air is described by the region $Z \geq 0$. The dipole is oriented in the X direction and is located at a depth d in meters with coordinates (0, 0, -d). The observation point in $Z \geq 0$, is given in spherical coordinates, $(r,\phi,\theta,)$.

The propagation constant is given by

$$k_1^2 = \omega^2 \mu_0 \epsilon + i\omega\mu_0\sigma \quad \text{for earth} \tag{2-1}$$

and

$$k_0^2 = \omega^2 \mu_0 \epsilon_0 \quad \text{for air} \tag{2-2}$$

and the refractive index, n, is defined from

$$n^2 = k_1^2/k_0^2 = \epsilon_g + i\sigma/\omega\epsilon_0 \tag{2-3}$$

where $\epsilon_g = \epsilon/\epsilon_0$, the relative dielectric constant of the earth. When $\sigma/\omega\epsilon >> 1$, $n^2 \simeq \sigma/\omega\epsilon_0$, which is the usual approximation made for buried antennas and holds for low frequencies in earth but not for high frequencies in which we are interested.

For the range $|k_0 r/n^2| >> 1$, the surface wave electric field components in $Z \geq 0$ are given by Biggs & Swarm (Ref. 18, page 45) in volts/meter as

$$E_r = 60 M_h \cos\phi \frac{D}{r^2} \tag{2-4}$$

$$E_\theta = -60 M_h \cos\phi \sin\theta \left[\frac{n^2}{(n^2-\sin^2\theta)^{1/2}}\right] \frac{D}{r^2} \tag{2-5}$$

$$E_\phi = 60 M_h \sin\phi \sin\theta \left[\frac{1}{n^2-\sin^2\theta}\right] \frac{D}{r^2} \tag{2-6}$$

where $D = \exp[i k_0 (r + d (n^2-\sin^2\theta)^{1/2}]$

M_h = dipole moment = $\int_{-L/2}^{+L/2} I(x) \exp(i k_0 x \cos\phi)\, dx$. When the refractive index is large, the horizontally polarized ϕ

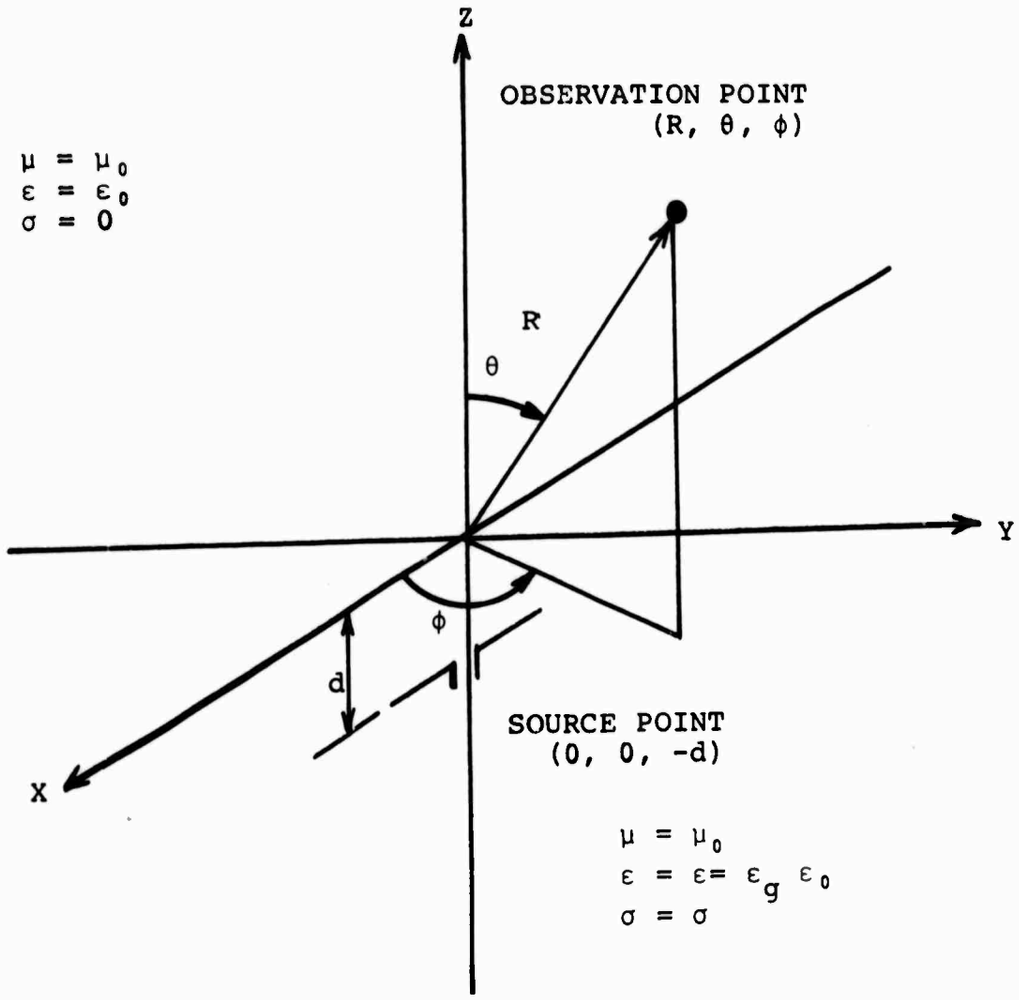

Figure 2-1. Coordinate System for Subsurface Electric Dipole

component in Eq. (2-6) is negligible. The ratio of the vertically polarized component of the electric field intensity, E_θ, to the accompanying horizontal component, E_r, corresponds to the "wave tilt" as discussed in the literature and at $\theta = 0$ is equal to the refractive index, n.

The space wave electric field components are given by (Ref. 18, page 46)

$$E_\theta = i\ 60\ k_0\ M_h \cos\phi \left[\frac{\cos\theta\,(n^2-\sin^2\theta)^{1/2}}{n^2\cos\theta+(n^2-\sin^2\theta)^{1/2}}\right] \frac{D}{r} \qquad (2\text{-}7)$$

$$E_\phi = i\ 60\ k_0\ M_h \sin\phi \left[\frac{\cos\phi}{\cos\phi+(n^2-\sin^2\theta)^{1/2}}\right] \frac{D}{r} \qquad (2\text{-}8)$$

In both sets of field equations the effect of burial is seen only in the term

$$\exp\ [i\ k_0\ d\ (n^2 - \sin^2\ \theta)^{1/2}]$$

at $\theta = 0$, the magnitude of this term can be written as

$$|D| = |\exp\ [i\ k_0 dn]| = |\exp\ [i\ k_1 d]| = \exp\ [-d/\delta] \qquad (2\text{-}9)$$

where δ is the skin depth of the medium and is given by

$$\delta = \left[\left[\left(\frac{\omega^2\mu_0\epsilon}{2}\right)^2 + \left(\frac{\omega\mu\sigma}{2}\right)^2\right]^{1/2} - \frac{\omega^2\mu_0\epsilon}{2}\right]^{-1/2} \text{ meters} \qquad (2\text{-}10)$$

For $\sigma/\omega\epsilon >> 1$ this becomes the well-known expression

$$\delta = \sqrt{\frac{2}{\omega\mu\delta}} \quad \text{meters} \qquad (2\text{-}11)$$

Plots of Eq. (2-10) are shown in Figure 2-2. The range of validity of Eqs. (2-4) through (2-8) extends to within several kilometers of the antenna. When distances are shorter, the vertical component of the surface wave is given by (Ref. 18, page 47)

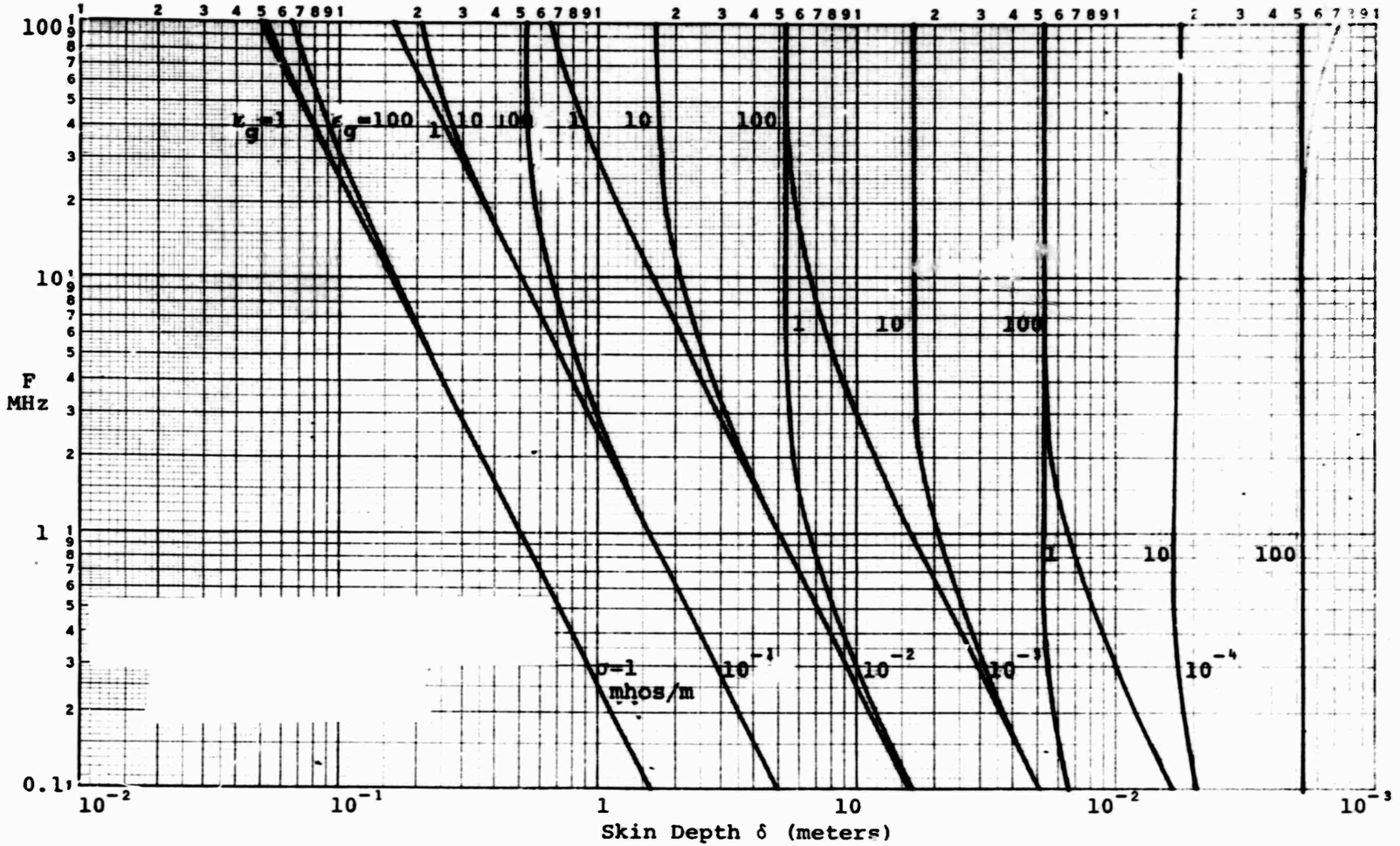

Figure 2-2. Skin Depth Vs. Frequency

$$E_\theta = i\ 60\ k_0 M_h\ \cos\phi \left[\frac{n}{(1+n^2)^{3/2}}\right]^{1/2} F(p)\ \frac{D'}{r} \qquad (2\text{-}12)$$

which reduces to

$$E_\theta = i\ 60\ k_0 M_h \cos\phi\ \frac{1}{n}\ F(p)\ \frac{D'}{r} \qquad (2\text{-}13)$$

when $n^2 >> 1$. $D' = \exp\left[i\ k_0 \left(r+d\ \frac{n^2}{(1+n^2)^{1/2}}\right)\right]$ with $F(p)$ representing the ground wave attenuation function

$$F(p) = 1 + i\sqrt{\pi p}\ \exp(-p)\ \text{erfc}\ (i\sqrt{p}) \qquad (2\text{-}14)$$

and

$$p = i\ k_0 r/2n^2 \qquad (2\text{-}15)$$

Erfc is the complimentary error function. The asymptotic expansion of erfc results in

$$F(p) = i\ \frac{n^2}{k_0 r} + 3\left[\frac{n^2}{k_0 r}\right]^2 + \ldots \qquad (2\text{-}16)$$

Substitution of the first term of this asymptotic expansion in Eq. (2-12) reduces it to Eq. (2-5) when $n^2 >> 1$ and $\theta = 90°$. Plots of surface wave field intensity are shown in Figure 2-3 as a function of distance and in Figure 2-4 for the space wave at a fixed distance as a function of θ.

C. RELATIVE GAIN OF SUBSURFACE DIPOLE

It is of value to compare the gain of the subsurface dipole to that of conventional antennas. Norton (Ref. 21, page 1212) and Jordan (Ref. 22, page 625) give the vertical electric component of the surface wave for a vertical dipole

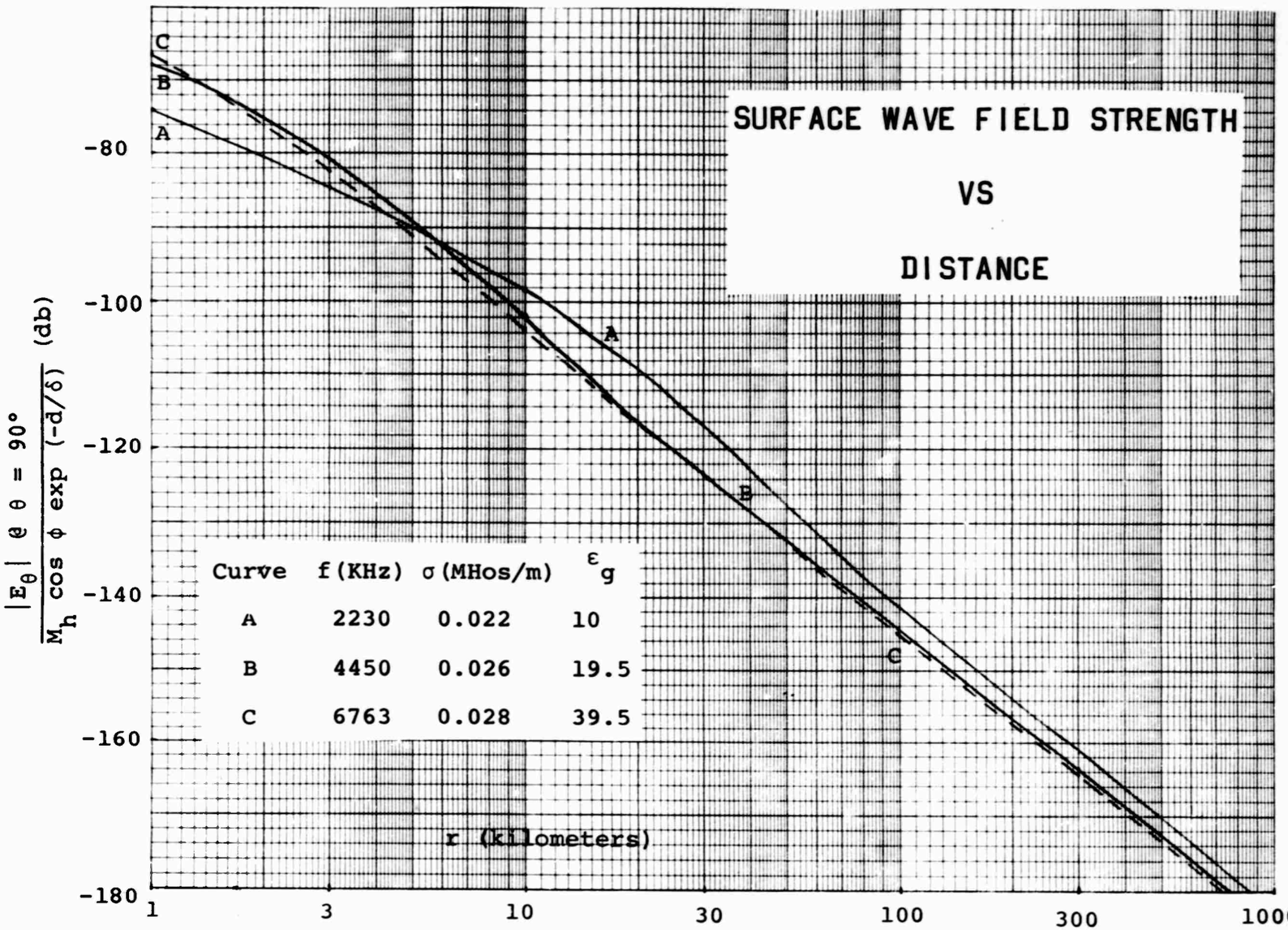
SURFACE WAVE FIELD STRENGTH
VS
DISTANCE
$\frac{|E_\theta| \text{ @ } \theta = 90°}{M_h \cos\phi \exp(-\bar{d}/\delta)}$ (db)
-80
-100
-120
-140
-160
-180
1
3
10
30
100
300
1000
r (kilometers)
A
B
C
Curve f(KHz) σ(MHos/m) ε_g
A 2230 0.022 10
B 4450 0.026 19.5
C 6763 0.028 39.5

Figure 2-3.

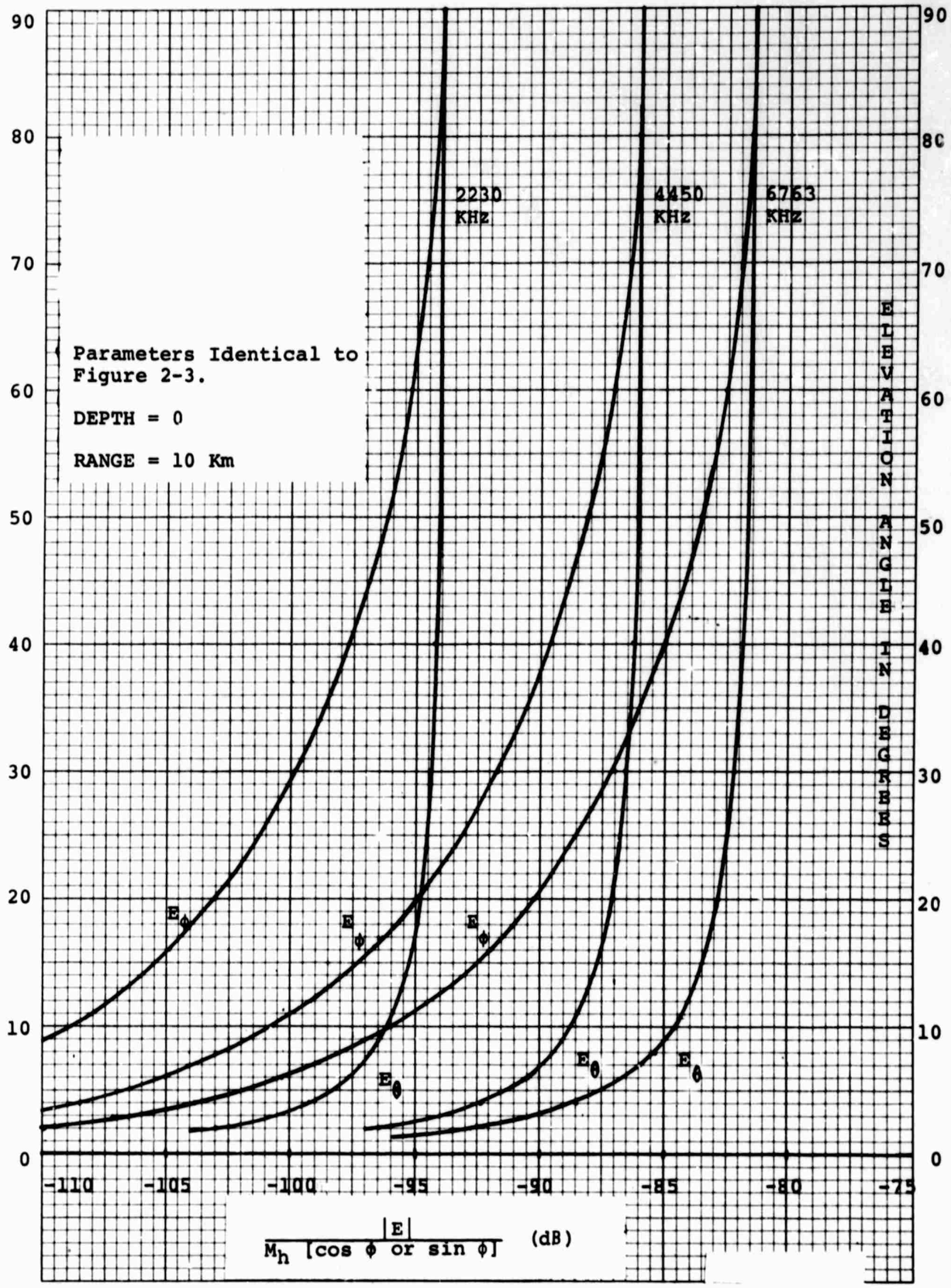

Figure 2-4. Space Wave Field Strength Vs. Elevation Angle Subsurface Dipole

at the surface of the earth as

$$E_{zv} = i\ 60\ k_0 M_v \left(\frac{n^2-1}{n^2}\right) F(p)\ \frac{\exp(-ik_0 r)}{r} \qquad (2\text{-}17)$$

for $r >> \lambda_0$.

For the case of $n^2 >> 1$, this reduces to

$$E_{zv} = i\ 60\ k_0 M_v\ F(p)\ \frac{\exp(-ik_0 r)}{r} \qquad (2\text{-}18)$$

which is the usual form found in the literature.

A comparison of Eqs. (2-13) and (2-18) show that the basic difference between the surface wave fields of a vertical dipole above the surface and a horizontal dipole below the surface are that the horizontal dipole is modified by

Refraction Term:	$1/n = (\varepsilon_g + i\ \sigma/\omega\varepsilon_0)^{-1/2}$
Pattern Factor:	$\cos\ \phi$
Depth Attenuation Factor:	$\exp\ (-d/\delta)$.

The radiation resistance of a short unloaded monopole of height h is given by

$$R_r = 10\ (k_0 h)^2 \qquad (2\text{-}19)$$

and since the radiated power $P_r = I_0^2 R_r$ we have (assuming linear current distribution)

$$M_v = \int_0^l I(x)\ dx = \sqrt{P_r/40k_0} \qquad (2\text{-}20)$$

where I(x) is the current distribution on the antenna. When substituted in Eq. (2-17) this becomes

$$E_{zv} = i \frac{3\sqrt{10P_r}}{r} \left(\frac{n^2-1}{n^2}\right) F(p) \qquad (2\text{-}21)$$

For the sub-surface horizontal dipole, M_h can be represented by

$$M_h = \frac{\sqrt{P_{in}/R_{in}}}{I_0} \int_{-L/2}^{L/2} I(x) \exp(i k_0 x \cos\phi)\, dx \qquad (2\text{-}22)$$

It is convenient to define a term $f(\phi)$ called the pattern-length factor (Ref. 13) which is given by

$$f(\phi) = \frac{k_0 \cos\phi}{I_0} \int_{-L/2}^{L/2} I(x) \exp(i k_0 x \cos\phi)\, dx \qquad (2\text{-}23)$$

where I_0 = input current

L = total antenna length

R_{in} = input resistance

x = distance along antenna from center feed point.

Substituting in Eq. (2-12), we have for the horizontal sub-surface antenna

$$E_{zh} = i\, 60 \sqrt{P_{in}/R_{in}}\, f(\phi) \left[\frac{n}{(1+n^2)^{3/2}}\right]^{1/2} F(p)\, D'/r \qquad (2\text{-}24)$$

Assuming that the vertical monopole is perfectly efficient ($P_r = P_{in}$) we define a relative gain (g_m) which is a comparison of the power radiated from a horizontal, subsurface linear antenna to that radiated from an ideal short vertical monopole above the surface.

$$g_m = \left|\frac{E_{zh}}{E_{zv}}\right|^2 = 40 \frac{|f(\phi)|^2}{R_{in}} |W| \exp(-2d/\delta) \qquad (2\text{-}25)$$

where

$$W = \frac{n^5}{(1+n^2)^{3/2}\ (n^2-1)^2} \tag{2-26}$$

When $\sigma/\omega\varepsilon >> 1$

this simplifies to

$$|W| = \left|\frac{1}{n}\right| \simeq \frac{\omega\varepsilon_0}{\sigma} \tag{2-27}$$

and

$$g_m = 40\ \frac{\omega\varepsilon_0}{\sigma}\ \frac{|f(\phi)|^2}{R_{in}} \exp\ (-2d/\delta) \tag{2-28}$$

D. IMPEDANCE CHARACTERISTICS

Guy and Hasserjian (Ref. 11, 14) have shown that an insulated wire with circular cross section in earth has a complex propagation constant, $\Gamma = \alpha + i\beta$, which is a function of the geometrical cross section of the wire, dielectric insulation, conductivity of the medium, depth from the interface, and distance from neighboring antennas. The antenna essentially behaves as a coaxial cable transmission line with a lossy shield. Guy and Hasserjian (Ref. 11, 14) have solved for the propagation constant and characteristic impedance as shown in Figures 2-5 and 2-6. Their results for 50 ohm coaxial cable with the shield removed and dimensions as shown in Figure 2-5 can be approximated by

$$\beta/k_0\sqrt{\varepsilon_r} = 1.631\ (b/\delta)^{-0.0554} \tag{2-29}$$

$$\alpha/k_0\sqrt{\varepsilon_r} = 0.179\ (b/\delta)^{0.0563} \tag{2-30}$$

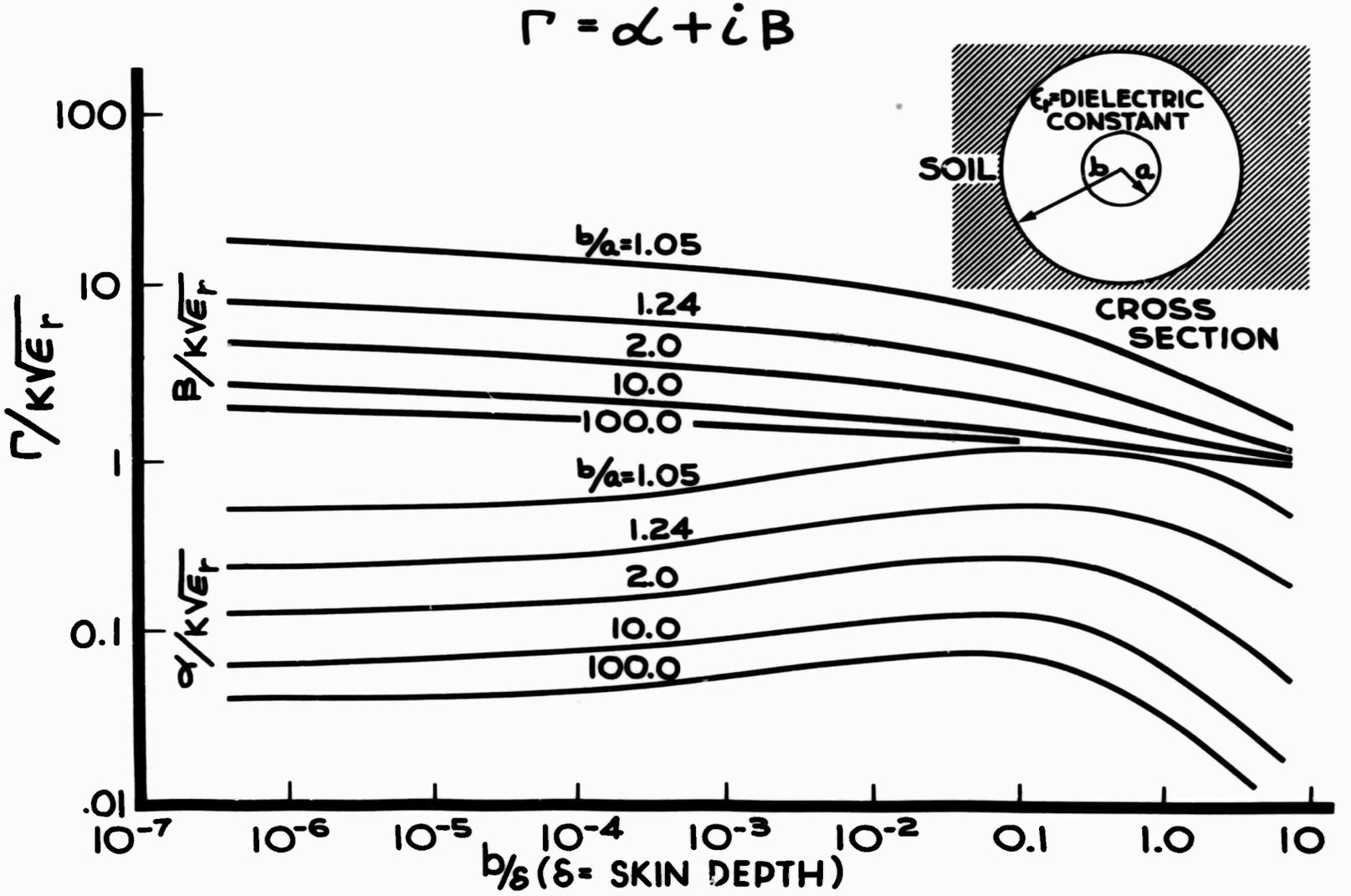

From: Hasserjian & Guy

Figure 2-5. Propagation Constant of Antenna

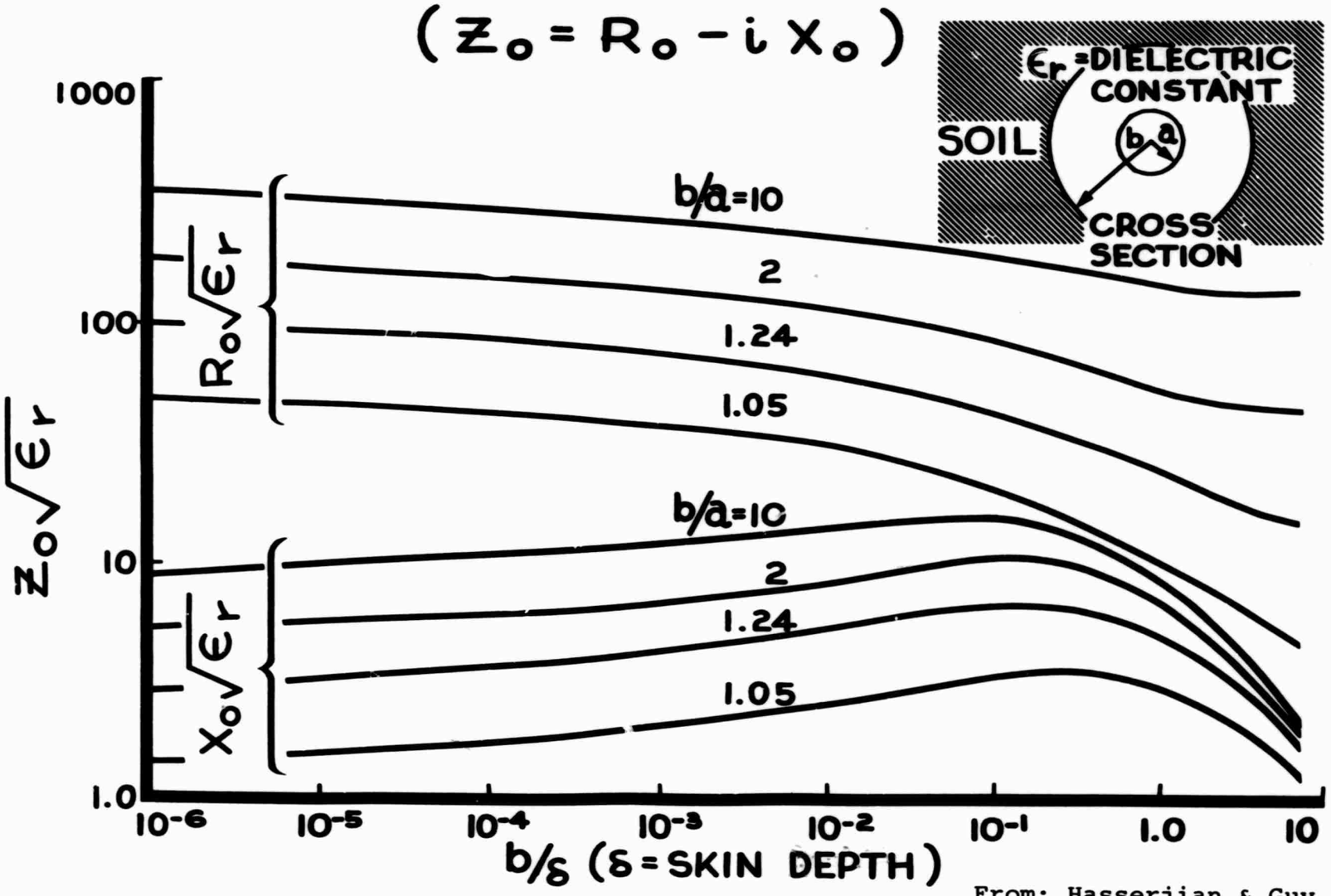

From: Hasserjian & Guy

Figure 2-6. Characteristic Impedance of Antenna

for practical values of b/δ, for $d/\delta > 1.6$, and $a/\delta >> 1$ and where ε_r is the relative dielectric constant of the cable dielectric covering. Input impedance of a subsurface dipole, as taken from the data by Guy and Hasserjian (Ref. 11), is shown in Figure 2-7 through 2-10.

E. RELATIVE GAIN OF SUBSURFACE ARRAY

Using calculated values of the propagation constant and input impedance, a normalized plot of $|f(\phi)|^2/R_{in}$ (Ref. 11) is shown in Figure 2-11. For ease in computation, two cases of interest can be approximated by the expressions given below:

Case I: $L = \lambda_{c/2}$

$$\frac{|f(\phi)|^2}{R_{in}} = 4.5 \times 10^{-3}[9.916\ (\beta/k)^{-0.894}] \qquad (2\text{-}31)$$

Case II: $L = \lambda_c$

$$\frac{|f(\phi)|^2}{R_{in}} = 4.5 \times 10^{-3}[7.522 - 0.647\ (\beta/k_0)] \qquad (2\text{-}32)$$

where λ_c = wavelength on the subsurface cable and

$\beta/k_0 = \lambda_0/\lambda_c$.

Eq. (2-29) through (2-32) enable computer calculation of the relative gain as given in Eq. (2-25). To simplify the presentation of the results, we can follow the example of a recent Boeing Report (Ref. 23) and separate the relative gain into three components. That is

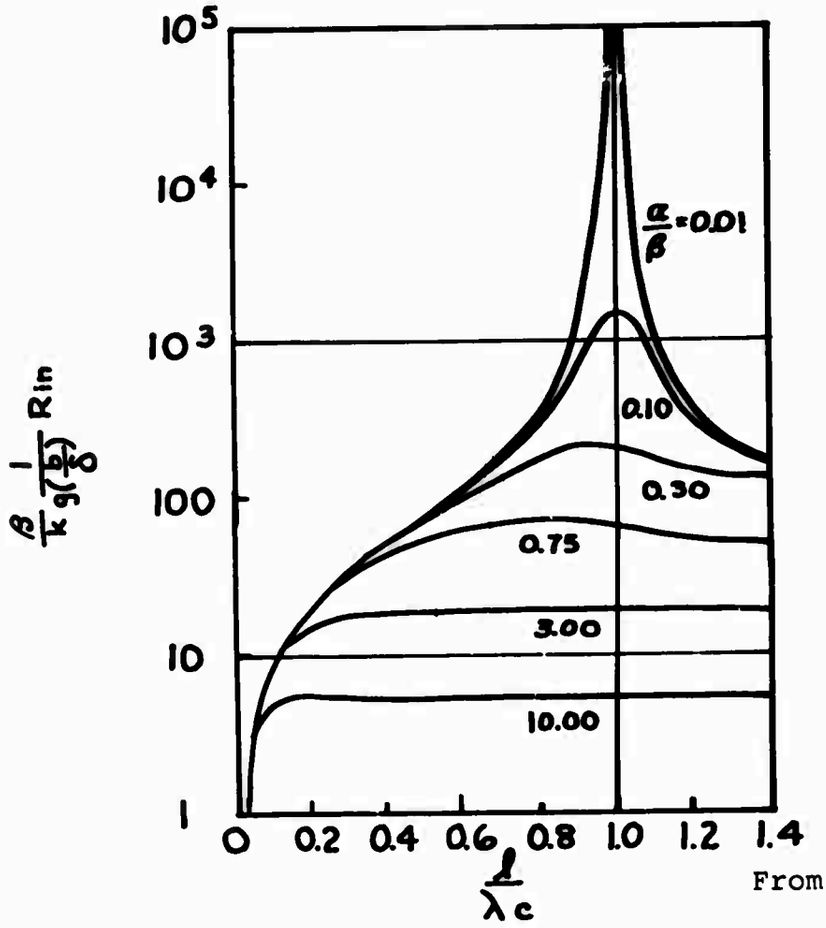

From: Hasserjian & Guy

Figure 2-7. Resistance of Open-Ended Antenna

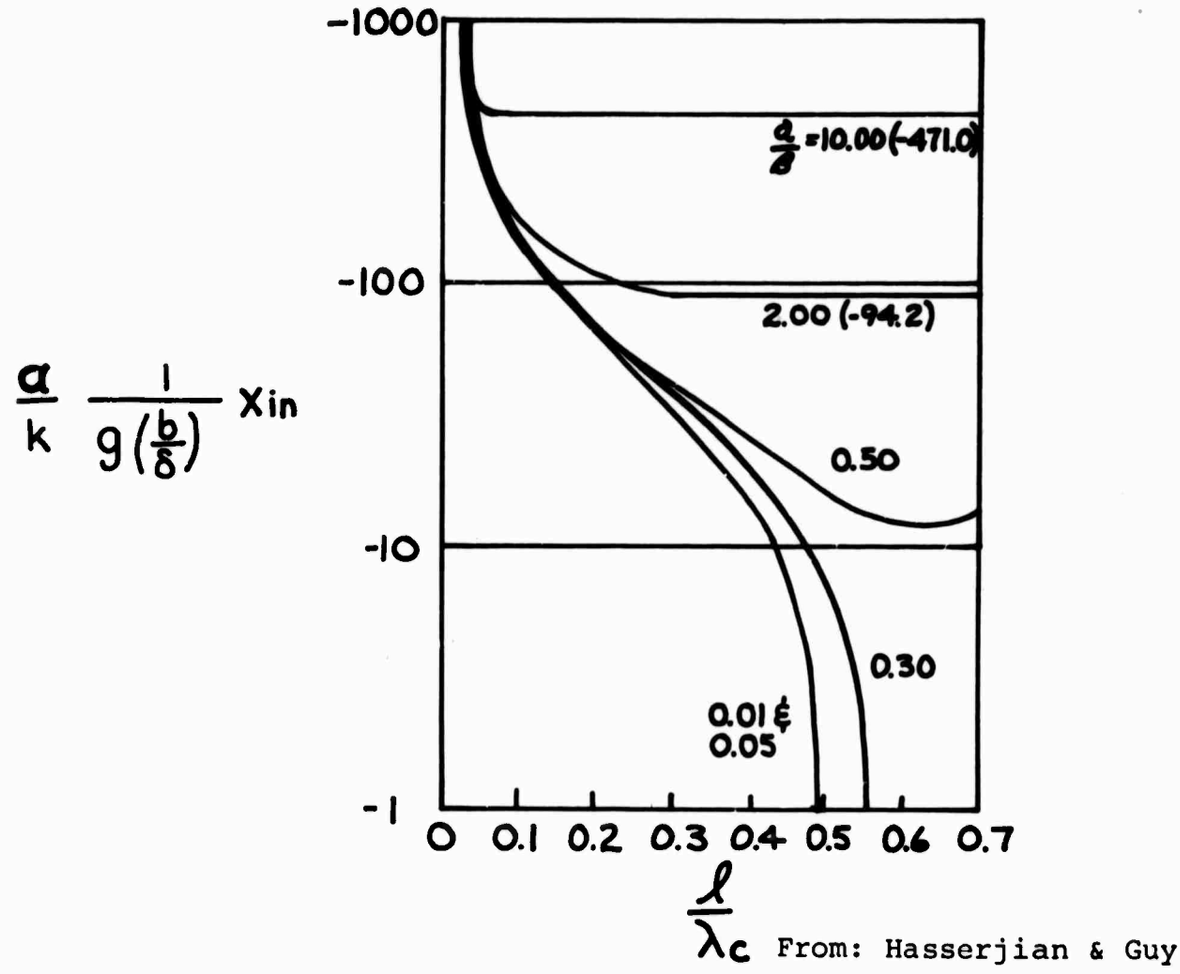

From: Hasserjian & Guy

Figure 2-8. Reactance of Open-Ended Antenna (Part One)

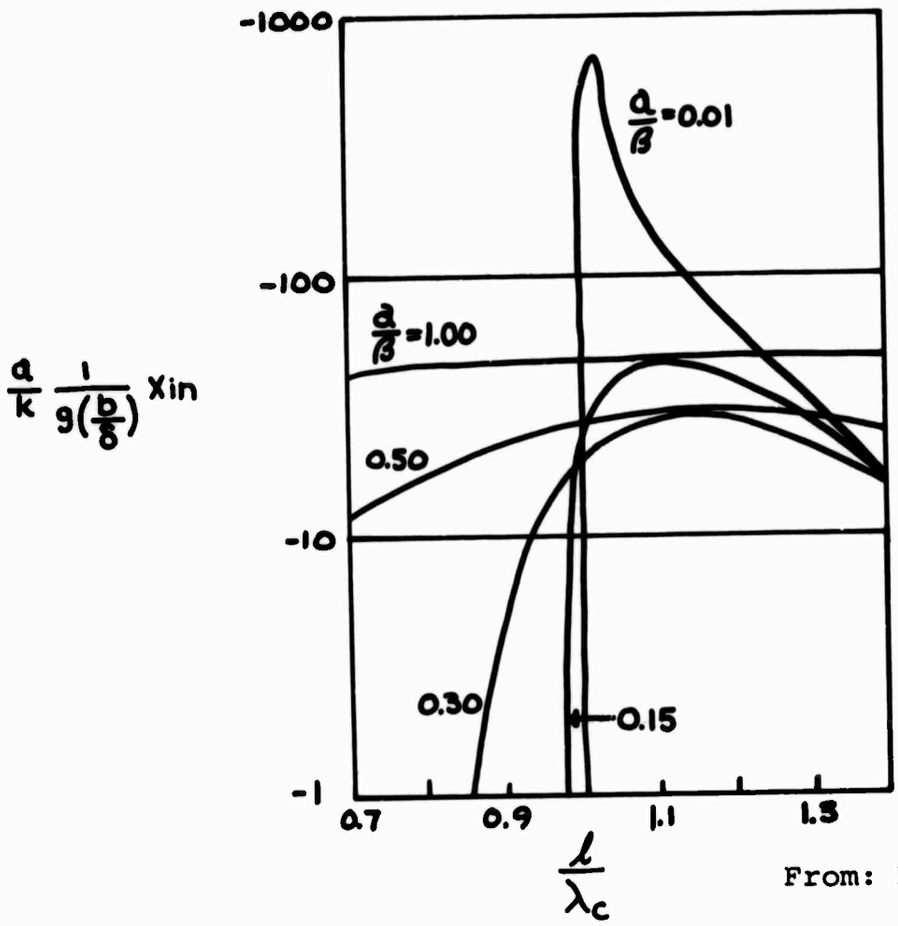

From: Hasserjian & Guy

Figure 2-9. Reactance of Open-Ended Antenna (Part Two)

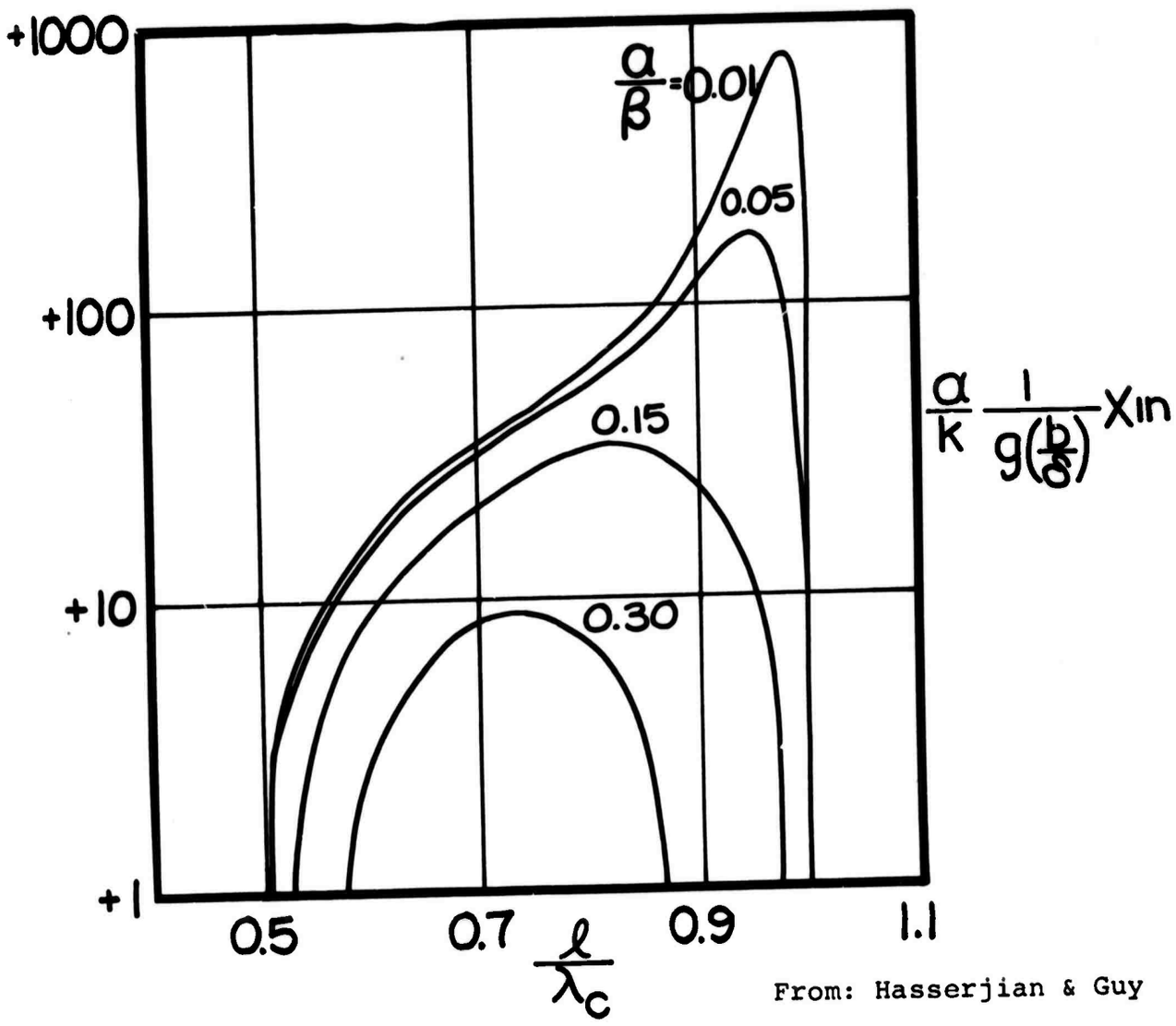

From: Hasserjian & Guy

Figure 2-10. Reactance of Open-Ended Antenna (Part Three)

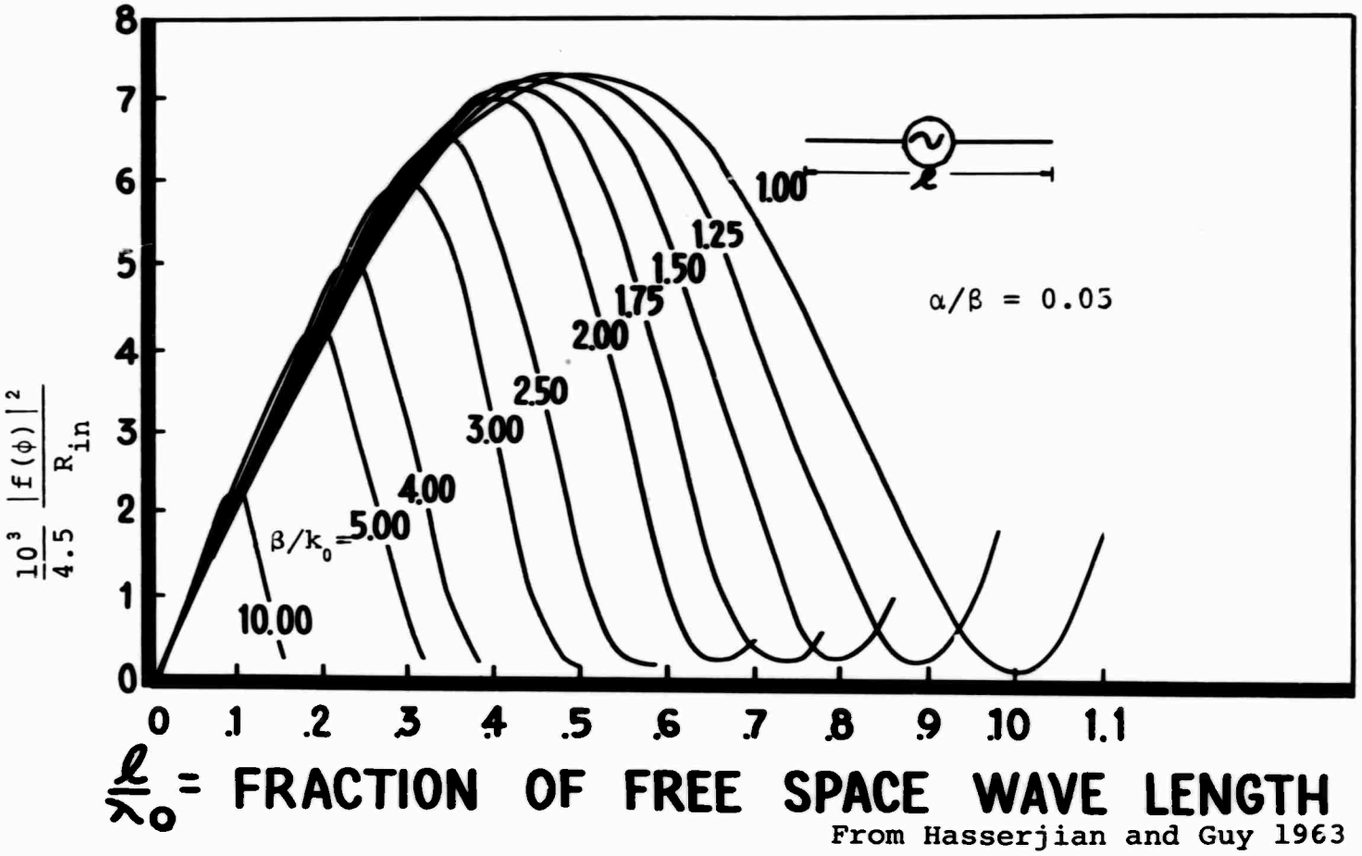

Figure 2-11. Normalized Power Gain - Subsurface Dipole

$$G_t = G_e - G_d + G_a \text{ (dB)} \qquad (2\text{-}33)$$

where G_t = the total relative gain g_m expressed in db plus the gain due to parallel elements, G_a.

G_e = the theoretical relative surface wave gain of a single horizontal insulated dipole at zero depth, referenced to a short loss-free monopole on the earth's surface (expressed in dB).

G_d = the depth loss incurred as a result of moving the dipole from the surface to a depth d, expressed in dB.

G_a = the array gain associated with utilizing multiple elements, expressed in dB above G_e.

Figures 2-12 through 2-15 are plots of G_e for different antenna resonant lengths and presented as a function of frequency and ground constants. G_e is calculated from Eq. (2-25) with d = 0 and expressed in db. The plots of G_e are for shieldless RG-19 coaxial cable as an example but computer runs for smaller cable such as RG-8 show a decrease in gain of only 0.1 to 0.2 dB. Figure 2-16 is a plot of the depth attenuation factor, $G_d = \exp(2d/\delta)$ expressed in dB/meter.

Significant improvement in gain can be achieved by paralleling identical elements close together. (Ref. 11, 13, 14). As long as the mutual coupling between parallel elements is negligible, then for an array of m identical elements the gain due to paralleling the elements is directly proportional to m, and G_a then becomes

$$G_a = 10 \log m. \qquad (2\text{-}34)$$

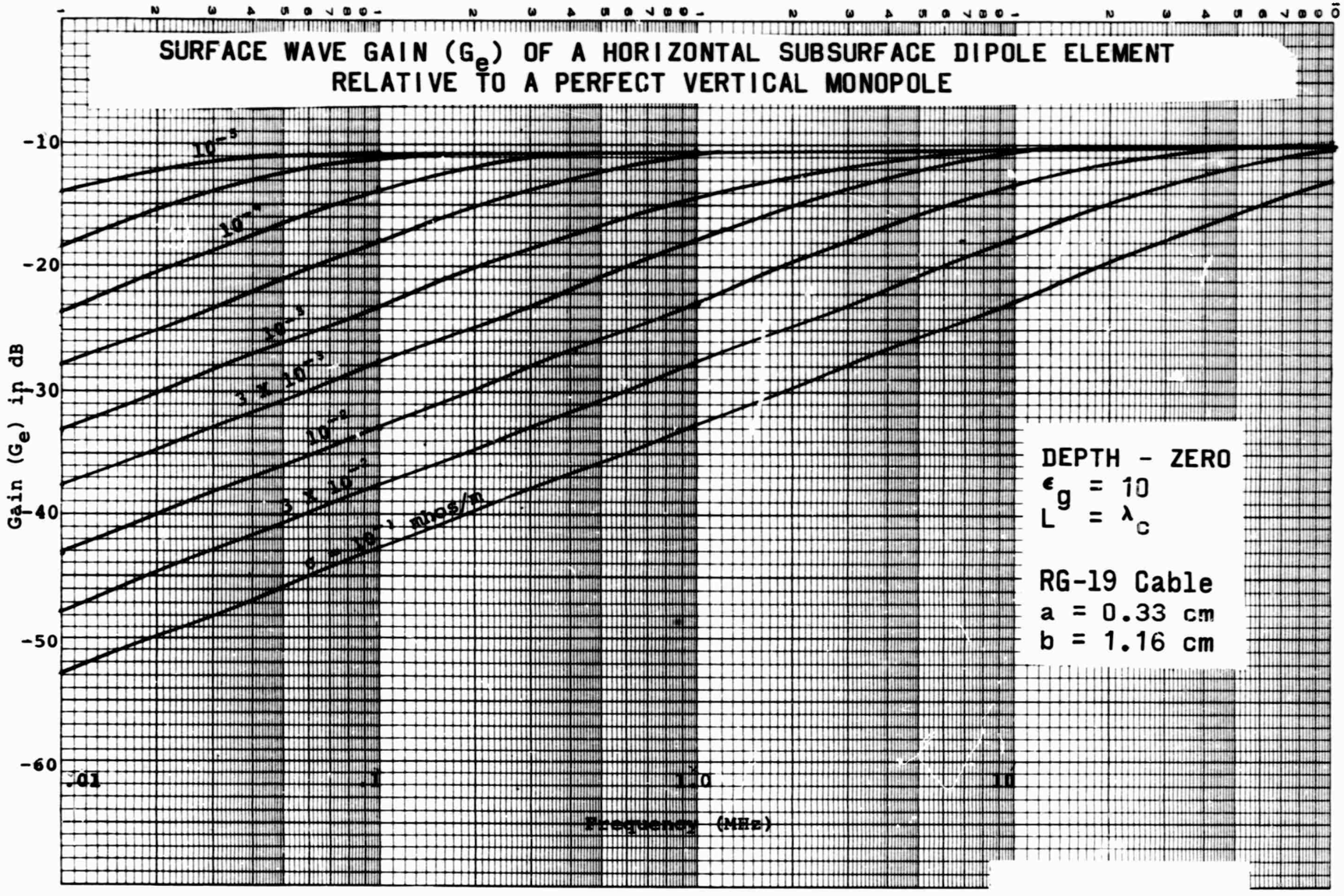
SURFACE WAVE GAIN (G_e) OF A HORIZONTAL SUBSURFACE DIPOLE ELEMENT
RELATIVE TO A PERFECT VERTICAL MONOPOLE
Gain (G_e) in dB
-10
-20
-30
-40
-50
-60
10^{-5}
10^{-4}
10^{-3}
3×10^{-3}
10^{-2}
3×10^{-2}
10^{-1} mhos/m
.01
.1
1.0
10
Frequency (MHz)
DEPTH - ZERO
$\epsilon_g = 10$
$L = \lambda_c$
RG-19 Cable
a = 0.33 cm
b = 1.16 cm

Figure 2-12.

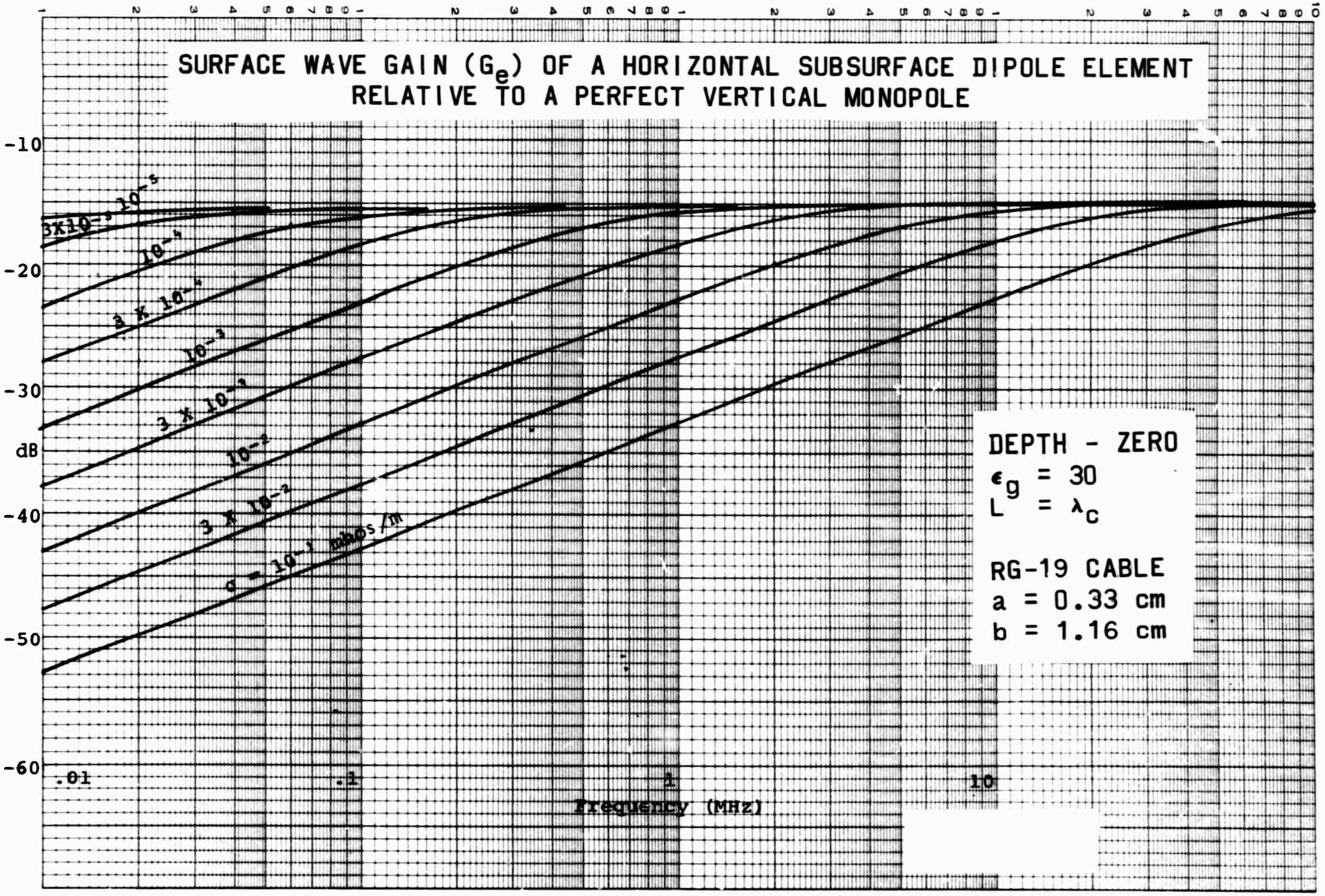
SURFACE WAVE GAIN (G_e) OF A HORIZONTAL SUBSURFACE DIPOLE ELEMENT
RELATIVE TO A PERFECT VERTICAL MONOPOLE
-10
-20
-30
-40
-50
-60
dB
3X10⁻⁵
10⁻⁴
3 X 10⁻⁴
10⁻³
3 X 10⁻³
10⁻²
3 X 10⁻²
σ = 10⁻¹ mhos/m
DEPTH - ZERO
ϵ_g = 30
L = λ_c
RG-19 CABLE
a = 0.33 cm
b = 1.16 cm
.01
.1
1
10
Frequency (MHz)

Figure 2-13.

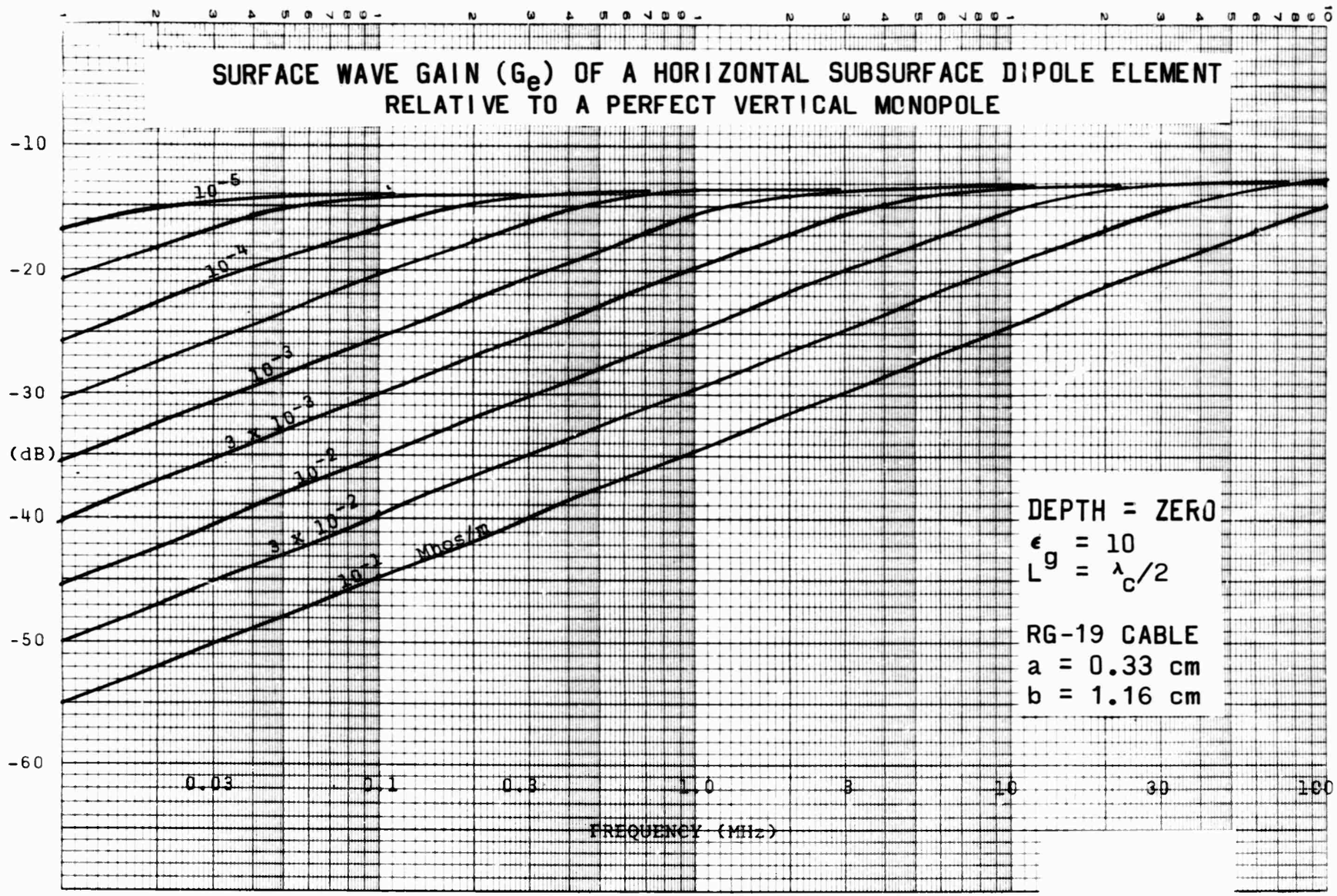
SURFACE WAVE GAIN (G_e) OF A HORIZONTAL SUBSURFACE DIPOLE ELEMENT
RELATIVE TO A PERFECT VERTICAL MONOPOLE
-10
-20
-30
-40
-50
-60
(dB)
10^{-5}
10^{-4}
10^{-3}
3×10^{-3}
10^{-2}
3×10^{-2}
10^{-1} Mhos/m
DEPTH = ZERO
$\epsilon_g = 10$
$L^g = \lambda_c/2$
RG-19 CABLE
a = 0.33 cm
b = 1.16 cm
0.03
0.1
0.3
1.0
3
10
30
100
FREQUENCY (MHz)

Figure 2-14.

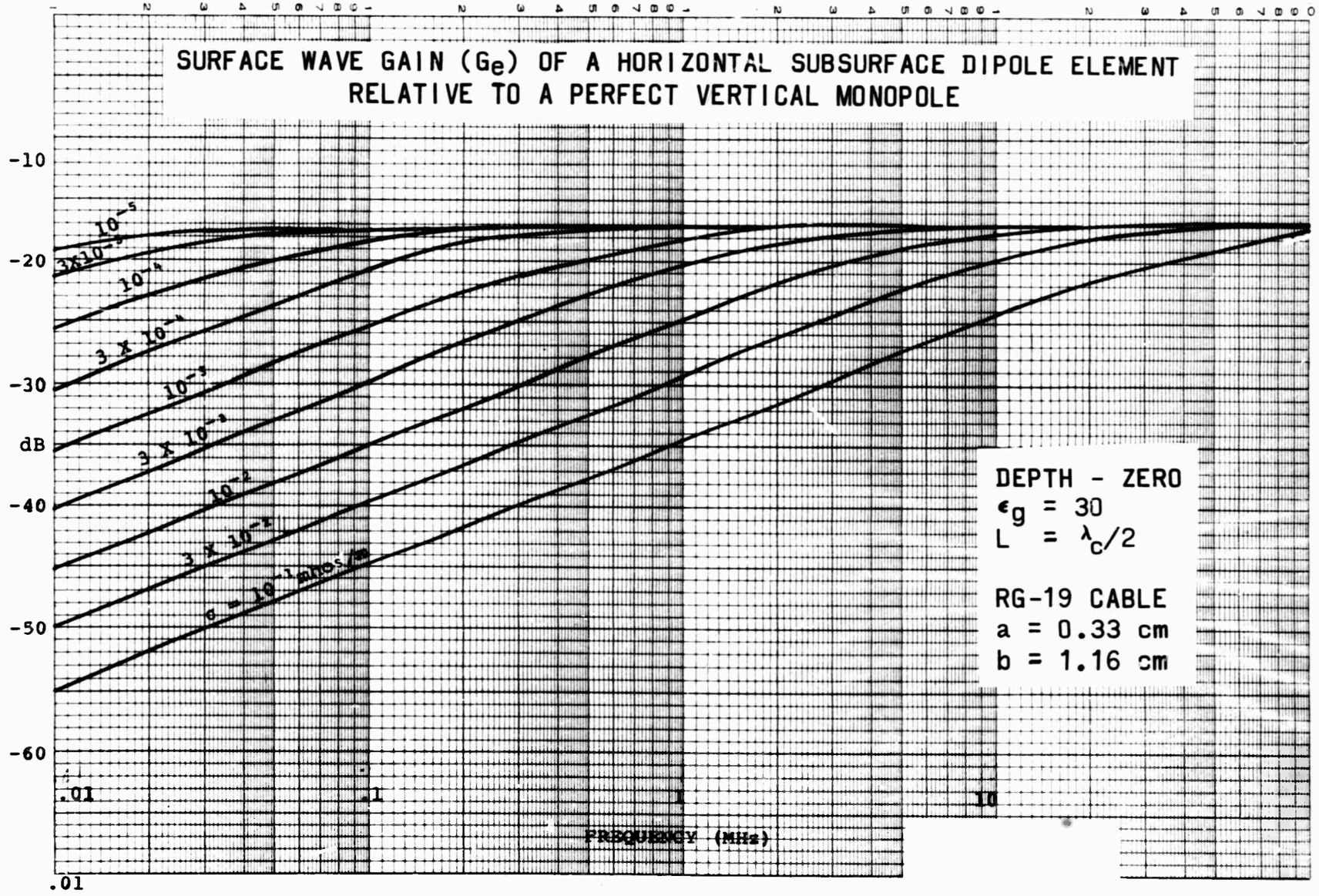
SURFACE WAVE GAIN (G_e) OF A HORIZONTAL SUBSURFACE DIPOLE ELEMENT
RELATIVE TO A PERFECT VERTICAL MONOPOLE
-10
-20
-30
dB
-40
-50
-60
10^{-5}
$3X10^{-5}$
10^{-4}
3×10^{-4}
10^{-3}
3×10^{-3}
10^{-2}
3×10^{-2}
$\sigma = 10^{-1}$ mhos/m
DEPTH - ZERO
$\epsilon_g = 30$
$L = \lambda_c/2$
RG-19 CABLE
a = 0.33 cm
b = 1.16 cm
.01
.1
1
10
FREQUENCY (MHz)
.01

Figure 2-15.

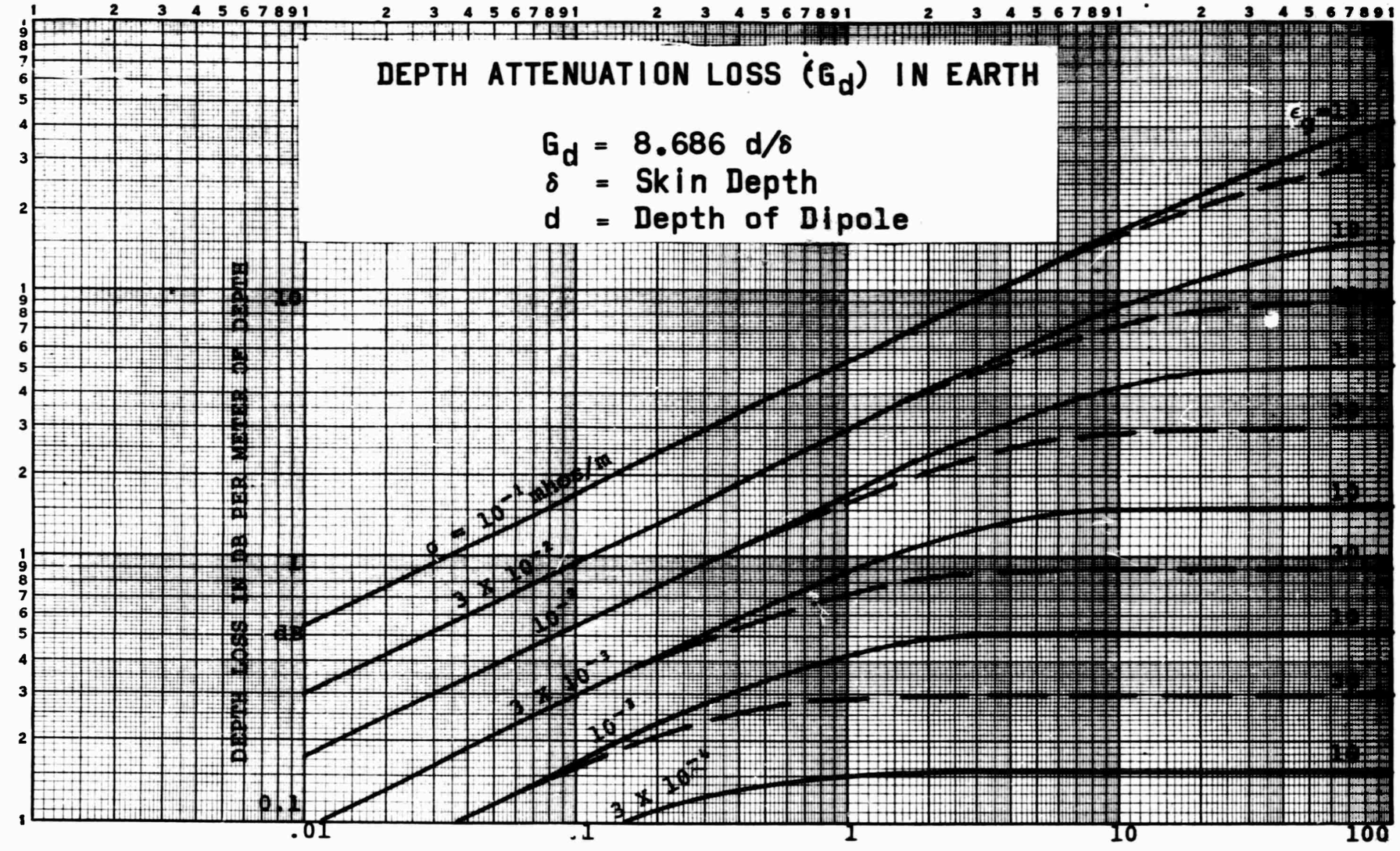
DEPTH ATTENUATION LOSS (G_d) IN EARTH
G_d = 8.686 d/δ
δ = Skin Depth
d = Depth of Dipole
DEPTH LOSS IN dB PER METER OF DEPTH
10
1
dB
0.1
$\sigma = 10^{-1}$ mhos/m
3×10^{-2}
10^{-2}
3×10^{-3}
10^{-3}
3×10^{-4}
ϵ_r
.01
.1
1
10
100
FREQUENCY (MHz)

FIGURE 2-1f

As the array width is increased beyond a half wavelength in free space, the pattern is no longer that of a single element, and directivity gain is achieved by loss of gain in certain directions. G_a can be expressed for computation as the number of elements spaced s meters apart and contained within an area w meters wide:

$$G_a = 10 \log (1 + w/s). \qquad (2\text{-}35)$$

Figures 2-17 and 2-18 are plots of G_a for $w = \lambda_0/2$ and for spacings of 1 and 1.5 skin depths, respectively. These plots do not include the effects of mutual coupling. The degradation due to mutual coupling between elements has recently been measured experimentally and at a spacing of 1 skin depth the array gain is reduced by as little as 2 db. (Ref. 24).

The total array gain, G_t, is shown in Figures 2-19 through 2-20 for typical parameters.

For the space wave of a subsurface dipole, we shall compare its gain to that of a horizontal half-wave dipole located a quarter wavelength above perfect ground. The field at the zenith for the half wave dipole can be expressed as (Ref. 25)

$$|E|_{hw} = \frac{120}{r} \sqrt{P_{in}/85.8} \qquad (2\text{-}36)$$

For the subsurface dipole, either Eq. (2-7) or (2-8) at $\phi = 0$ and $\theta = 90°$ become

$$|E|_{ssd} = \frac{60}{r} \sqrt{\frac{P_{in}}{R_{in}}} |f(\phi)| . \left|\frac{1}{n+1}\right| \exp(-d/\delta) \qquad (2\text{-}37)$$

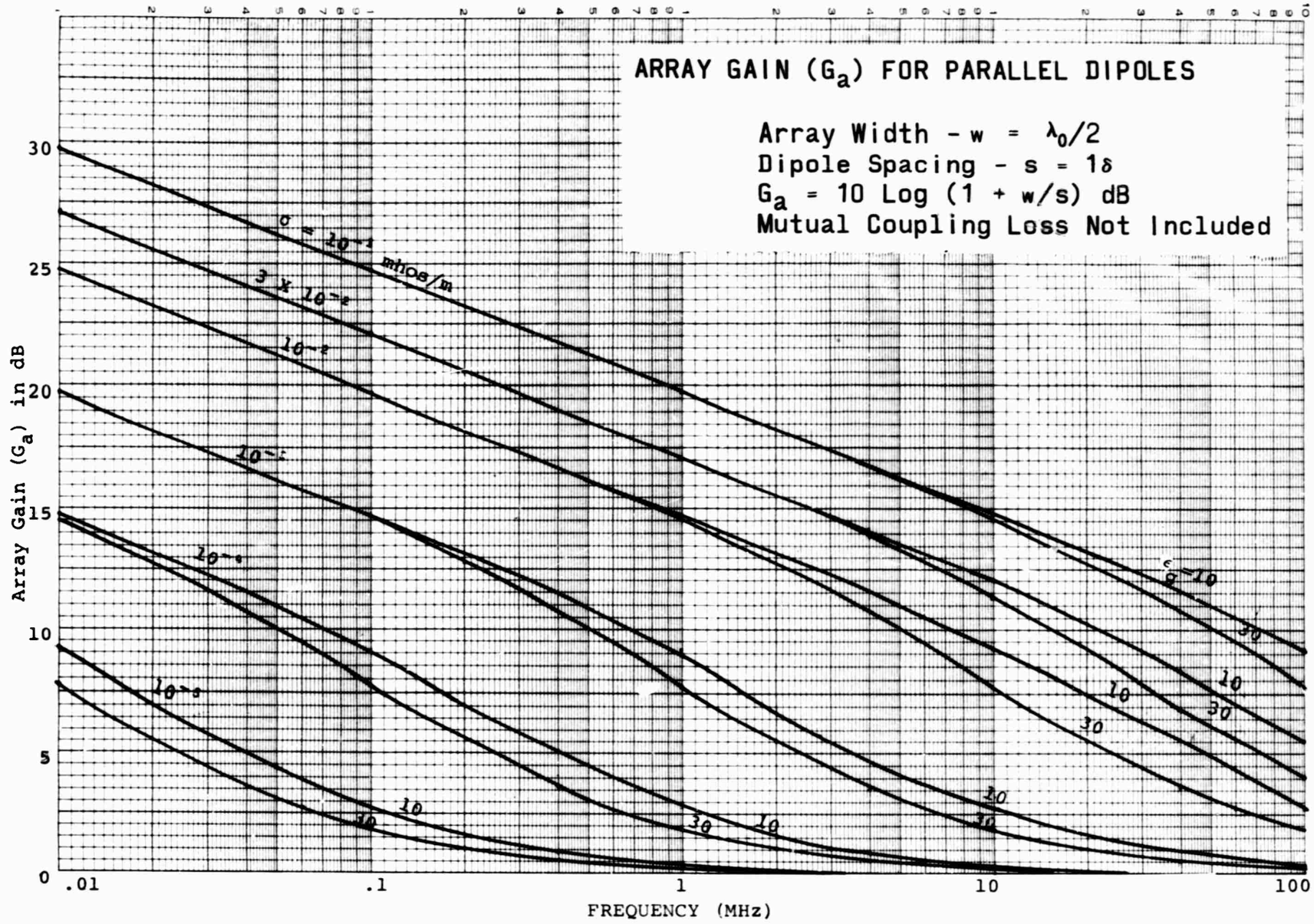
ARRAY GAIN (G_a) FOR PARALLEL DIPOLES
Array Width - w = $\lambda_0/2$
Dipole Spacing - s = 1δ
G_a = 10 Log (1 + w/s) dB
Mutual Coupling Loss Not Included
Array Gain (G_a) in dB
FREQUENCY (MHz)
0
5
10
15
20
25
30
.01
.1
1
10
100
σ = 10⁻¹ mhos/m
3 X 10⁻²
10⁻²
10⁻³
10⁻⁴
10⁻⁵
ε = 10
30
10
30
10
30
10
30
10
30

Figure 2-17.

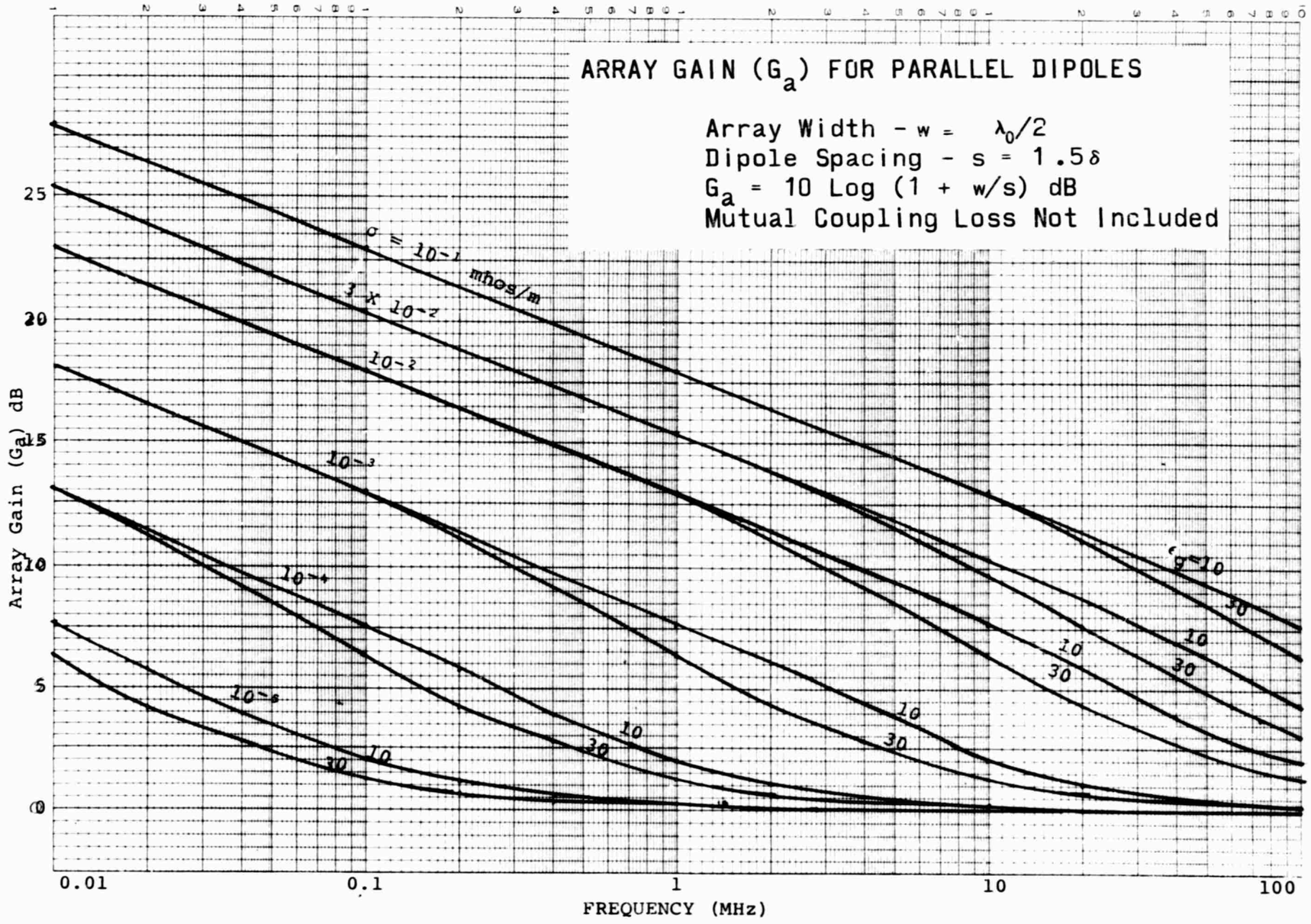
ARRAY GAIN (G_a) FOR PARALLEL DIPOLES
Array Width - w = $\lambda_0/2$
Dipole Spacing - s = 1.5δ
G_a = 10 Log (1 + w/s) dB
Mutual Coupling Loss Not Included
σ = 10-1 mhos/m
3 x 10-2
10-2
10-3
10-4
10-5
10
30
Array Gain (G_a) dB
0
5
10
15
20
25
0.01
0.1
1
10
100
FREQUENCY (MHz)

Figure 2-18.

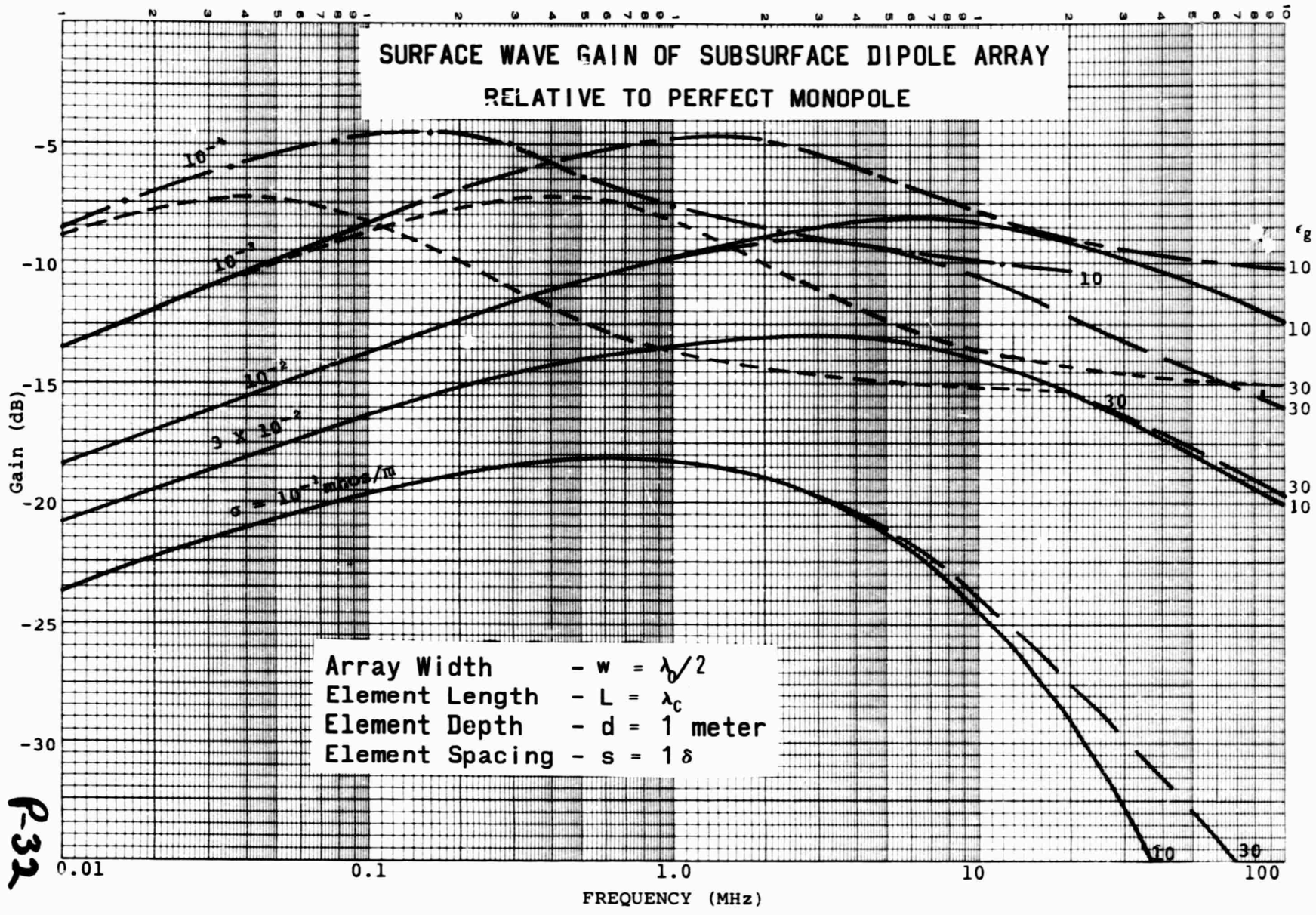
SURFACE WAVE GAIN OF SUBSURFACE DIPOLE ARRAY
RELATIVE TO PERFECT MONOPOLE
Gain (dB)
-5
-10
-15
-20
-25
-30
10^{-1}
10^{-2}
3×10^{-2}
$\sigma = 10^{-3}$ mhos/m
ϵ_g
10
10
10
30
30
30
10
10
10
30
Array Width - w = $\lambda_0/2$
Element Length - L = λ_c
Element Depth - d = 1 meter
Element Spacing - s = 1 δ
0.01
0.1
1.0
10
100
FREQUENCY (MHz)

Figure 2-19.

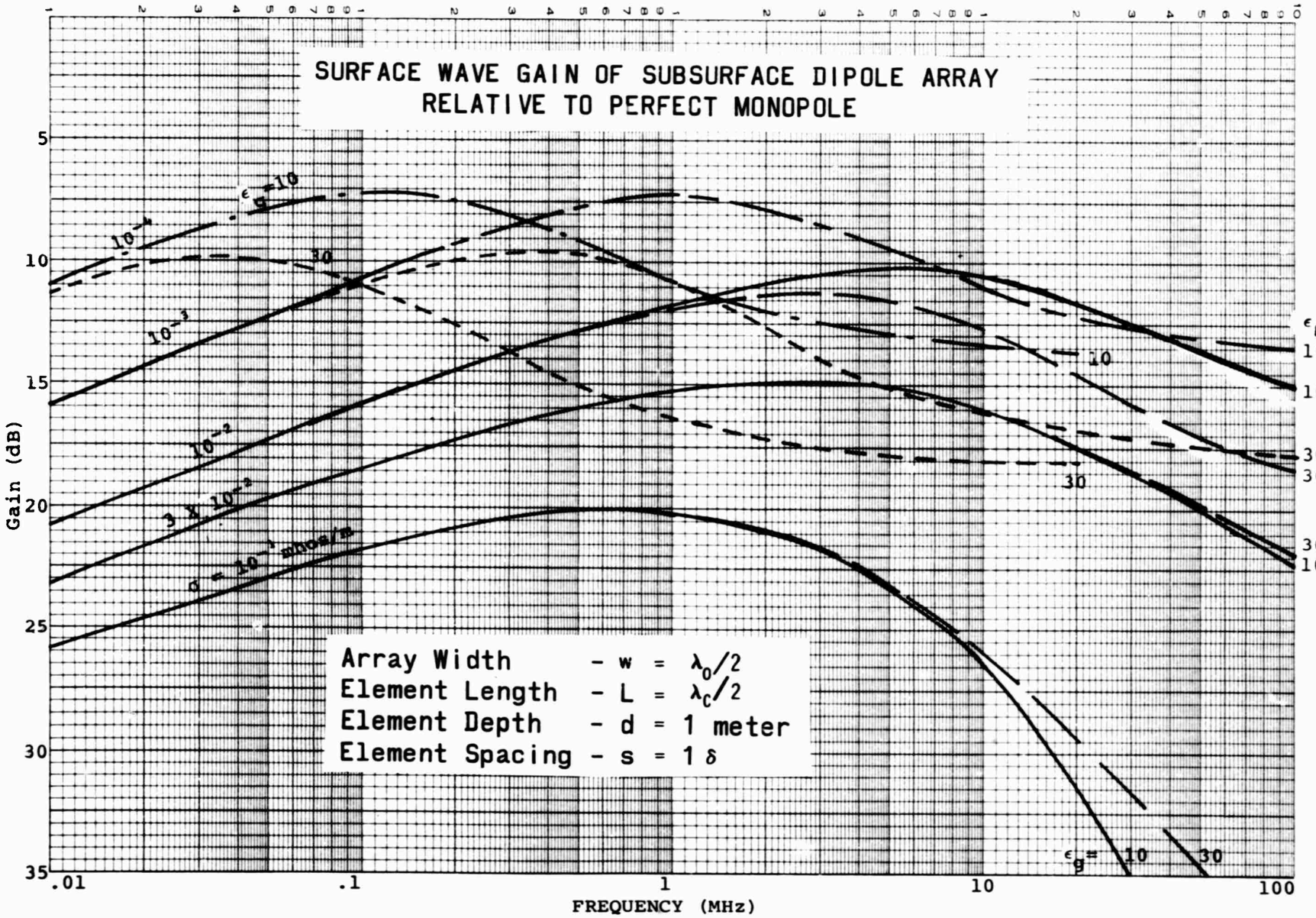
SURFACE WAVE GAIN OF SUBSURFACE DIPOLE ARRAY
RELATIVE TO PERFECT MONOPOLE
Gain (dB)
5
10
15
20
25
30
35
.01
.1
1
10
100
FREQUENCY (MHz)
ϵ_g=10
30
10^{-4}
10^{-3}
10^{-2}
3×10^{-2}
$\sigma = 10^{-1}$ mhos/m
10
30
ϵ_g
10
10
30
30
30
10
Array Width - w = $\lambda_0/2$
Element Length - L = $\lambda_c/2$
Element Depth - d = 1 meter
Element Spacing - s = 1 δ

Figure 2-20.

Squaring these and taking the ratio, we have a relative gain similar to that calculated for the monopole. This new relative gain which we shall call g_d can be expressed in terms of the previously derived relative gain compared to the monopole (g_m) as:

$$g_d = 0.536 \left| \frac{(1+n^2)^{3/2}}{n(1+n^2)} \right| g_m \qquad (2\text{-}38)$$

For $n >> 1$, this reduces to

$$g_d/g_m \simeq 0.536 = -2.7 \text{ db} \qquad (2\text{-}39)$$

and for $|n| = 10$, which is a typical example,

$$g_d/g_m \simeq 0.44 = -3.5 \text{ db}. \qquad (2\text{-}40)$$

It is now possible to use the previous figures to obtain the relative gain compared to the half wave dipole by simply adding approximately -3.5 db for most practical uses or computing the exact quantity from Eq. (2-38).

3. MEASURED PERFORMANCE

A. INTRODUCTION

An experimental program was conducted to verify the theoretical prediction of subsurface dipole performance at high frequencies and investigate misleading results from a previous experiment. (Ref. 1) Previous experimental work has been concentrated mainly on lower frequencies (Ref. 12, 26-28). Experimental work in the HF range had established some performance parameters in a qualitative fashion (Ref. 29-33). However, most of this work is not available in the open literature and for the most part is buried in company proprietary literature.

The main objective of the RADC experiment was to measure the gain of the surface and space wave radiation from subsurface HF dipoles. This was accomplished by burying the dipoles, measuring their input characteristics, and comparing the radiated field with that produced from known reference antennas.

This section is devoted to a detailed description of the test set-up and measurements.

B. PHYSICAL DESCRIPTION OF TRANSMITTER SITE

The transmitting site for the experiment was located at Rome Air Development Center's Verona Test Facility at coordinates 75° 37.1'W and 43° 9.12'N. This location provided an antenna site with level ground extending for more than

several miles in any direction and free of any concentrated wooded areas. The region in which the test facility is located has a rather high water table with wet-weather marshes. The soil would best be described as good agricultural land and its electrical properties are discussed in 3.C.1. The location of the test antennas in relationship to each other and to nearby structures is shown in Figure 3-1. The subsurface and reference dipoles were positioned perpendicular to each other. With this arrangement, it was possible to measure the maximum radiation from both antennas while flying on a 239° heading. The distance separating the reference dipole from the subsurface dipole is approximately 340' and the separation between the monopole and the subsurface dipole is 60'. Figure 3-2 contains a photo which shows approximately the same area as Figure 3-1. The subsurface dipoles are visible in the center. There were some metal structures nearby, but the antenna radiation patterns were not appreciably affected.

The subsurface antennas consisted of five buried dipoles as shown in Figure 3-3. The elements of dipoles 1 and 2 were constructed of shieldless RG-8 cable and were buried one foot below the surface. Dipoles 3, 4, and 5 were constructed of shieldless RG-19 cable and were buried a depth of three feet. Dipole number 5 was placed 13.8' from number 4 and was used to measure the effects of mutual impedance. Figures 3-4

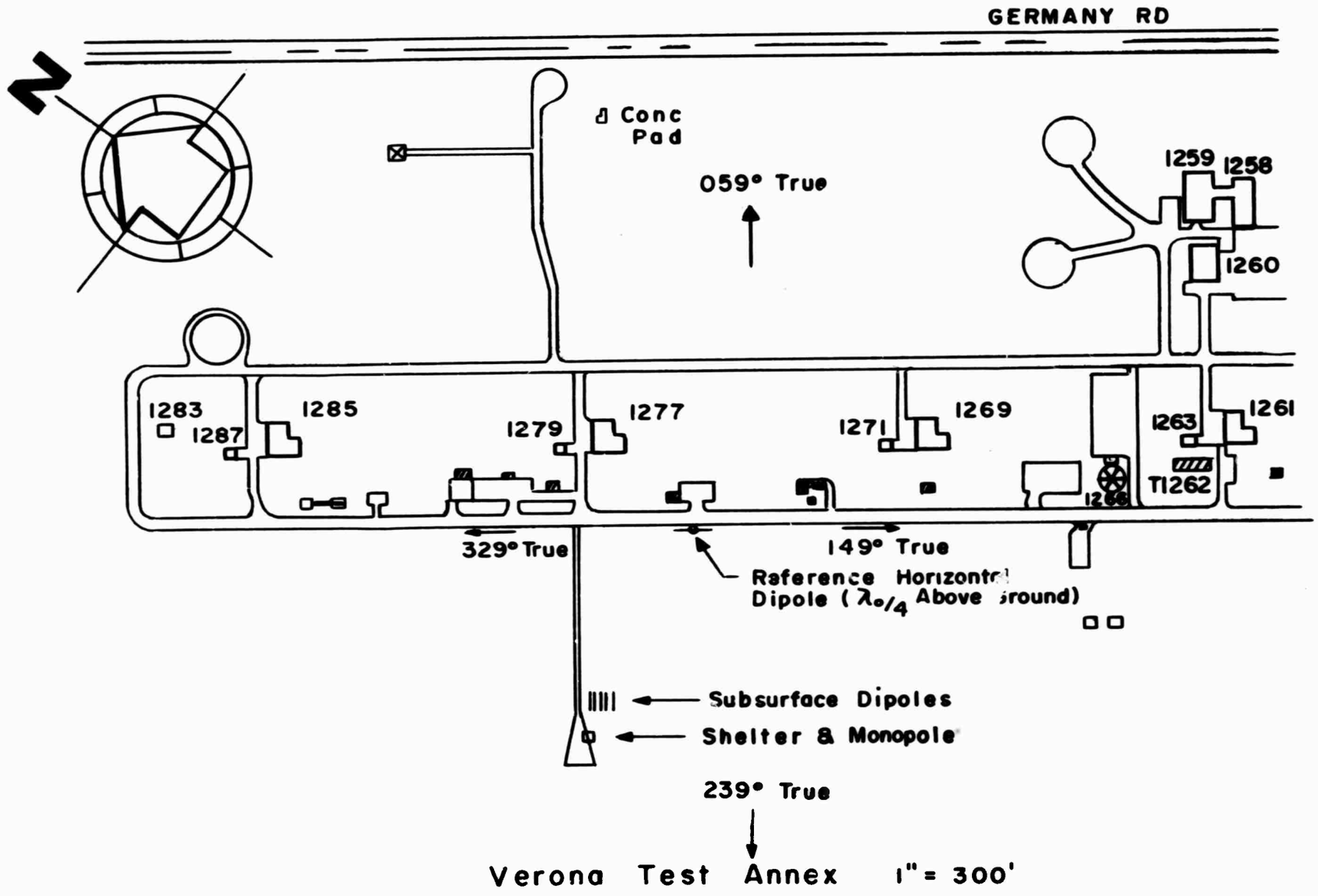

Figure 3-1. Antenna Site Layout

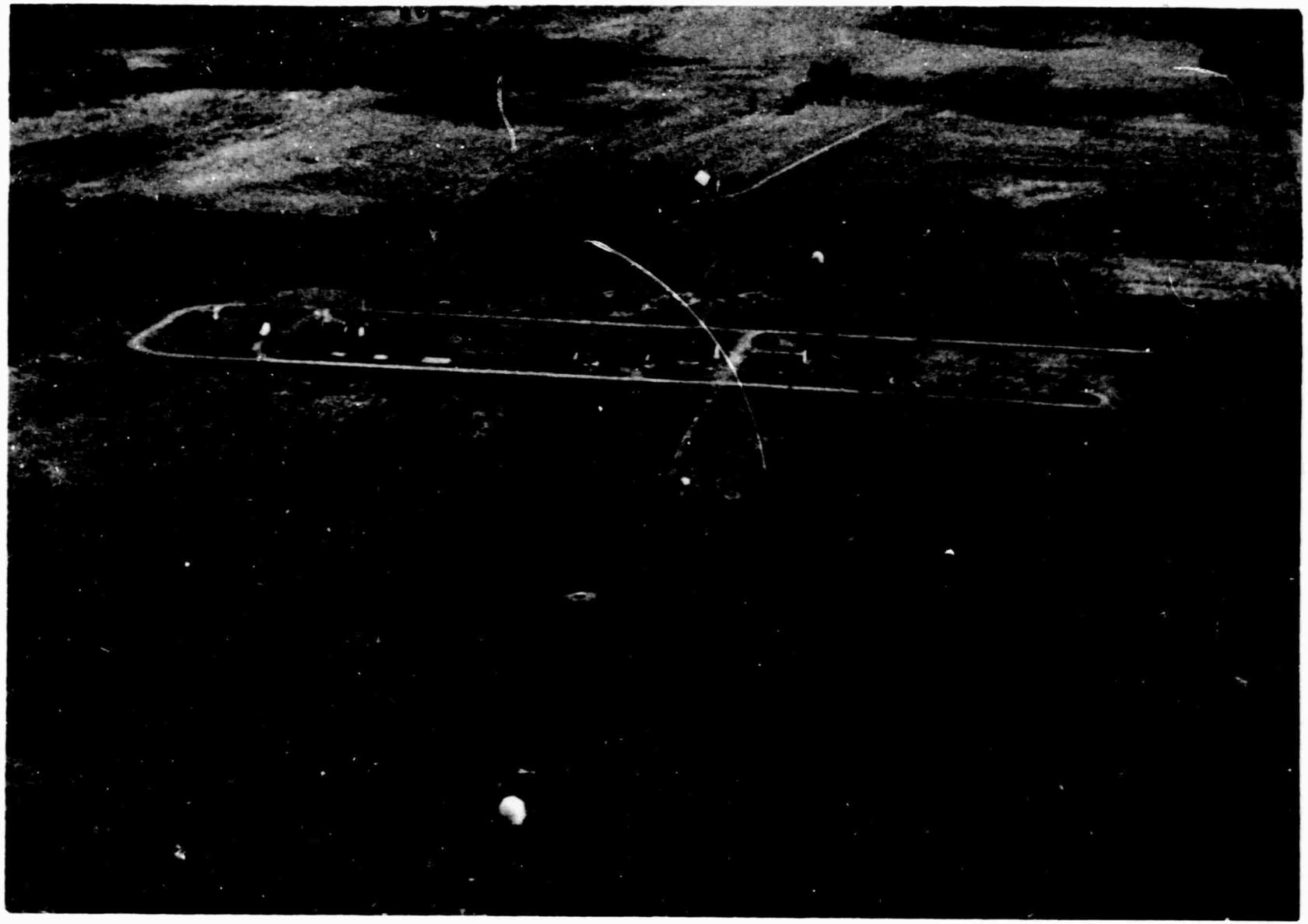

Figure 3-2. Aerial Photo of Antenna Site

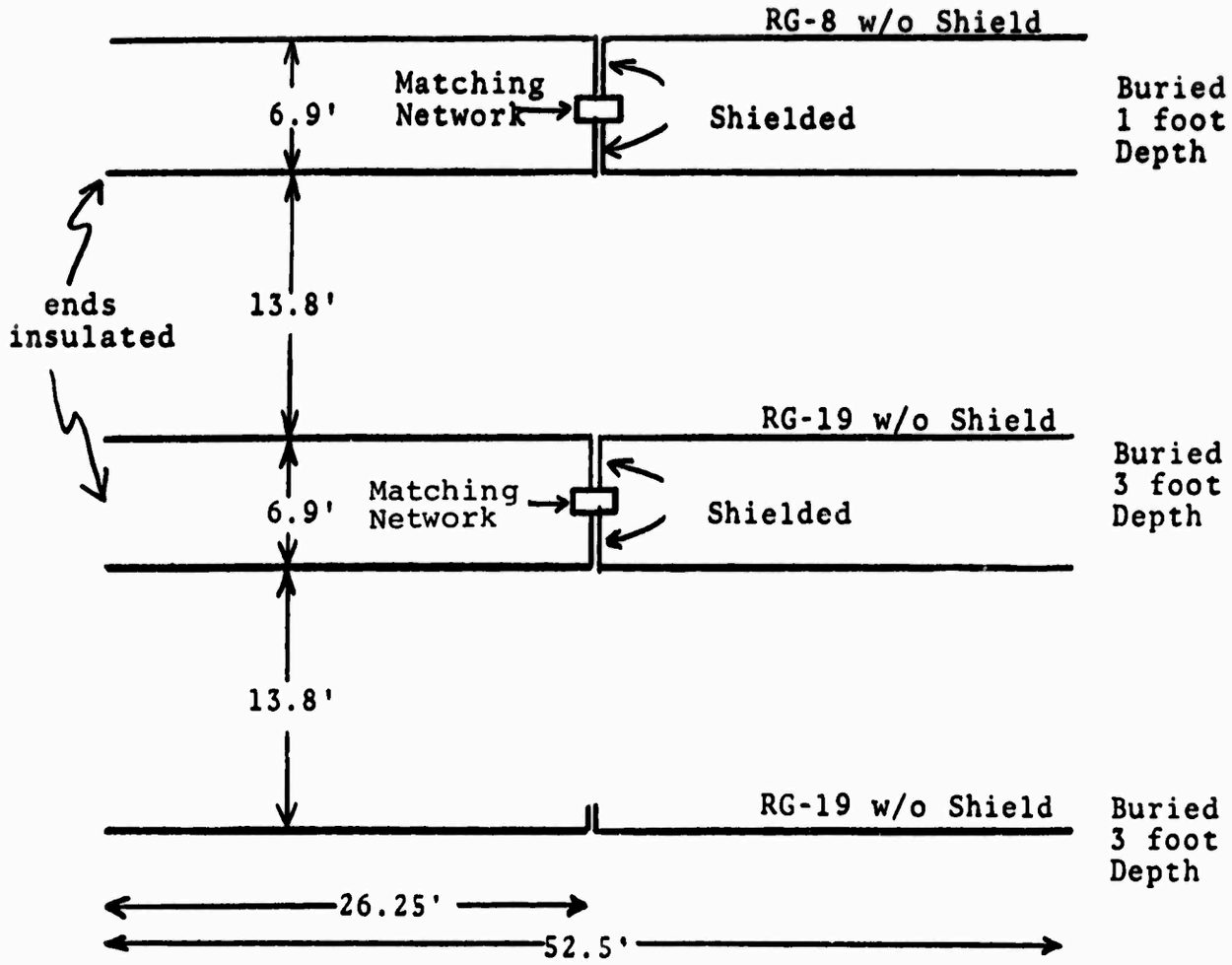

TOP VIEW OF DIPOLE PLACEMENT

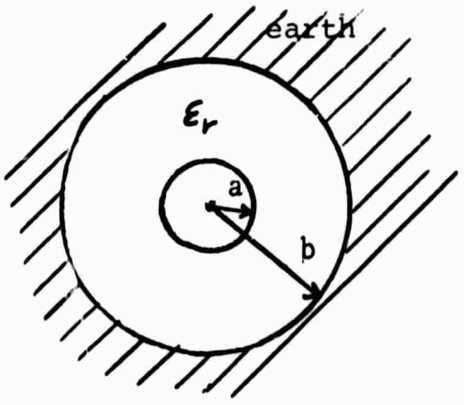

	2a(in)	2b(in)
RG-8	0.086"	0.283"
RG-19	0.260"	0.910"

$\epsilon_r \simeq 2.23$

Figure 3-3. Subsurface Dipole Construction

Figure 3-4. One-Foot Trenches for Dipoles 1 & 2

Figure 3-5. Three Foot Trenches Dipoles 3 & 4

Figure 3-6. Completed Subsurface Dipoles

through 3-6 show the dipoles in various stages of construction.

For the tests, 1 and 2 were combined together in parallel as were 3 and 4, to form two element arrays. The 6.9' spacing between the elements of the arrays is approximately 1.4 skin depth at 7 MHz and resulted in very little mutual coupling between elements.

Approximately one-hundred feet of RG-17 was used as a feed line to the subsurface dipole matching unit. It approached the antennas perpendicular to the elements so that it did not affect the radiation.

The reference dipole was constructed of copper wire cut to half-wave length and trimmed for resonance. The dipole was positioned a quarter of a wave length above ground.

The reference 35' monopole was located on top of an eight-foot shelter with a ground plane consisting of 30' lengths of copper wire spaced every 22.5° around the antenna base and tied to a central ground rod under the monopole.

Standard equipments were utilized in the instrumentation, however, it was necessary to perform modifications to enable pulsed operation. A block diagram illustrating transmitting stations is shown in Figure 3-7. The power levels delivered to the antennas were continuously monitored by calibrated in-line wattmeters and oscilloscopes. Both pulse and CW signals were transmitted from the reference and subsurface antennas. CW was used primarily for the airborne antenna

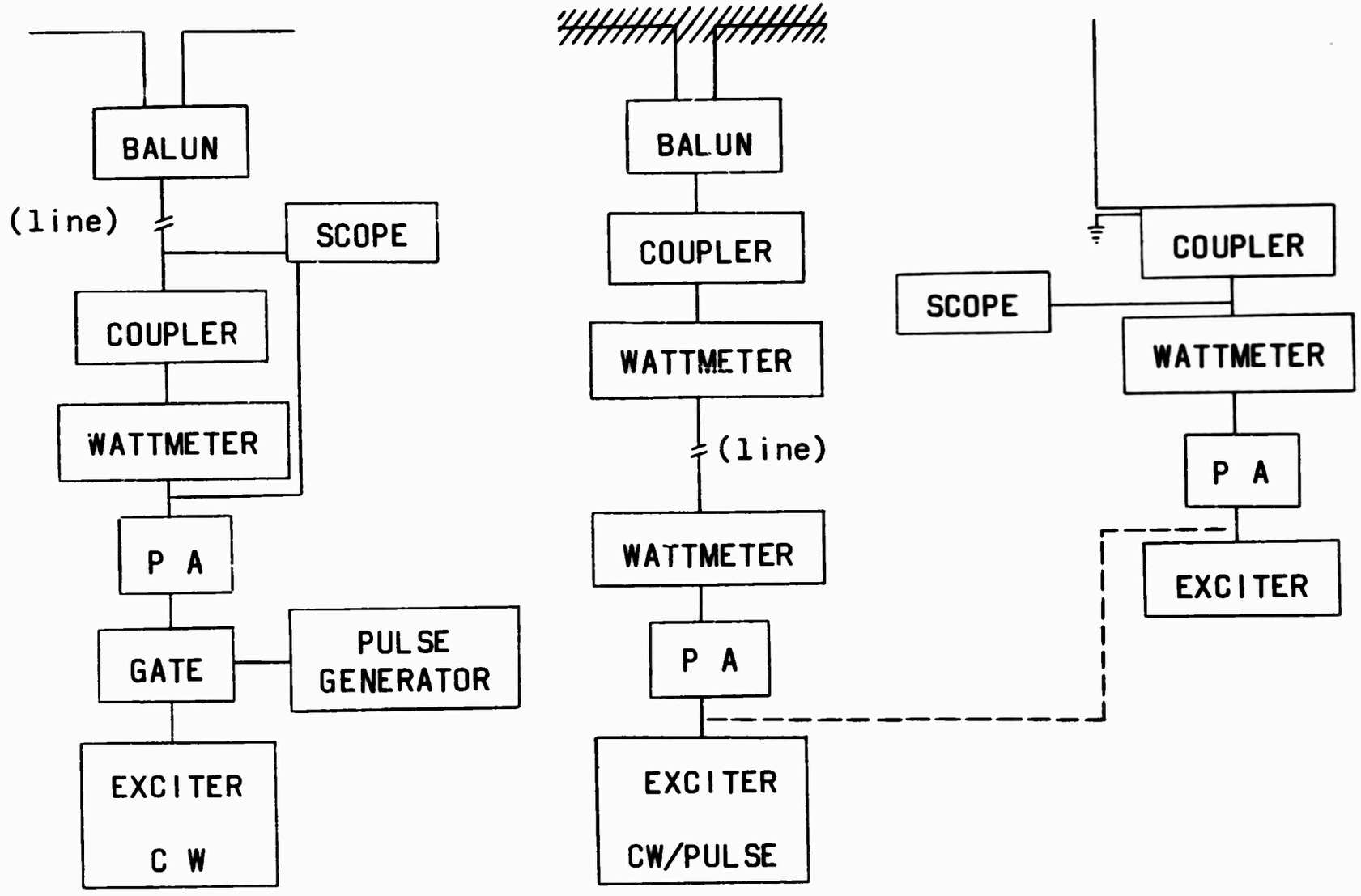

Figure 3-7. Transmitting Stations

patterns and the close-in surface wave measurements where contamination of the data with skywave signals was not a problem. Pulse transmissions were utilized for the point to point tests beyond 2 miles to provide mode resolution. The 100 microsecond (μS) pulse used with the reference whip and the subsurface antennas was adequate to resolve all the major propagation modes encountered during the tests but the 1.4 ms pulse of the reference dipole was too long to separate the 1 hop E and 1 hop F modes existing a few times during tests. The 100 μS pulse was lengthened to 400 μS for a portion of the test because it looked too much like the noise spikes and was difficult to identify in the photographs at low signal levels.

Vertical sounding data taken simultaneously with the measurements was provided by a Type C-2/A Automatic Ionosphere Recorder located at RADC's Stockbridge Test Facility approximately 8.6 miles from the transmitting site at Verona.

C. ELECTRICAL CHARACTERISTICS OF TRANSMITTER SITE

1. SOIL PARAMETERS

Accurate values of the soil constants were required in order to make theoretical predictions of the subsurface antenna's capabilities. Originally, it was planned to repeat the required measurements several times during the test program but equipment non-availability prevented it.

The soil constant measurements were based on measurements of the wave tilt of an electromagnetic wave near the earth's

surface. The instruments and techniques utilized for the measurements are described in a recent report (Ref. 34).

Data resulting from measurements completed early in the test program are shown in Figure 3-8 and 3-9.

2. SUBSURFACE DIPOLES

The input impedance of the subsurface dipole antennas was measured as a function of frequency with and without the transmitting baluns. The measurements without the balun were made to determine the actual balanced input impedance of the antennas, and the measurements with the balun were made to determine the unbalanced impedance which would have to be matched to the transmitter.

Figures 3-10 and 3-11 show the balanced input impedance of subsurface dipole 2 and subsurface dipole 4. Figures 3-12 and 3-13, respectively, show the balanced input impedance of the paralleled combinations of dipoles 1 and 2 and of dipoles 3 and 4. Figure 3-14 shows the balanced input impedance of subsurface dipole 4 and subsurface dipole 5 plotted on the same graph to display the effects of coupling between dipole 3 and dipole 4.

The balanced input impedance of the subsurface dipoles was measured as shown in Figures 3-15 with a Wayne Kerr type B-801 admittance bridge. The R-390 receiver which had been frequency calibrated served as a frequency indicator and bridge detector. A standard HP-606A signal generator supplied the

GROUND CONDUCTIVITY MEASUREMENTS

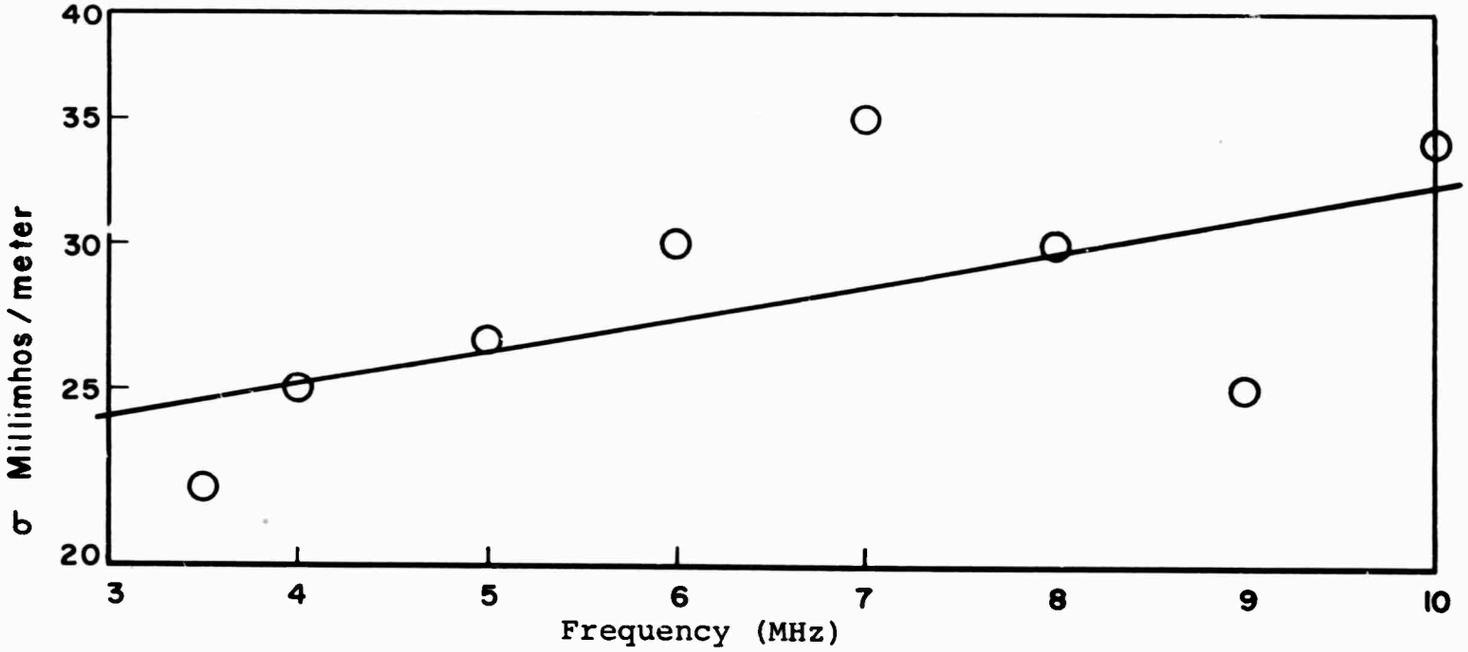

FIGURE 3-8

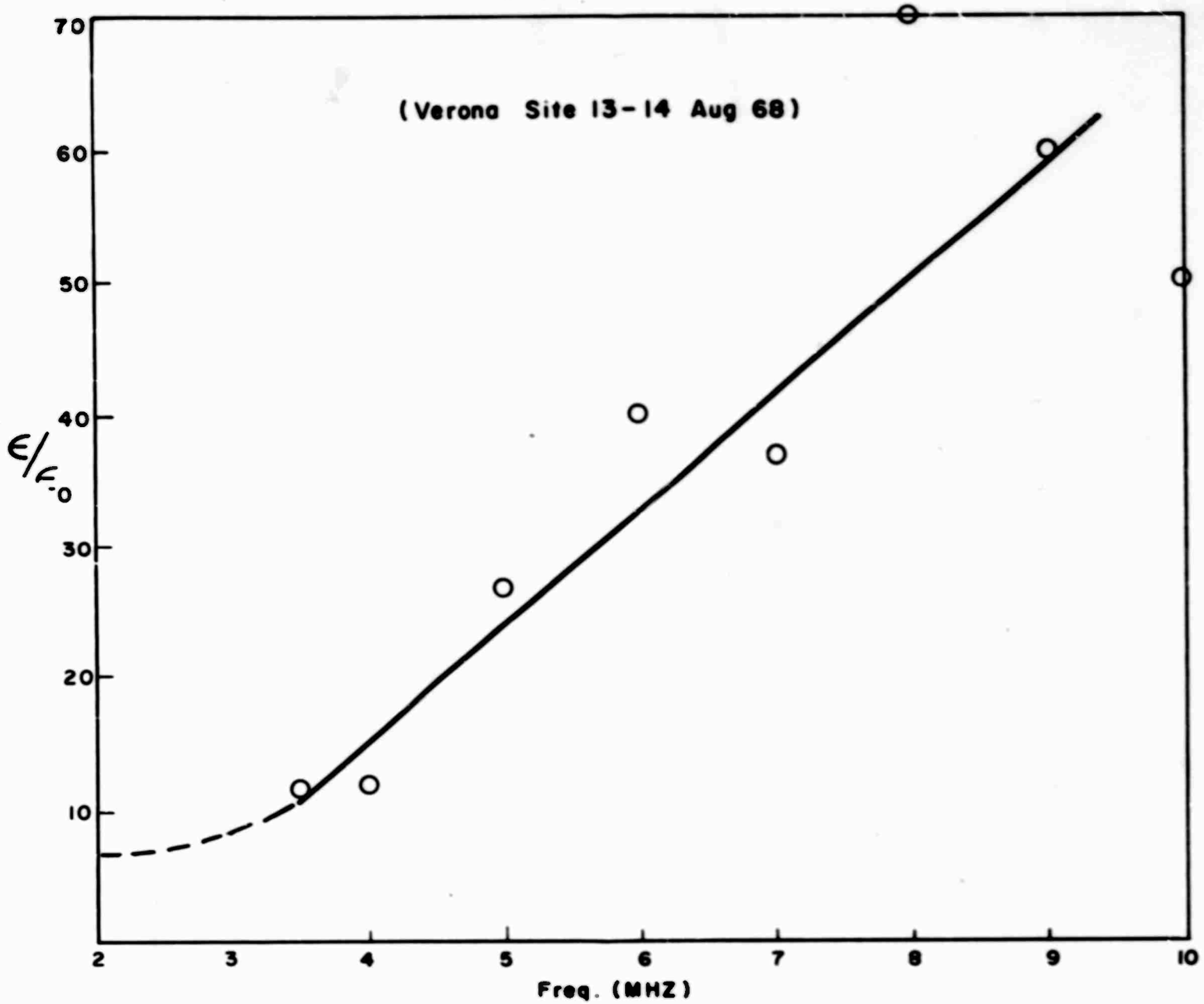

Figure 3-9. Dielectric Constant Measurements

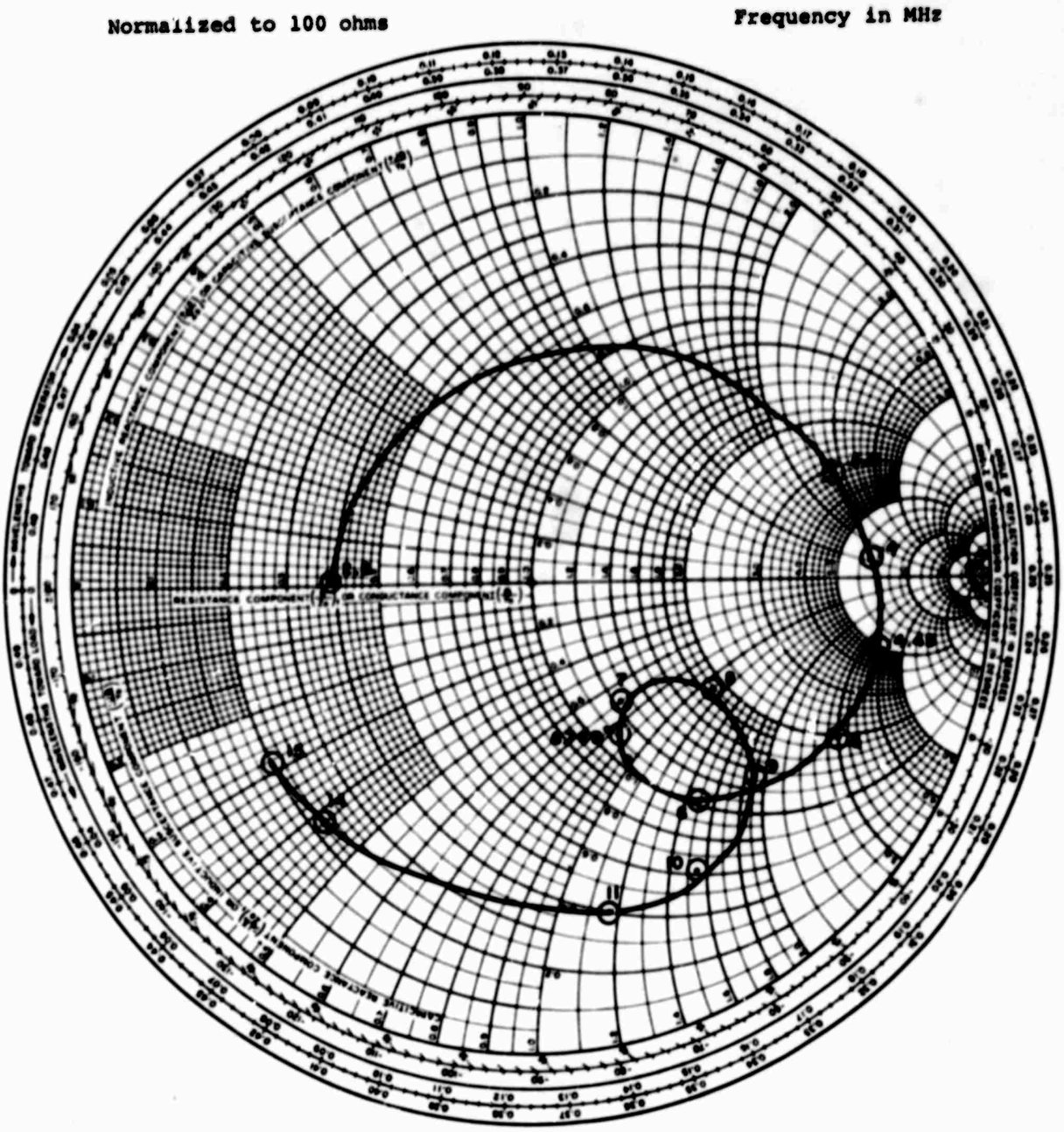

Figure 3-10. SUBSURFACE DIPOLE 2 BALANCED INPUT IMPEDANCE

Normalized to 100 ohms

Frequency in MHz

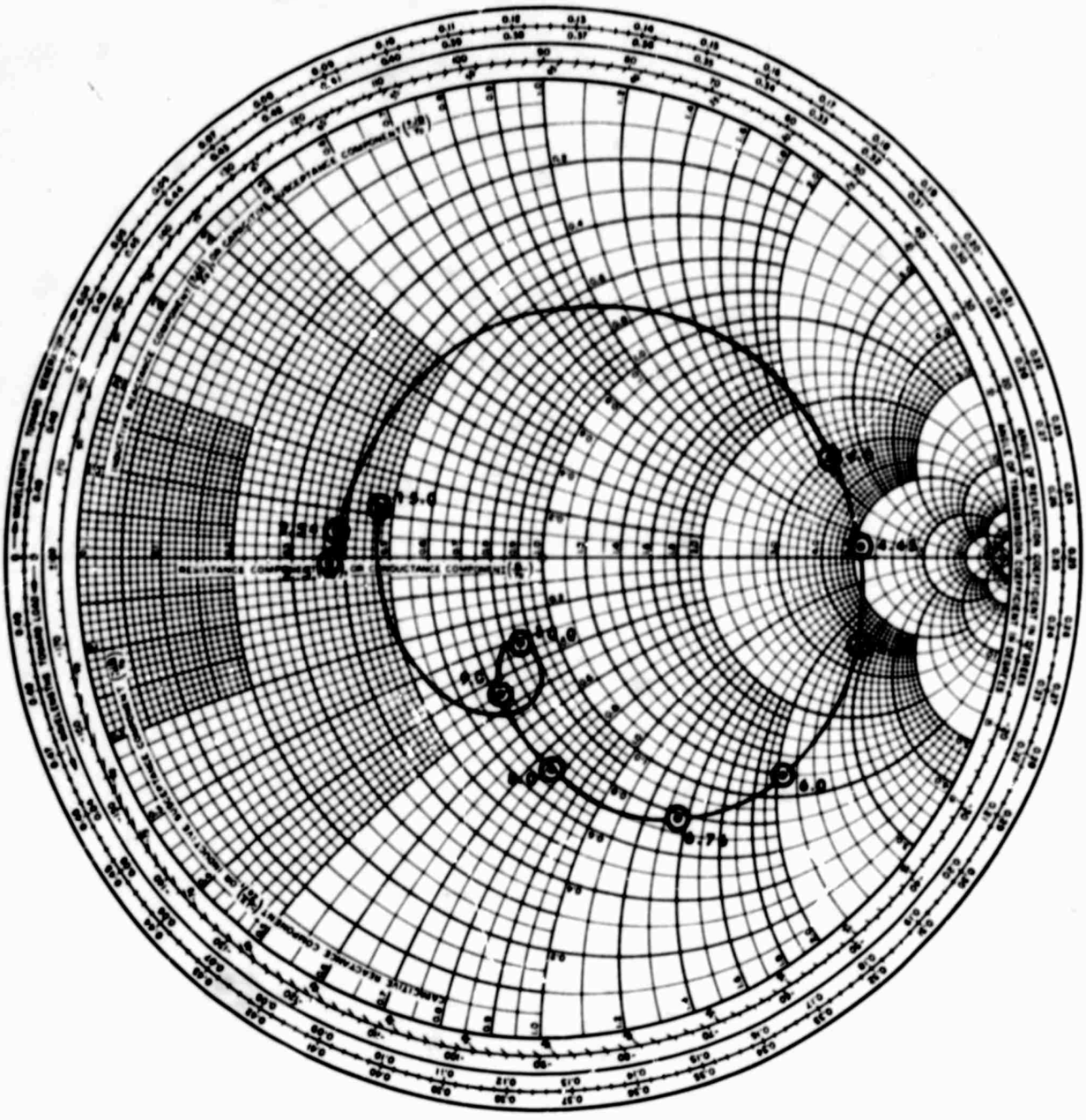

Figure 3-11. SUBSURFACE DIPOLE 4 BALANCED INPUT IMPEDANCE

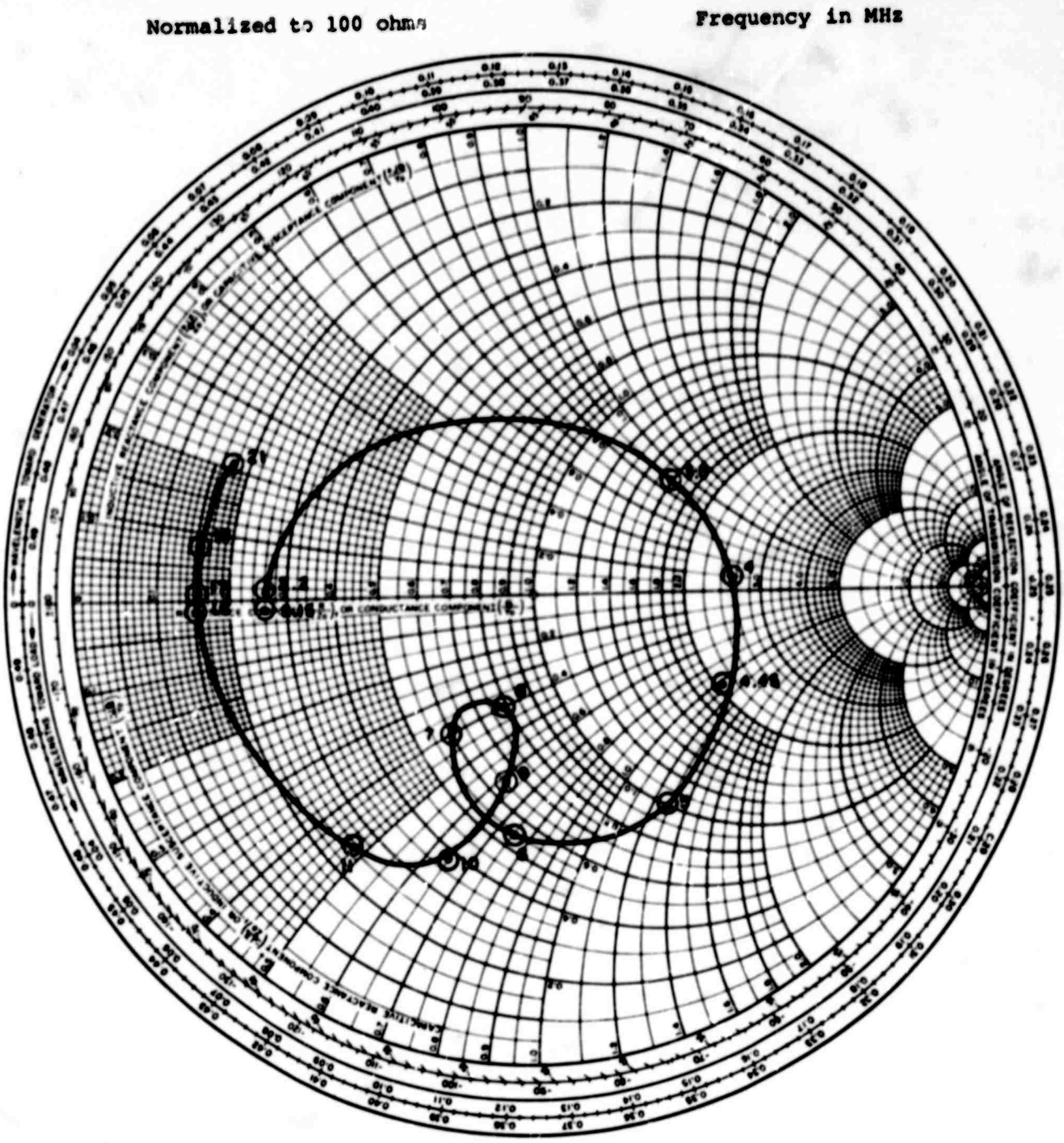

Figure 3-12. SUBSURFACE DIPOLES 1 AND 2 BALANCED INPUT IMPEDANCE

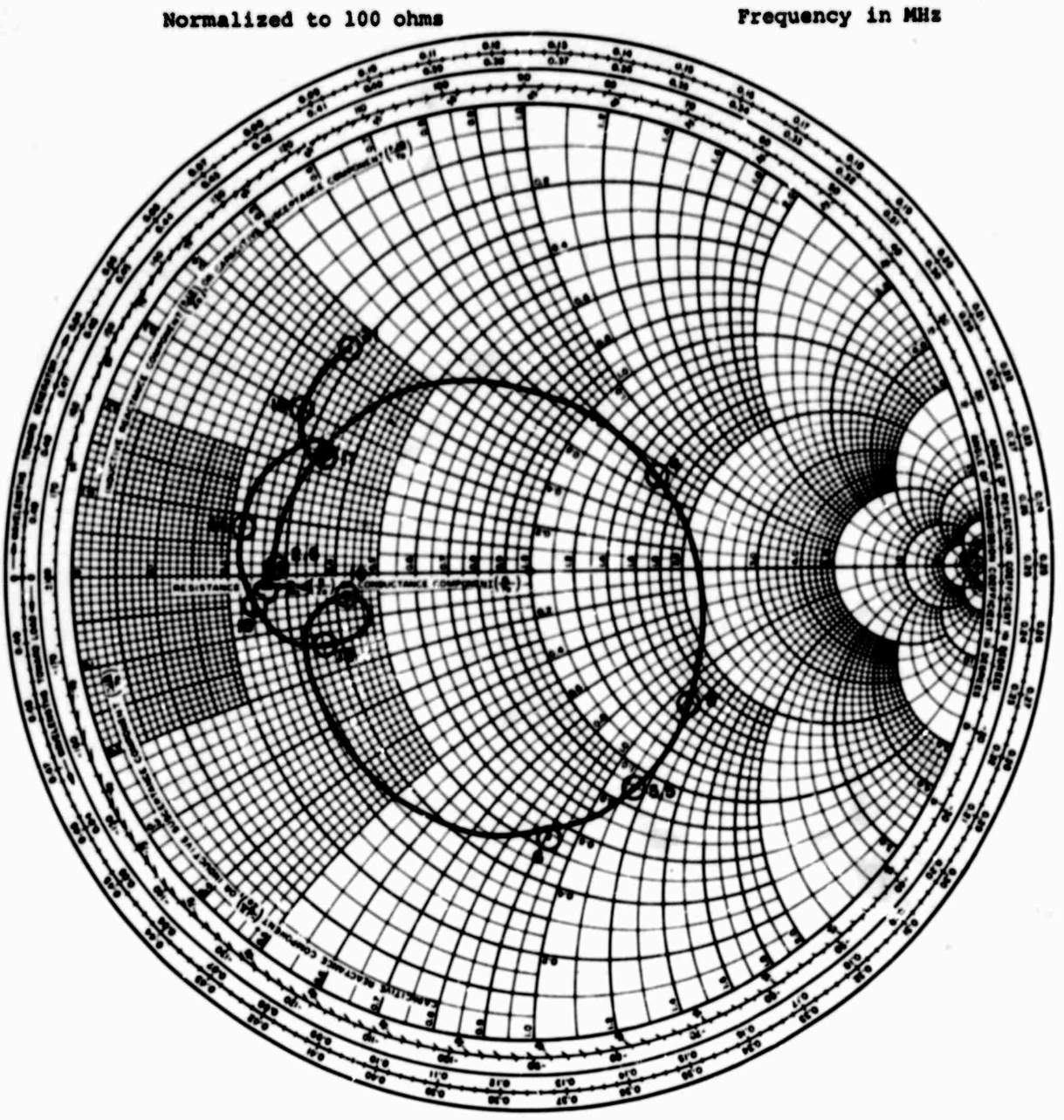

Figure 3-13. SUBSURFACE DIPOLES 3 AND 4 BALANCED INPUT IMPEDANCE

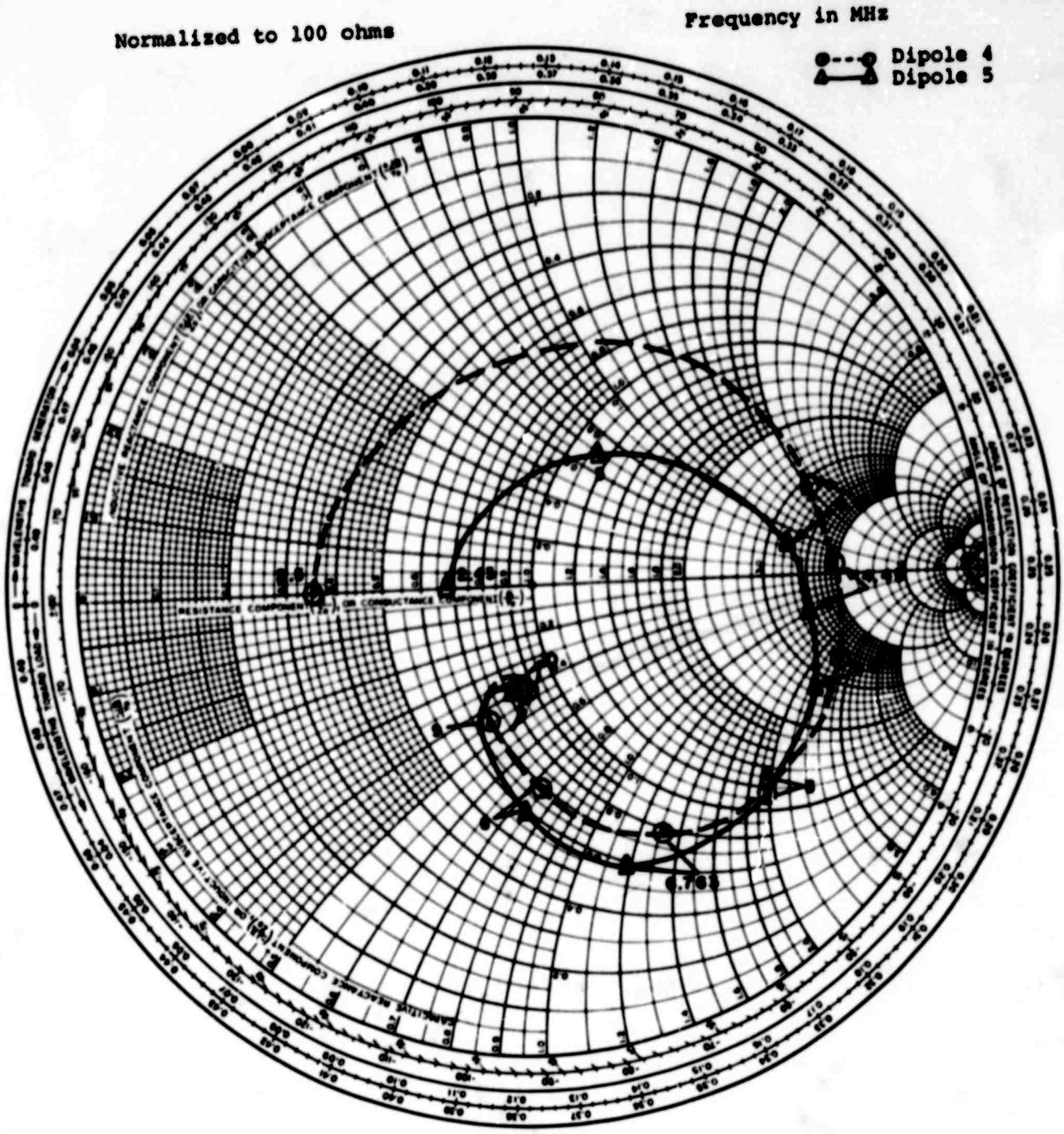

Figure 3-14. MUTUAL COUPLING BALANCED INPUT IMPEDANCE

signal for the bridge. As shown in Figure 3-15, the antenna leads were connected to the balanced input terminals of the bridge and the shields were connected to a common ground. The same arrangement was used in connecting the antenna to the transmitting balun (see Figure 3-21).

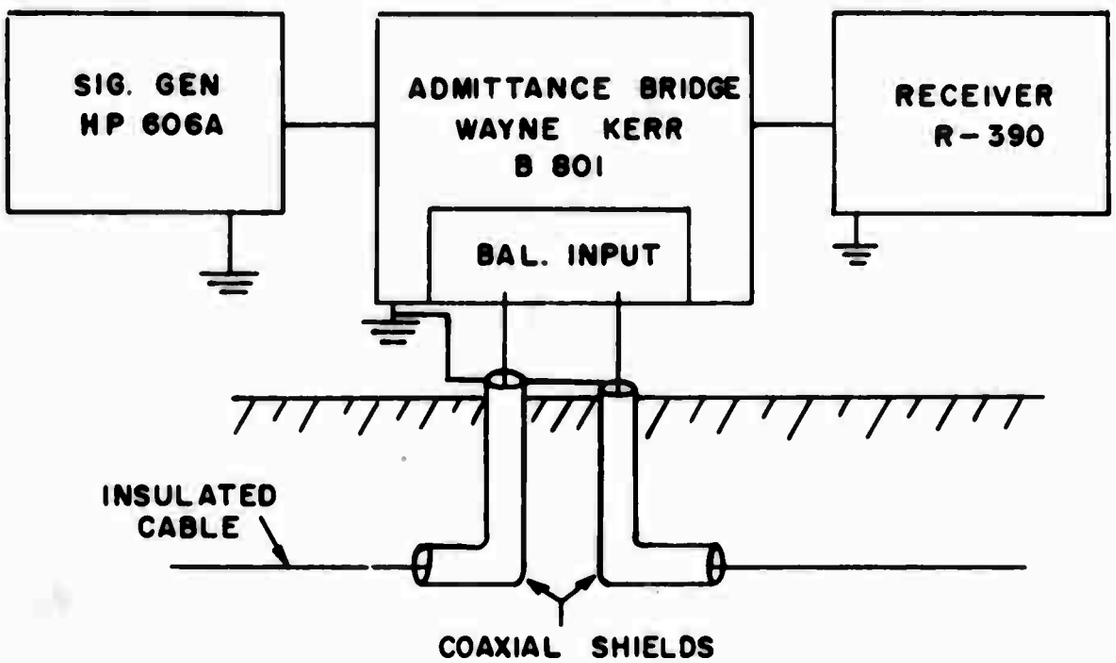

Figure 3-15. Balanced Impedance Measurements.

A Hewlett-Packard Model 4815A Vector Impedance Meter was used to make the unbalanced impedance measurements. A frequency counter was used in conjunction with the Vector Impedance Meter to give an accurate indication of frequency. The test set up is shown in Figure 3-16 below.

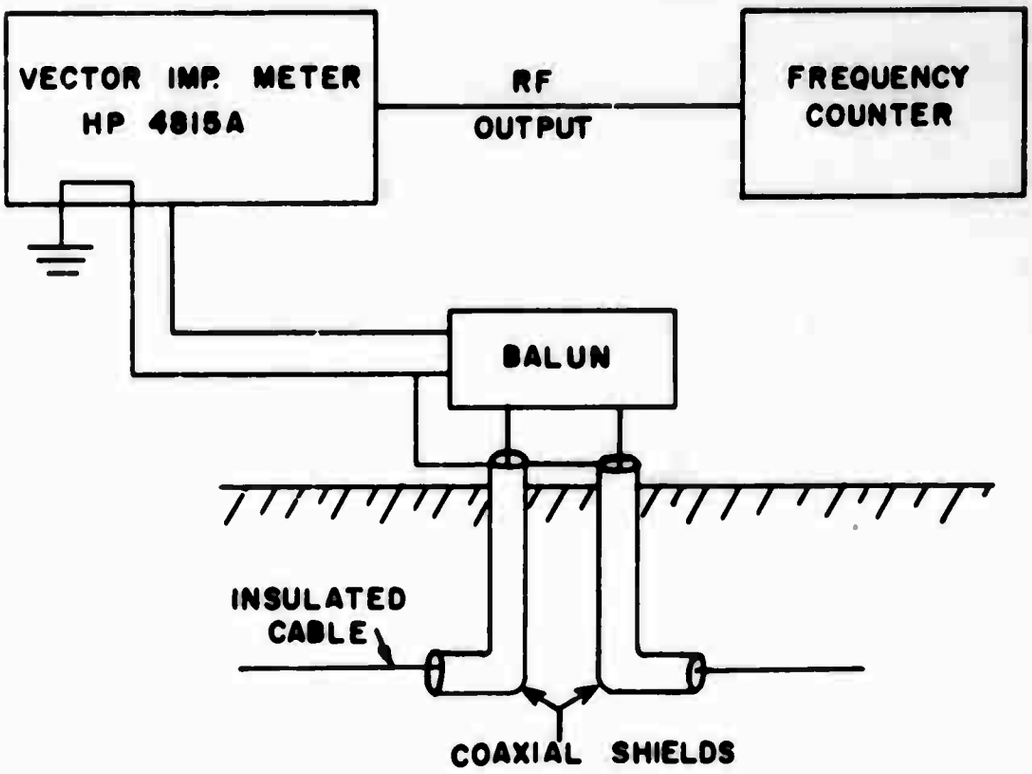

Figure 3-16. Unbalanced Impedance Measurements.

Figure 3-17 contains curves illustrating the unbalanced input impedance of subsurface dipoles 1 and 2 through a 50 to 50 ohm balun over a 2 to 20 MHz frequency range and from 4.2 to 4.45 MHz through a 200 to 50 ohm balun. Similar information for subsurface dipoles 3 and 4 is contained in Figures 3-18a and 3-18b.

The impedance measurements indicate that half-wave and full-wave resonance of the subsurface dipoles occurs at approximately 2-3 MHz and 4-5 MHz, respectively. Further analysis, which will be discussed later on, indicates that the actual current distribution is resonant at slightly

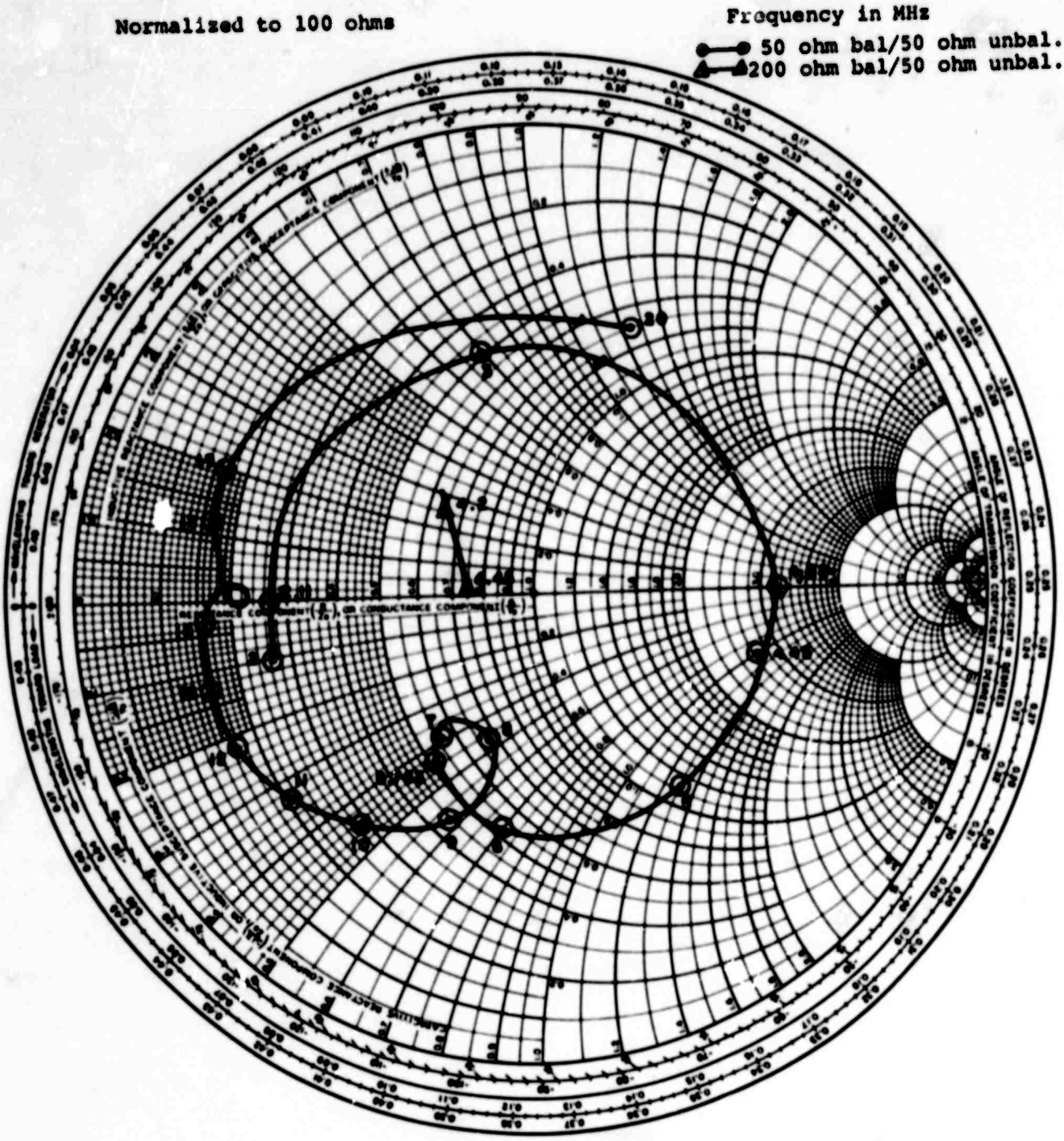

Figure 3-17. SUBSURFACE DIPOLES 1 AND 2 WITH BALUN UNBALANCED INPUT IMPEDANCE

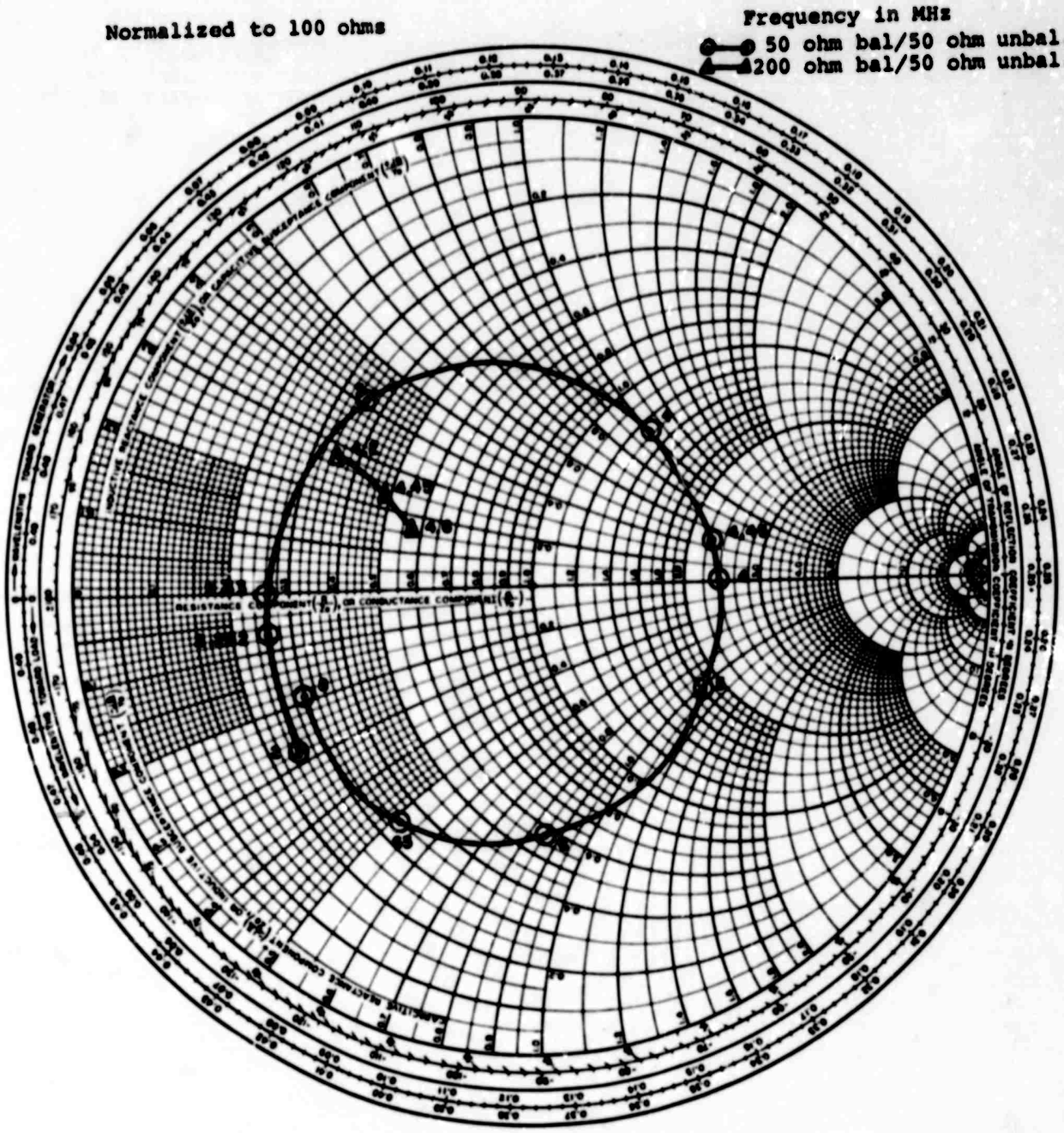

Figure 3-18a. SUBSURFACE DIPOLES 3 AND 4
UNBALANCED (THRU BALUN)

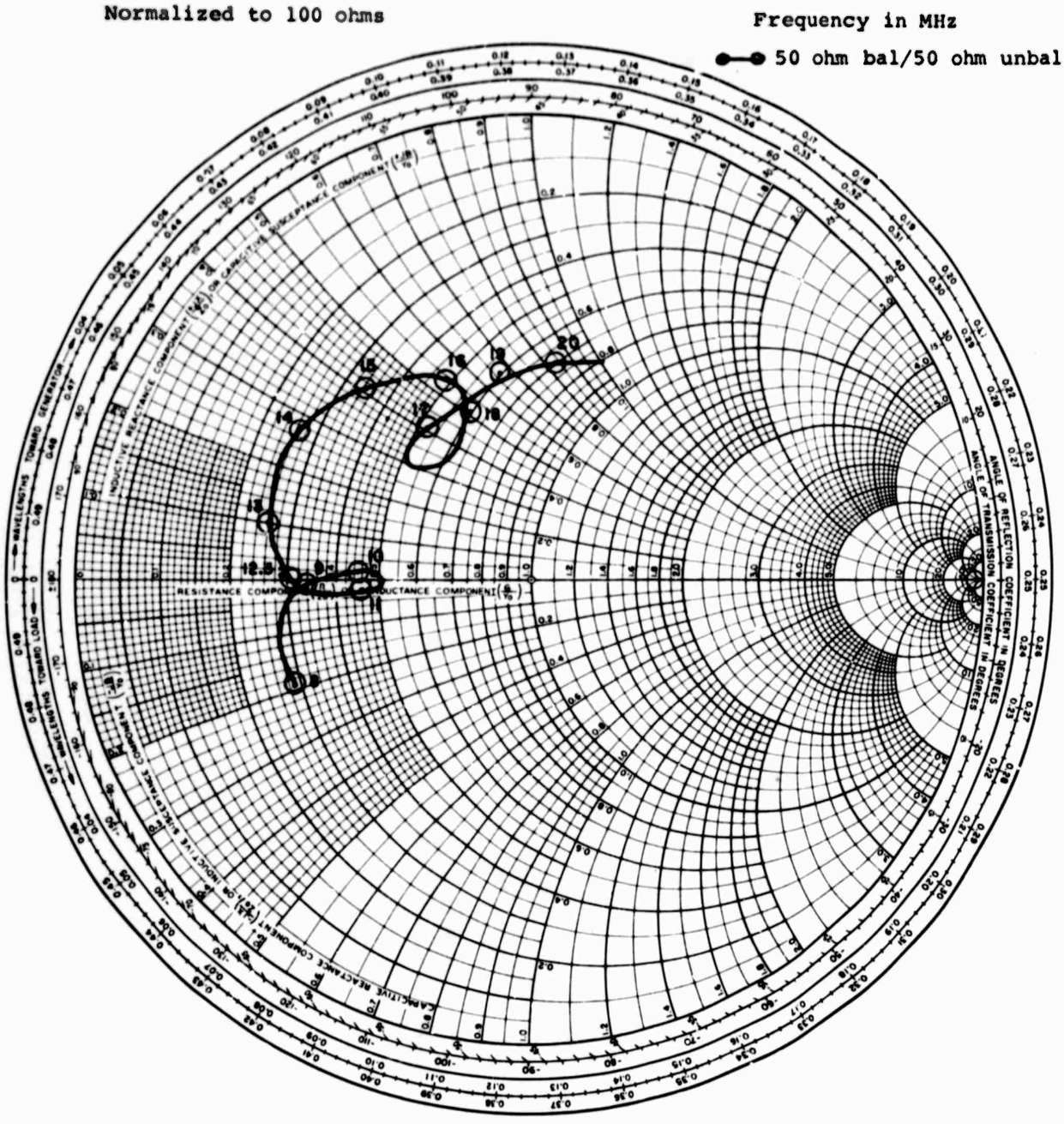

Figure 3-18b. SUBSURFACE DIPOLES 3 AND 4 WITH BALUN

UNBALANCED INPUT IMPEDANCE

higher frequencies than indicated by the impedance measurements. The difference is most probably due to stray capacitance and inductance of lead-in cables and mutual coupling.

The level of mutual coupling between the parallel dipoles was determined by impedance measurements. This was accomplished by breaking the parallel connection of dipoles 3 and 4 and performing measurements of dipole 4 alone. In Figure 3-19, the results of these measurements are compared with the impedance of subsurface dipole 5 which had been installed a sufficient distance from the others to significantly isolate it from any mutual coupling effects. The difference in impedance between dipoles 4 and 5 may be attributed to the mutual coupling between dipoles 3 and 4. From Figure 3-19 it may be observed that significant coupling is present from 1 skin depth spacing (2 MHz) and below, but decreases to a very low level at larger spacings (higher frequencies). Figure 3-20 is a plot of the balanced input impedance of a theoretical subsurface dipole and the measured impedance of dipole 5. The theoretical impedance was based on the dimensions and measured ground constants of the Verona dipoles. The actual length of the dipole (20 meters) includes approximately 4 meters of shielded coaxial cable as lead in and this was used as the length for the theoretical impedance.

In order to make a minimum number of meaningful measurements of the radiation field, allocated frequencies near resonances and slightly above were chosen. This resulted in selecting the test frequencies of 2.232, 4.450, and 6.763 MHz. Matching the antenna impedance to the transmitter at these frequencies was accomplished with a balun and an antenna matching unit. A

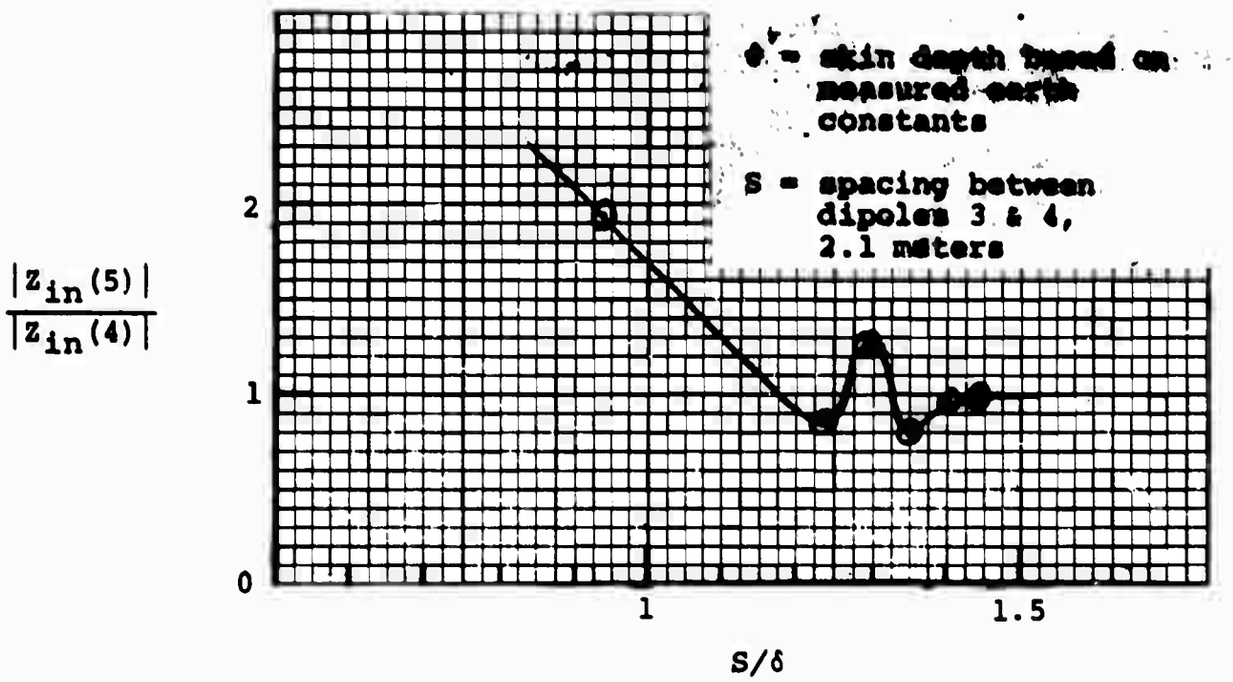

Figure 3-19. Impedance Ratio of Dipoles 4 and 5 Illustrating Mutual Coupling Effects.

50 ohm balanced/50 ohm unbalanced TRANSLAB Model 6010 Ferrite Balun was used in conjunction with a Collins Model 180S-1 Antenna Tuner to match the antenna impedance to 50 ohms for 2.232 and 6.763 MHz. A 200 ohm balanced/50 ohm unbalanced TRANSLAB Model 6011 Balun was used with the same antenna tuner for 4.450 MHz. This combination worked very well and it was possible to keep the VSWR at the ends of the transmission line connecting the transmitter and antenna to such a low value that it was not measurable using forward and reflected power reading from a thruline wattmeter.

Both the transmitter and antenna tuner were adjusted before each test. The transmitter was first tuned while

— X — Theoretical $\frac{\sigma}{\omega\varepsilon} >> 1$ Theoretical RG-19 Cable $\alpha/\beta = 0.075$

L = 20 meters $\beta/k_o = 3.27$

—O— Balanced SSD No. 5 (16 meters buried) $\alpha/k_o = 0.25$

— Δ — Unbalanced SSD No. 5 Verona Earth

Normalized to 100 ohm Frequency (MHz)

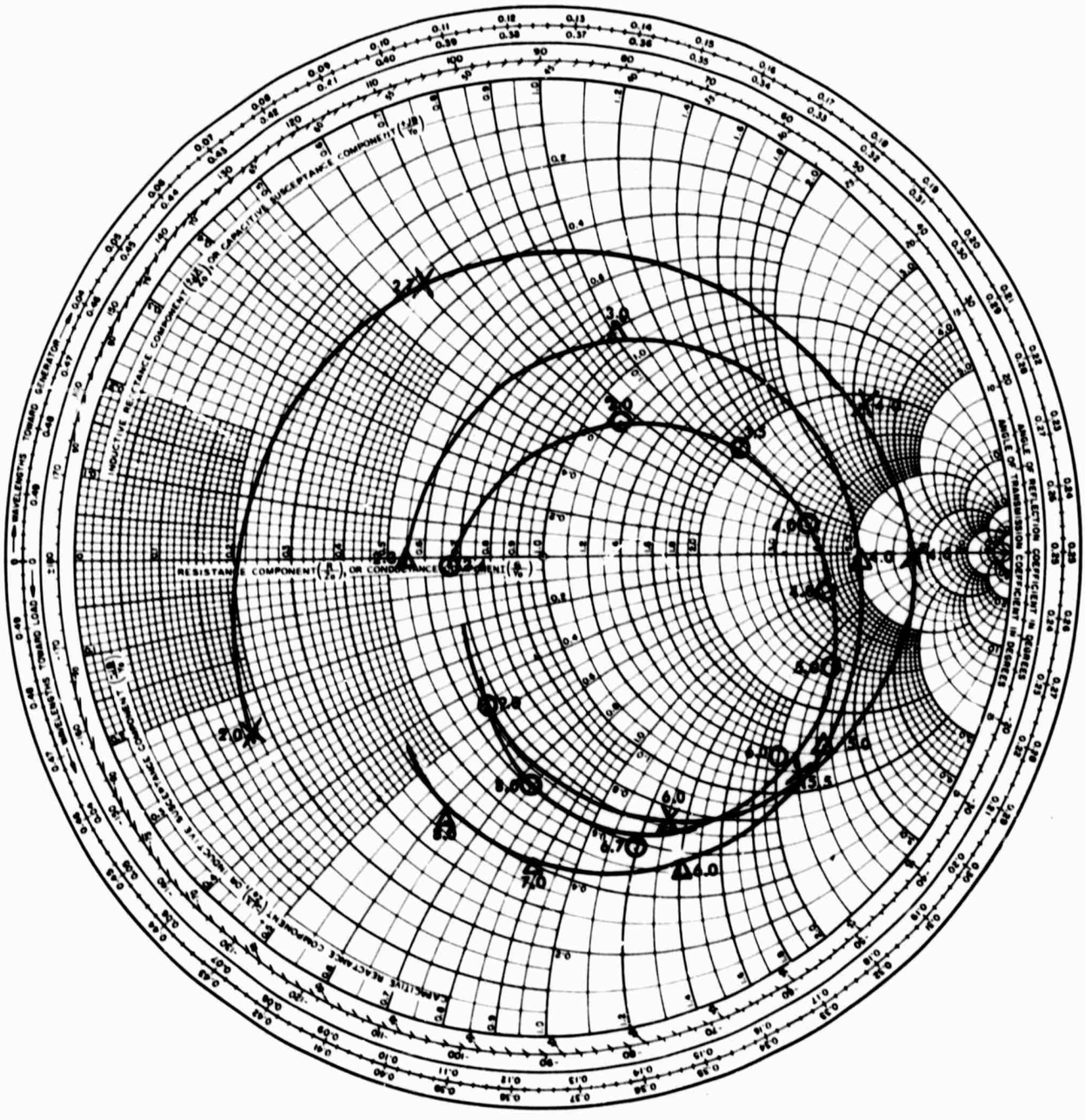

Figure 3-20. THEORETICAL AND MEASURED IMPEDANCE OF A SUBSURFACE DIPOLE

connected to a 50 ohm dummy load to ensure that its output impedance was 50 ohms. It was then connected to the transmission line leading to the antenna and used as a signal source to perform the tuning of the antenna tuner. In this manner, one was assured that both ends of the transmission line were terminated in 50 ohms and that there were no standing waves on the line to cause radiation. Keeping the transmission line radiation to a minimum was critical for these tests since the test antenna has a very low efficiency. Figure 3-21 shows the block diagram of the transmitter configuration.

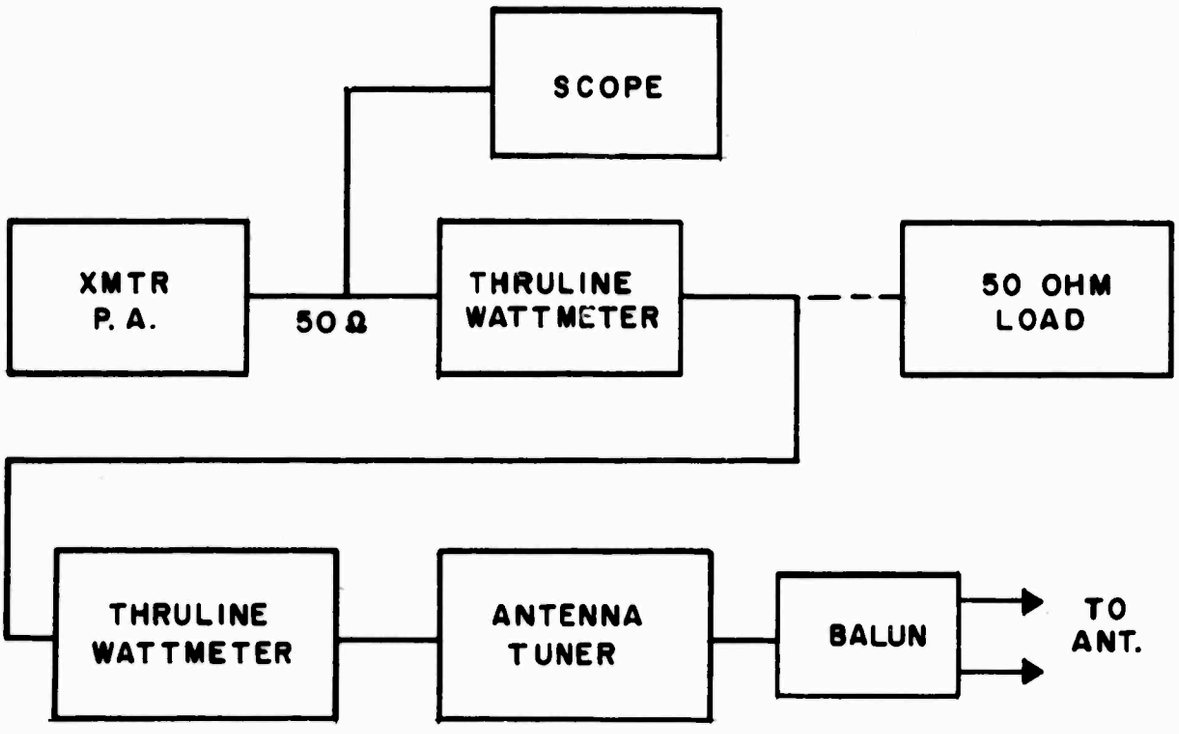

Figure 3-21. Transmitter Configuration.

A photo of the antenna matching unit is shown in Figure 3-22.

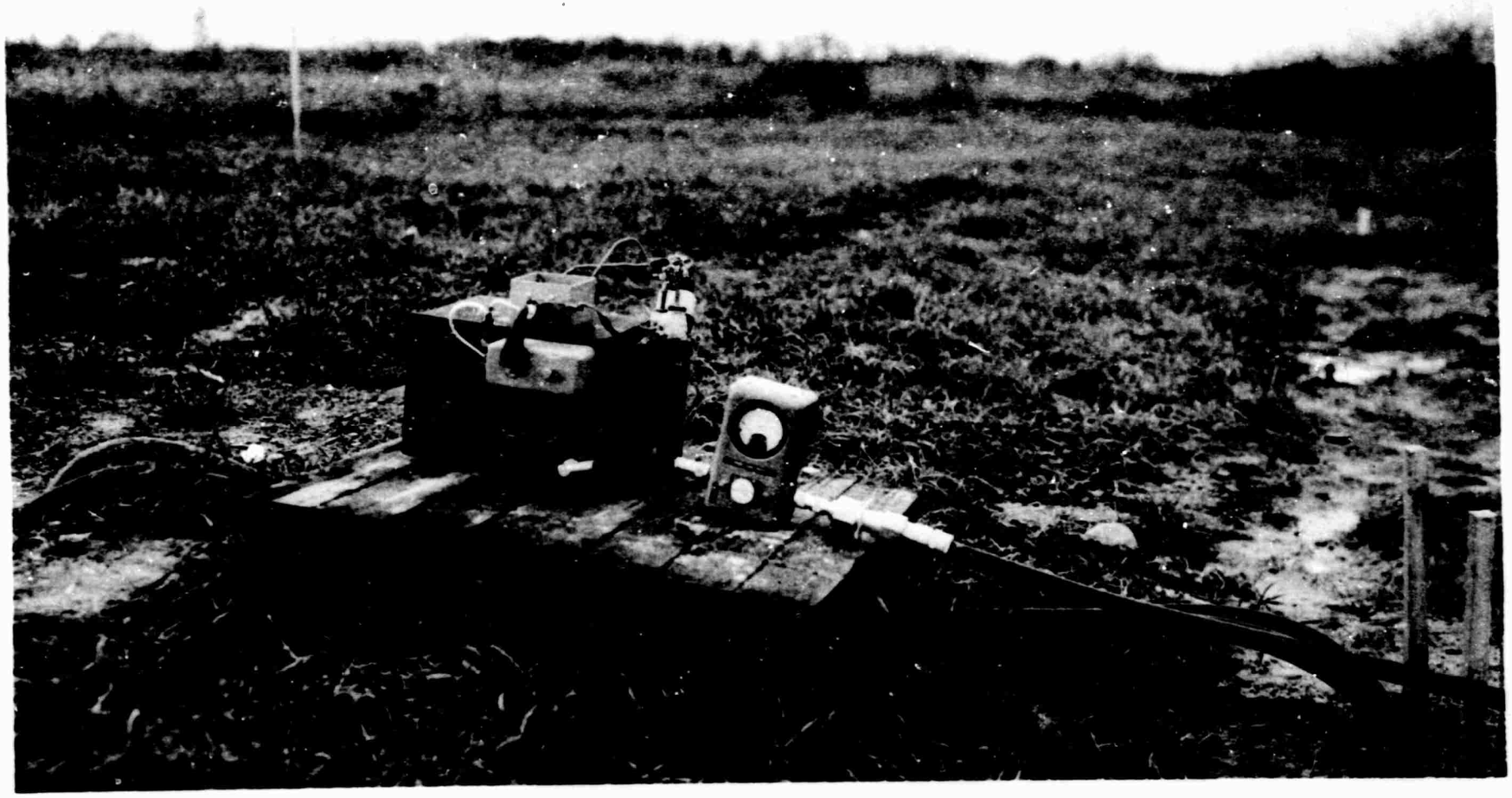

Figure 3-22. Antenna Matching Unit

The baluns were bifilar wound ferrite toroids as shown in Figure 3-23 below.

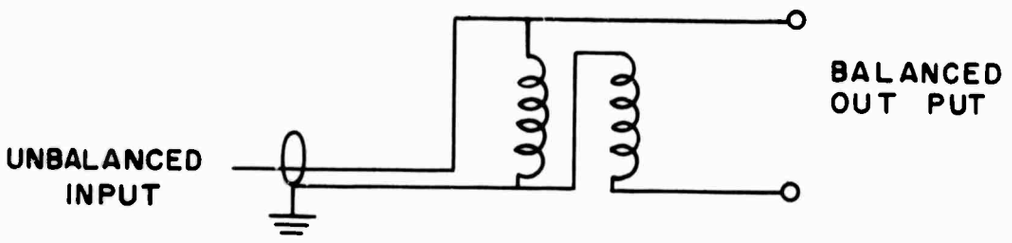

Figure 3-23. Subsurface Dipole Balun.

The antenna tuner consisted of two variable capacitors and one variable inductor. The three components can be configured in two basic schemes to give a wide flexibility in matching different loads. (Figure 3-24 below shows the two basic schemes were C_1 is 2.7 - 770 μμf, L is 0-15 μh and C_o is 4-500 μμf.

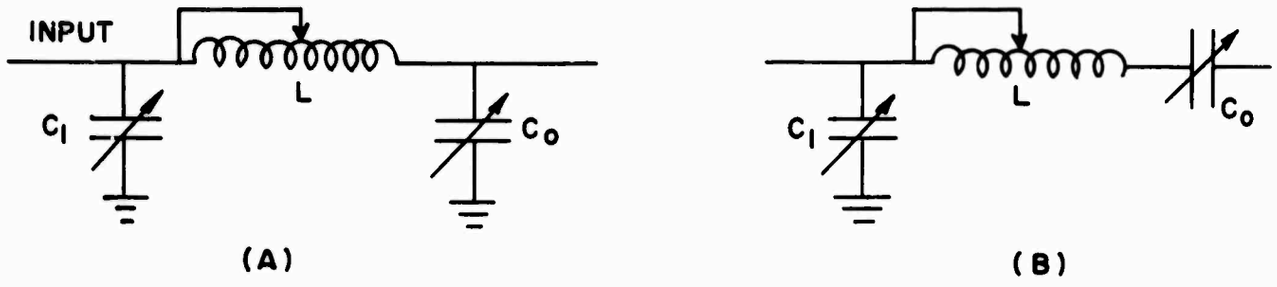

Figure 3-24. Antenna Tuner.

About 75 feet of RG-17 was used between the subsurface antennas and the transmitter. The manufacturer's published data on this cable shows a nominal loss of 0.20 dB/100 feet at 7 MHz. The actual loss of the cable and connectors was measured at each test frequency and the data is shown in

Table 3-1 below. During the tests, thruline wattmeters were attached to each end of the transmission line to continuously monitor the power and to detect any changes in the VSWR on the line due to bad connections or breaks in the cable.

TABLE 3-1. SUBSURFACE DIPOLE TRANSMISSION LINE

Frequency	Loss in dB
2.232	0.15
4.450	0.2
6.763	0.3

To determine the relative gain of the subsurface antenna, one requires knowledge of the antenna matching network losses. This loss was evaluated using the relation:

$$L_c = -10 \log \frac{P_i}{P_o} \qquad (3\text{-}1)$$

where P_i is the power into the network and P_o is the power out of the network. Dummy antennas were made for each of the three major operating frequencies and connected to the balun output terminals. Using an HP 4815A RF Vector Impedance Meter as an indicator, the antenna tuner was then adjusted to obtain $50 + 0_j$ at the input. An HP 606A Signal Generator was attached to the tuner input and a reference signal applied to the network. The voltage applied across the tuner input and the resistive part of the dummy antennas were measured and P_i and

P_o computed. Figure 3-25 and Table 3-2 show the test setup and the data obtained. One can see from the data that losses in the matching network are small enough to neglect.

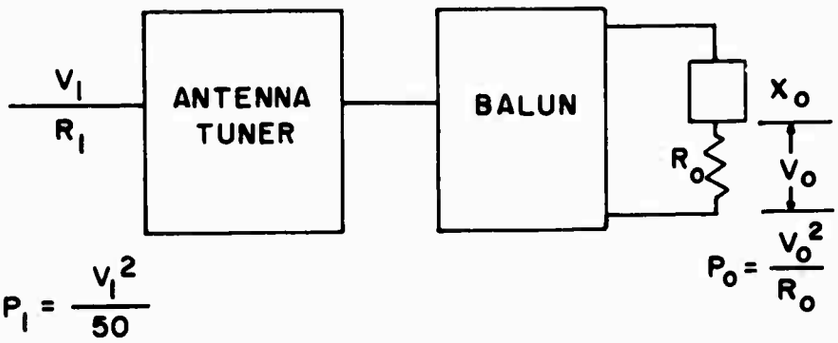

Figure 3-25. Subsurface Dipole Matching Network Losses.

TABLE 3-2. SUBSURFACE ANTENNA MATCHING NETWORK LOSS.

Freq MHz	Z_i	V_i Volts	P_i MW	Actual Ant. $R_o + j X_o$	Dummy Ant. $R_o + j X_o$	V_{R_o}	P_o MW	Loss db
2.232	$50 \angle 0°$	1.0	20	25.5 - 7j	31.5 + 0j	0.765	18.5	0.3
4.450	$50 \angle 0°$	1.0	20	230 + 43j	234 + 0j	2.07	18.4	0.3
6.763	$50 \angle 0°$	1.0	20	45.8 - 57.5j	48.4 - 55j	0.960	19.1	0.2

3. REFERENCE MONOPOLE

The impedance of the reference monopole (whip) antenna is shown in Figure 3-26. From this data, it can be seen that the primary test frequency (6.763 MHz) was very close to the $\lambda_o/4$ resonant frequency (7.22 MHz) of the reference monopole.

The efficiency of the reference monopole below a perfect loss-less monopole can be calculated from the measured impedance at resonance (97 ohm). The input resistance of a 1/4 wavelength monopole perpendicular to an infinite perfectly conducting ground plane is 36.5 ohms (Ref. 25, p. 262). The efficiency of the test monopole is then given by

$$\text{Eff} = -10 \log \frac{97}{36.5} = -4.25 \text{ db}$$

The TRC-69 radio equipment which was used to feed the whip has an auto-tune antenna coupler which matches the antenna impedance to the transmitter's 50 ohm output. Coupler losses were measured using a procedure similar to that used for the subsurface dipole matching unit. After the system was tuned in the usual manner, the coupler was disconnected from the antenna and power amplifier. A dummy antenna was then substituted to make loss measurements. It was not possible to get exactly 50 ohm at the input to the coupler using this technique so the actual input impedance was recorded and P_i computed from Eq. 3-1. P_o was obtained

Normalized to 100 ohms

Frequency in MHz

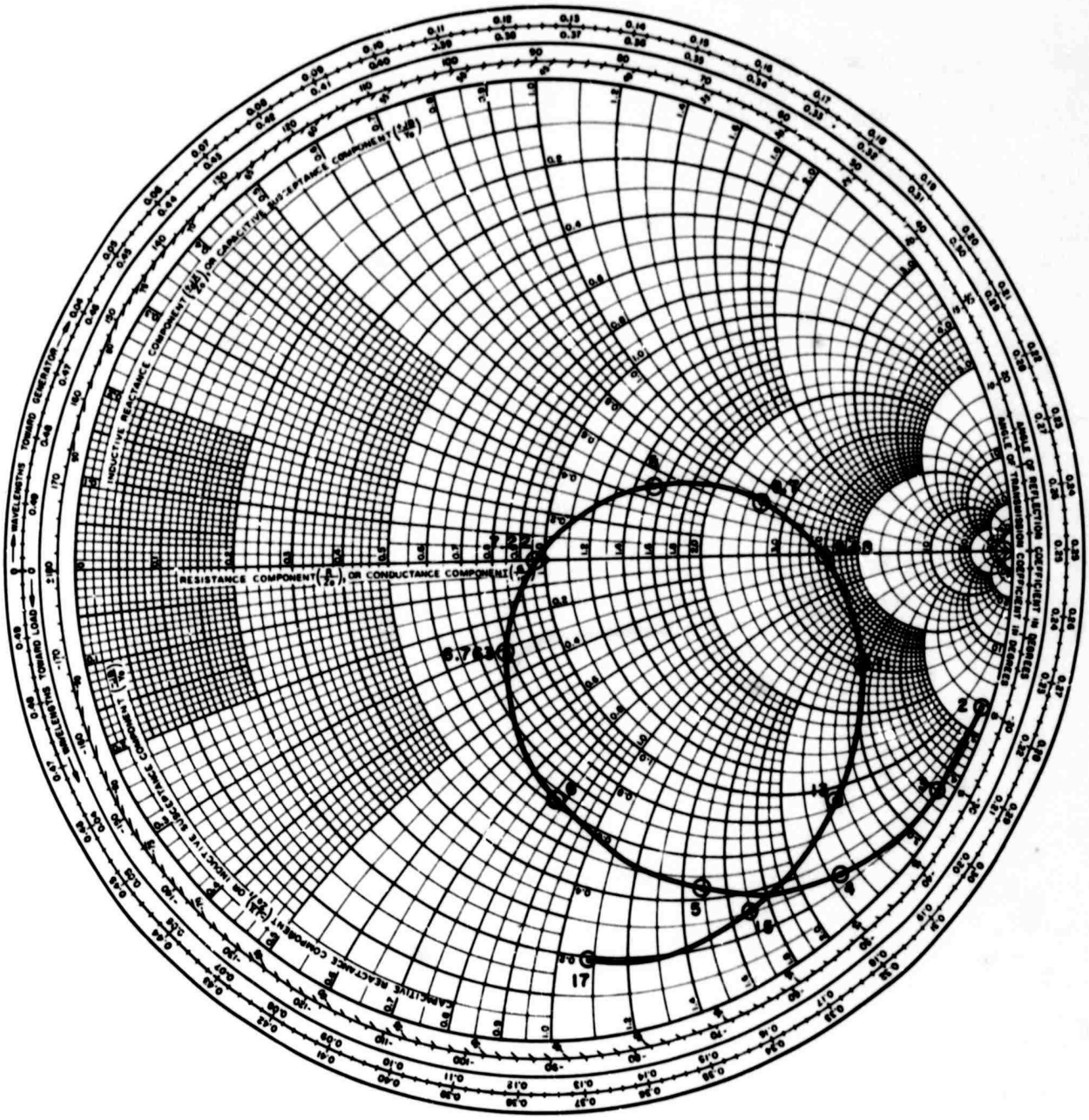

Figure 3-26. REFERENCE 30' MONOPOLE IMPEDANCE

the same as before. Figure 3-27 and Table 3-3 show the test configuration and test results. It can be seen that coupler losses were significant only at the 2.323 MHz operating frequency.

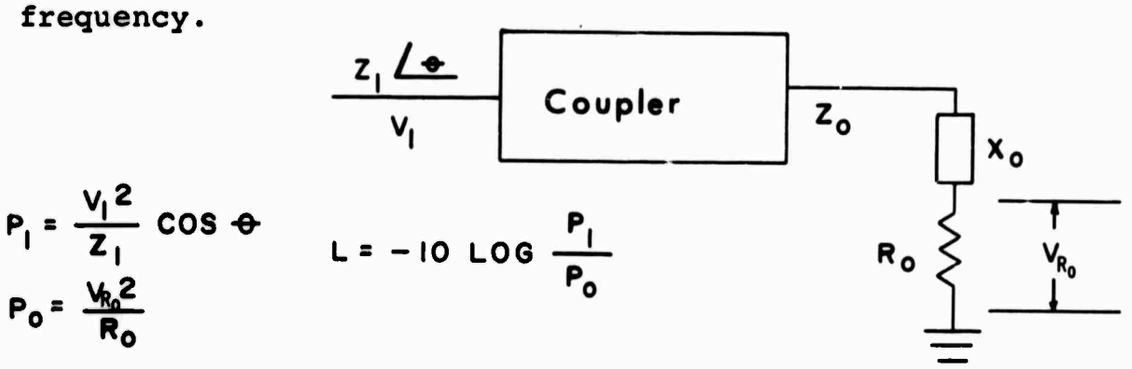

Figure 3-27. Monopole Coupler Losses.

4. REFERENCE DIPOLE

The reference half wave dipole was made from number 14 copper wire and was fed through a 1:1 balun. At each frequency, the elements were trimmed in length to come as close to resonance as possible. It was found that very little trimming was necessary after they were cut to (0.95) of a free space half wave length. The 6.763 and 4.450 MHz dipoles were raised to a height of one quarter wavelength above ground. The 2.232 MHz dipole was raised only one-eighth wavelength above ground because of pole height limitations.

TABLE 3-3

MONOPOLE COUPLER LOSS DATA

Freq (MHz)	Z_i	pf	V_i	P_i (w)	Z_o	R_o	X_o	V_{R_o}	P_o (w)	Loss dB
2.232	$54\angle -5°$	.9962	2.0	.0736	$495\angle -89°$	$16\angle +2°$	-490	0.92	.0527	-1.45
4.450	$50\angle -1°$	.9999	3.0	.080	$165\angle -76°$	$39\angle 0°$	-160	1.70	.074	-0.33
6.763	$56\angle 8°$	1	2.35	.098	$114\angle -6°$	$113\angle 0°$	-12	3.30	.097	<-.1

The impedances of the reference dipoles are shown in Table 3-4 below:

TABLE 3-4
REFERENCE DIPOLE CHARACTERISTICS

Freq (MHz)	Length	Height	Impedance
6.763	$\lambda_o/2$	$\lambda_o/4$	72 - 8j
4.450	$\lambda_o/2$	$\lambda_o/4$	75 - 9j
2.232	$\lambda_o/2$	$\lambda_o/4$	52 - 8j

The antenna coupler for the reference dipole was identical to the one used for the reference monopole. Based on the monopole coupler loss data and the fact that the reference dipole impedances were reasonably close to the transmitter 50 ohm output, it was assumed that the dipole coupler losses were negligible for all practical purposes.

The transmission line loss for the reference dipole was measured to be 1.7, 1.3, 1.1 dB for 6.763, 4.45, and 2.232 MHz, respectively.

D. AIRBORNE MEASUREMENTS OF RADIATED FIELDS

1. DESCRIPTION OF RECEIVING INSTRUMENTATION

Airborne measurements were conducted to establish space wave radiation characteristics of the subsurface dipole and verify results of the surface measurements. A modified KC-135 aircraft, shown in Figure 3-28, equipped with the necessary receiving and recording equipment served as the airborne measurement facility. Figure 3-29 contains a block diagram of the equipment installation in the aircraft. A balanced loop located on the end of the refueling boom and a 90-foot unbalanced long-wire fastened on top of the aircraft between the vertical stabilizer and the fuselage were utilized as receiving antennas. The balanced loop was capable of being oriented in either the vertical or horizontal plane.

The airborne receiving system was completely calibrated at the beginning of the test program and periodic checks were made to assure that system performance did not degrade during the test period. The ground transmitting facility was identical to that used during the surface measurements.

To achieve the goals of the test program a series of flights consisting of radials and orbits were conducted. The altitude of the aircraft was maintained at 20,000 feet for the duration of the test period and ground navigational aids were utilized by the navigator to ensure position and heading accuracy. A radar missile tracker and beacon transmitter were used to guide the aircraft.

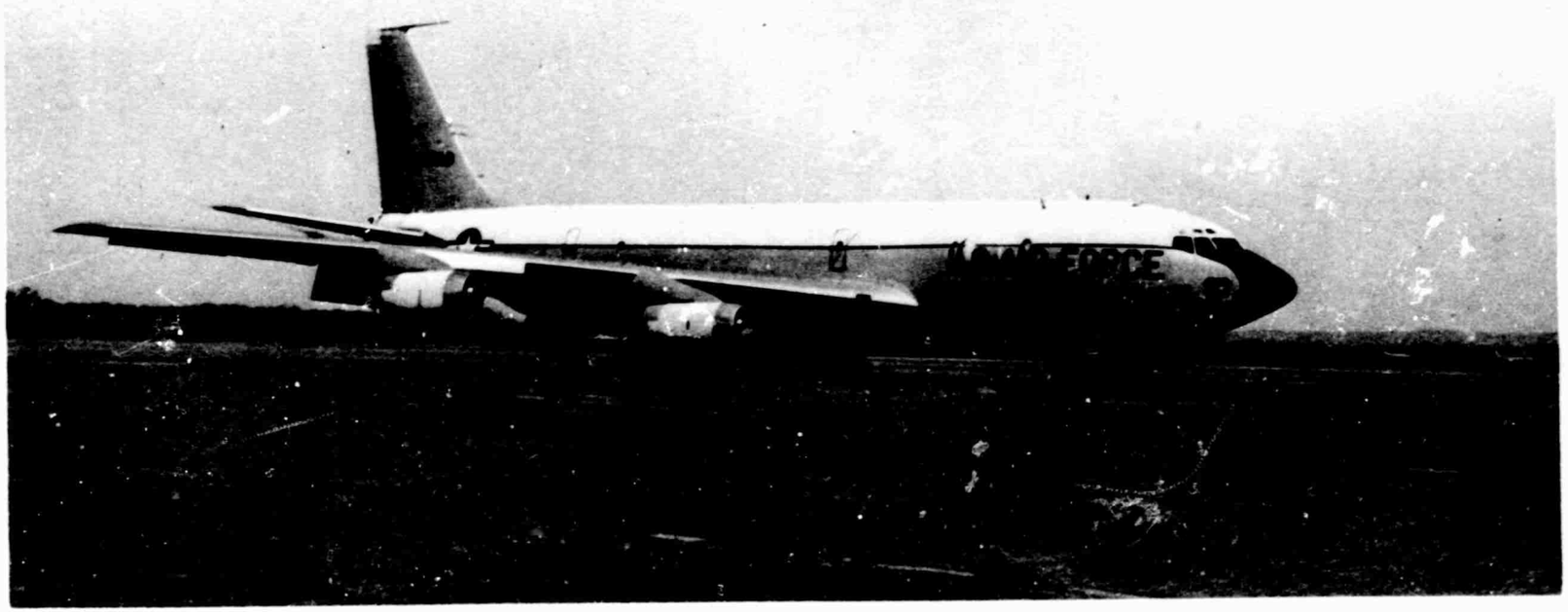

Figure 3-28 Photo of Flight Test Aircraft

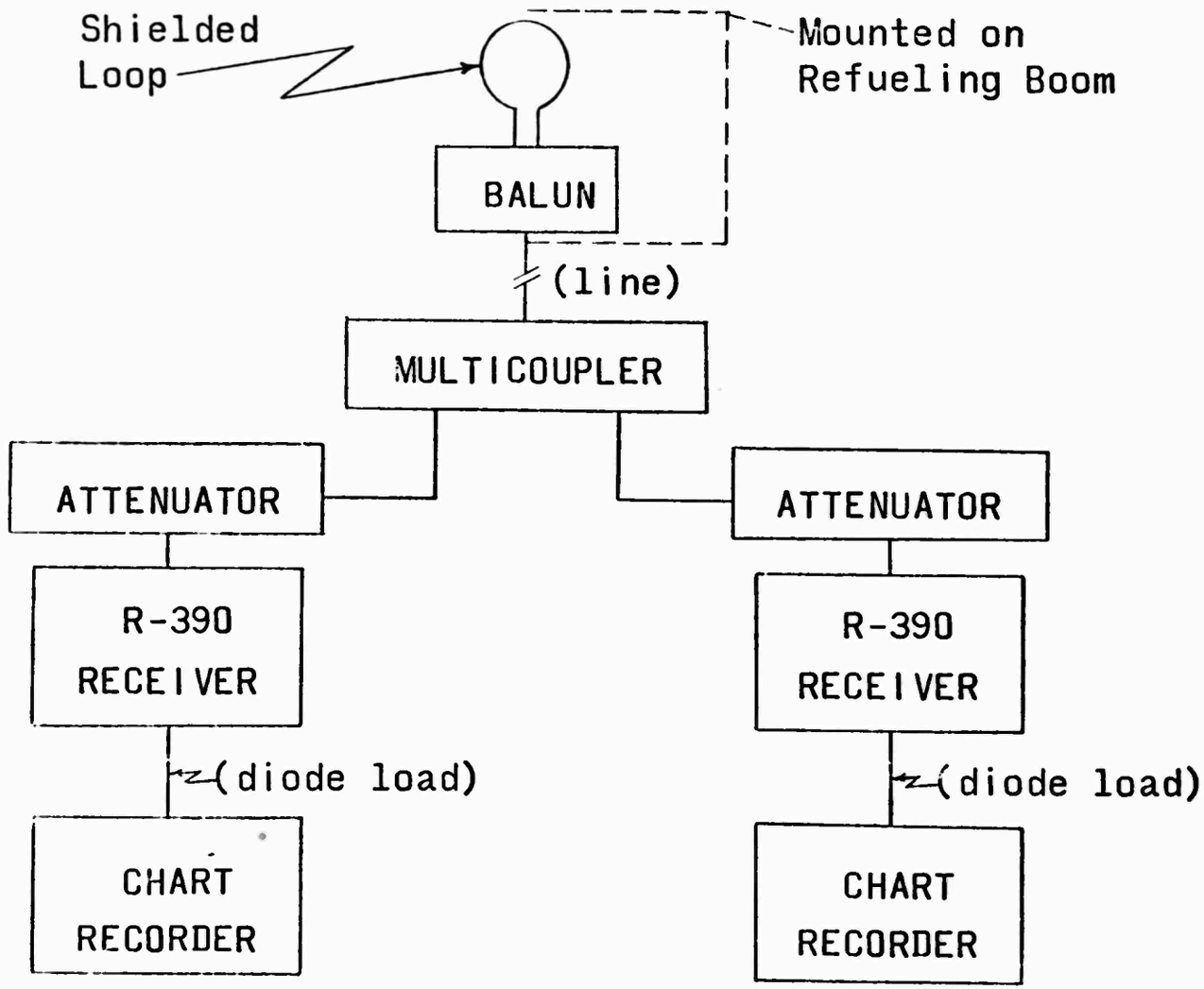

Figure 3-29. AIRCRAFT TEST EQUIPMENT NKC-135

2. SPACE WAVE GAIN

The relative space wave gain of the subsurface dipoles was measured by comparing their received field strength with that of the reference 35-foot monopole and the reference half-wave horizontal dipole located a quarter-wave length above ground. These measurements were made simultaneously by using frequencies approximately 5 kHz apart.

Figures 3-30 through 3-32 portray, in three dimensions, the theoretical patterns of all three antennas. Figure 3-33 shows the specific orientation of the subsurface and reference dipoles along with the polarization of their electric field vectors as a function of angle. The radials were flown both parallel and perpendicular to the subsurface dipole axis.

In measuring the various components of each antenna care had to be taken to orient the balanced loop on the aircraft in the proper position with respect to the received electric or magnetic field vector. This is complicated by the fact that balanced receiving loop, as shown in Figure 3-34, receives in both a magnetic dipole and electric dipole mode (Ref. 36, page 481).

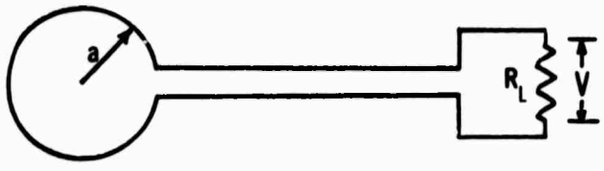

Figure 3-34. Balanced Receiving Loop.

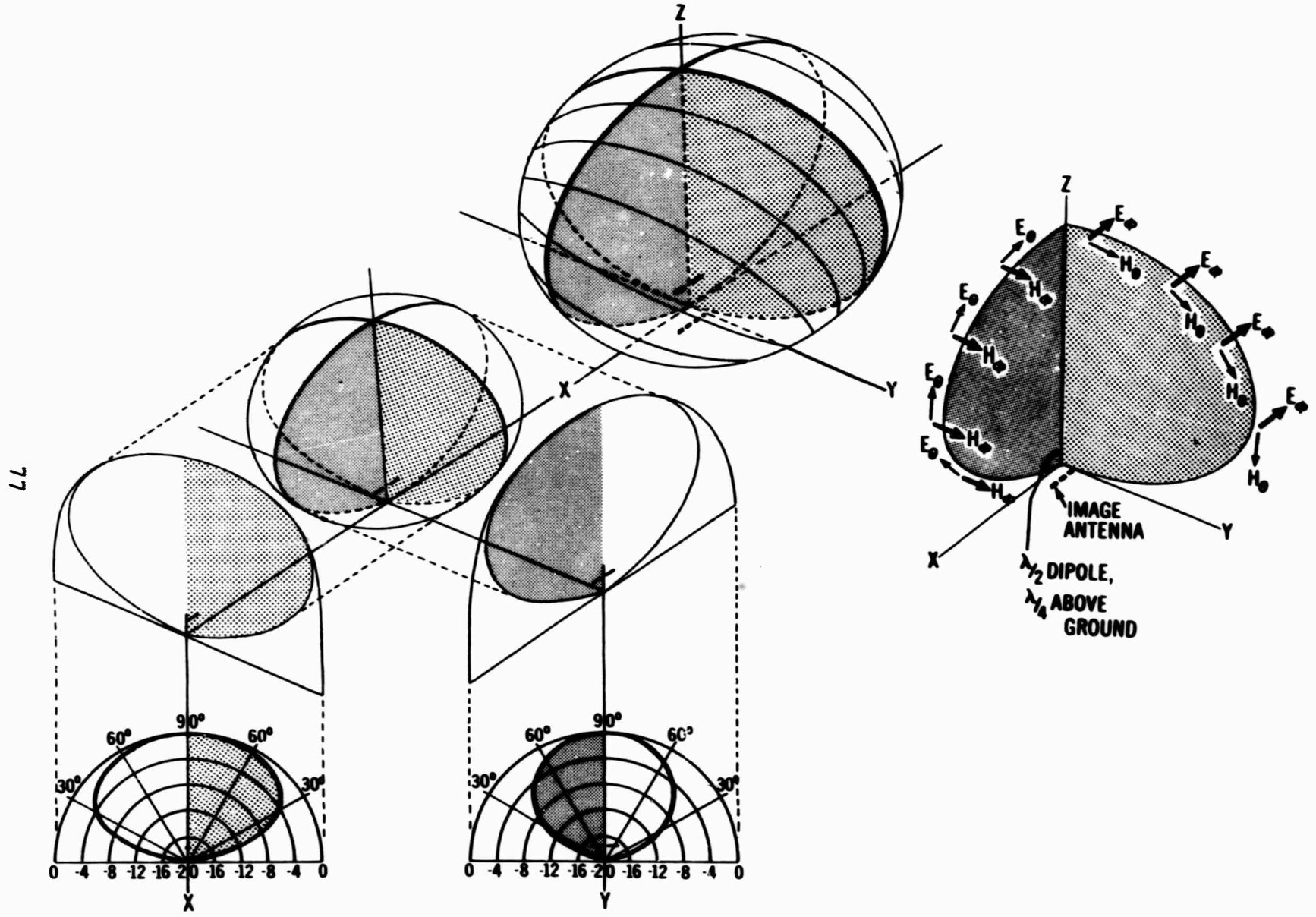

Figure 3-30. Horizontal Dipole Antenna

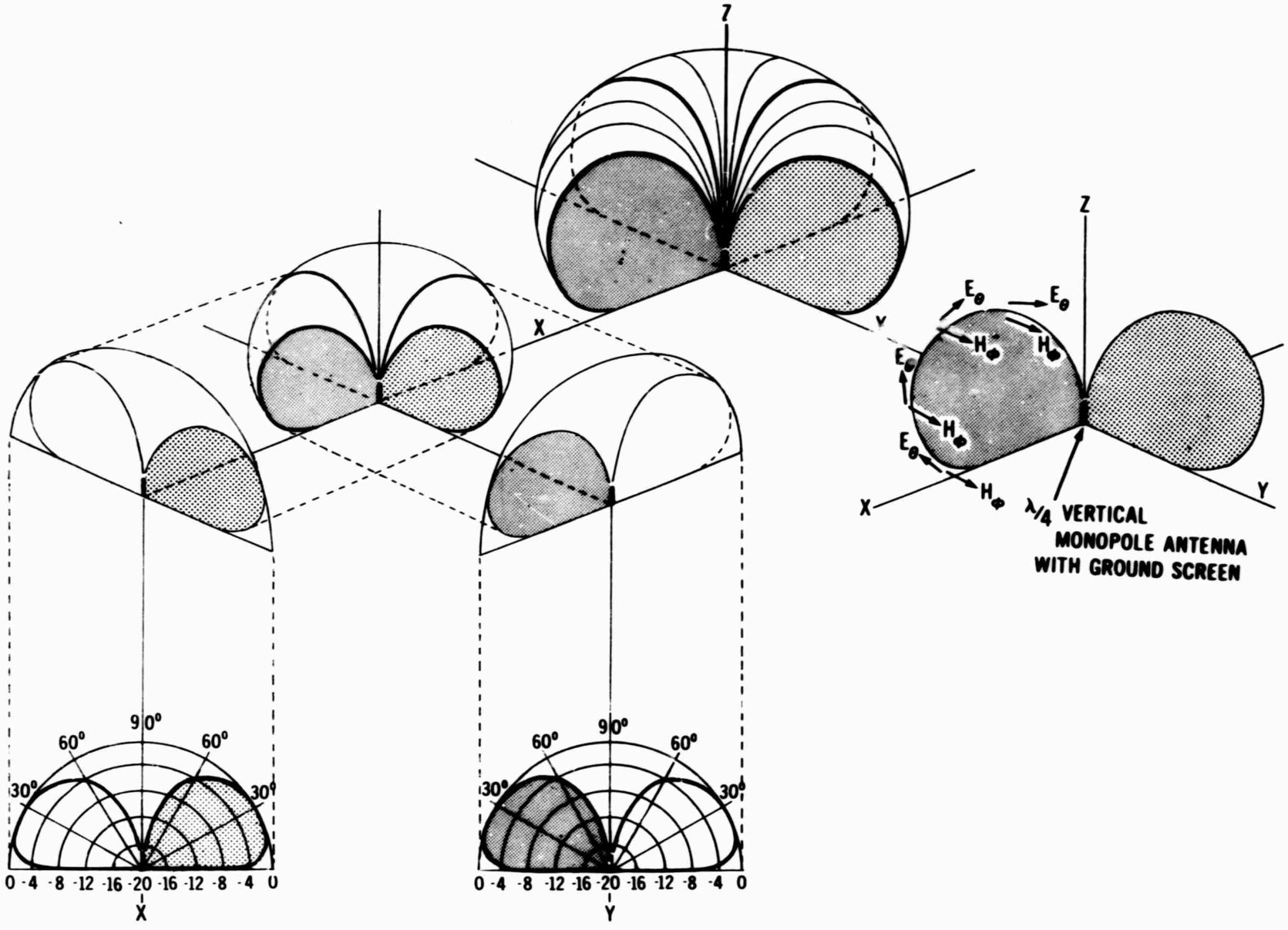

Figure 3-31. Vertical Monopole Antenna

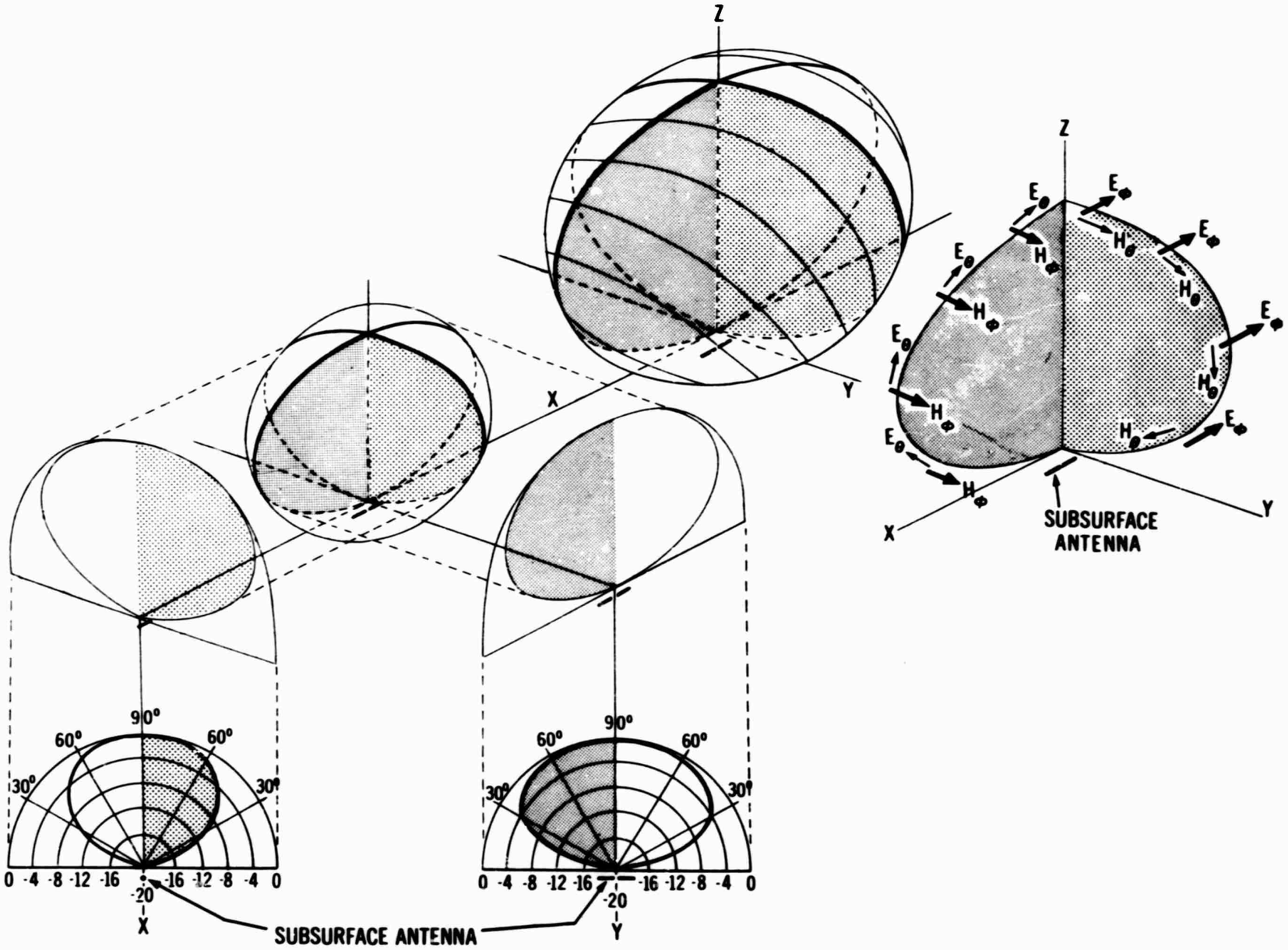

Figure 3-32. Subsurface Dipole Antenna

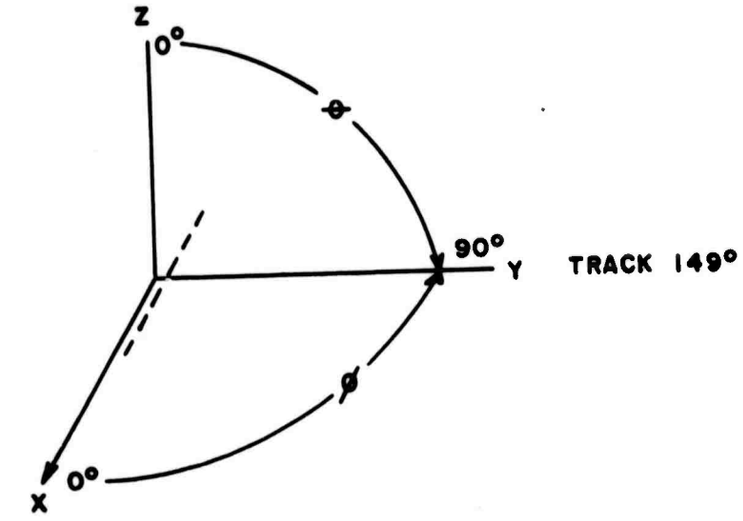

REFERENCE DIPOLE

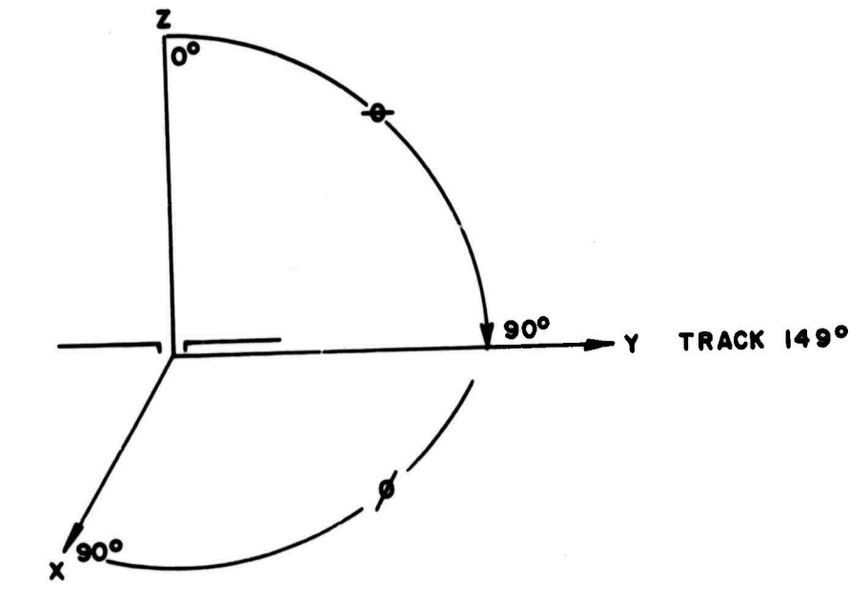

Figure 3-33. Subsurface Dipole/Reference Dipole

In the normal magnetic dipole mode, the voltage V is maximum when the normal to the loop is parallel to the local $\vec{H}$ vector. If, however, the $\vec{E}$ vector is in the plane of the loop and also perpendicular to the pair of wires, an extra voltage appears on R which comes from the electric dipole excitation and adds vectorally to the magnetic dipole mode.

Directly over the antennas, either reference or subsurface, the E_θ (or H_ϕ) component can be measured exclusively in the magnetic dipole mode by orienting the receiving loop in the vertical plane and flying along the dipole axis. At low angles, however, the electric dipole mode adds to the received voltage. The E_ϕ (or H_θ) component can be measured directly overhead exclusively in the electric dipole mode by orienting the receiving loop in the horizontal plane and flying perpendicular to the dipole axis. Again, though, at low angles the magnetic dipole mode adds to the received voltage.

Figures 3-35 and 3-36 are plots of the theoretical and measured vertical profiles of the reference and subsurface dipoles. The theoretical curve for the reference dipole E_ϕ component is taken from Berry and Chrisman (Ref. 35) for the dipole over "good" ground. The E_θ component for the reference dipole is not usually given except for the case of the dipole over perfect ground. The dashed line on Figure 3-35 is a plot of E_θ for the perfect ground case with a 3 db

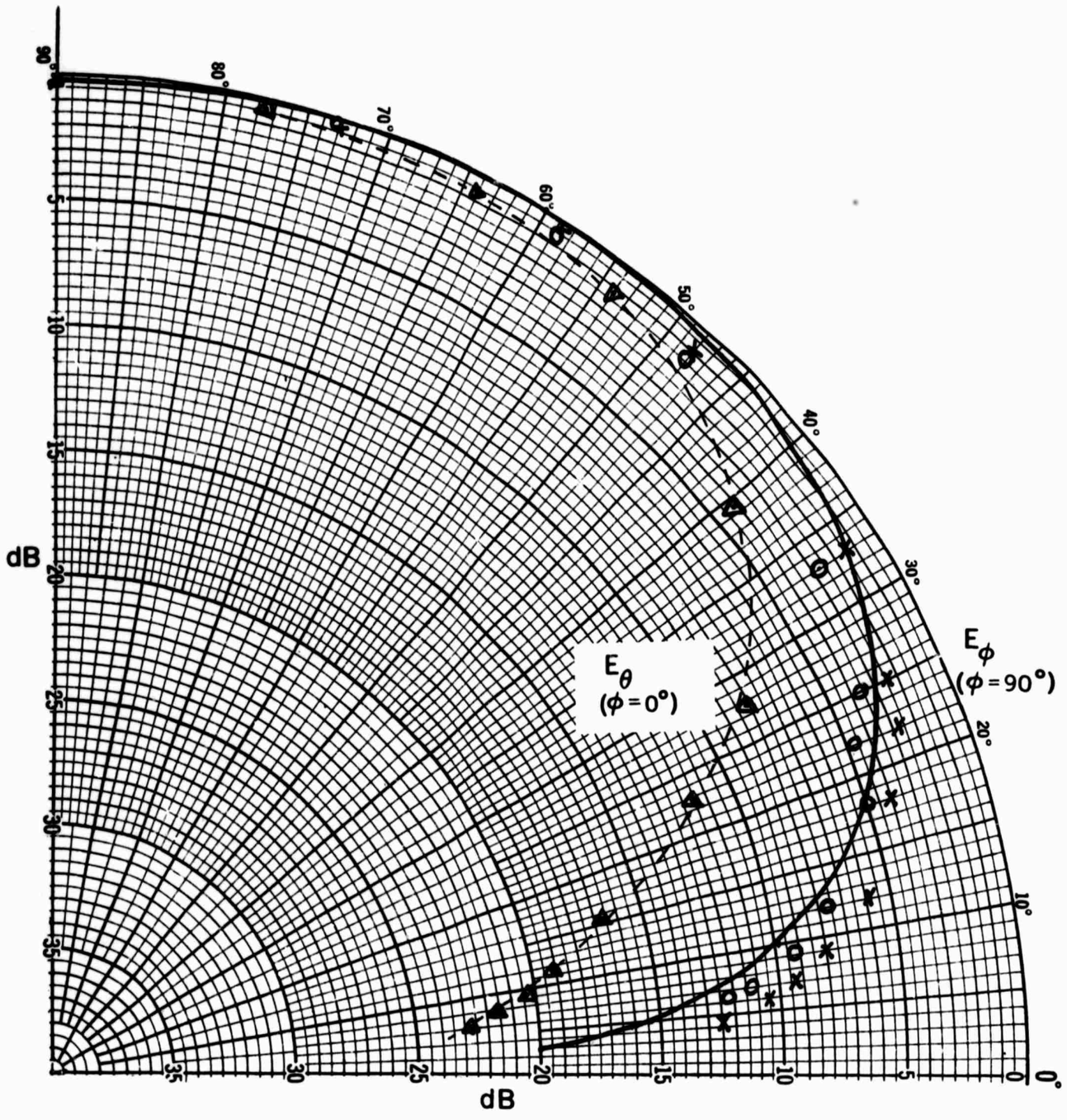

— Theoretical Curve $E_\phi(\phi=90°)$ Berry & Chrisman(1966)
Good Ground $\sigma = 0.01$ mhos/m
$\varepsilon = 10\varepsilon_o$ Fd/m

Measured Data-6763 kHz, Verona Ref. Dipole
o & x --E_ϕ ($\phi = 90°$)
△---△ --E_θ ($\phi = 0°$)

Figure 3-35. Theoretical and Measured Vertical Profiles for Halfwave Dipoles ($\lambda_0/4$ Above Ground)

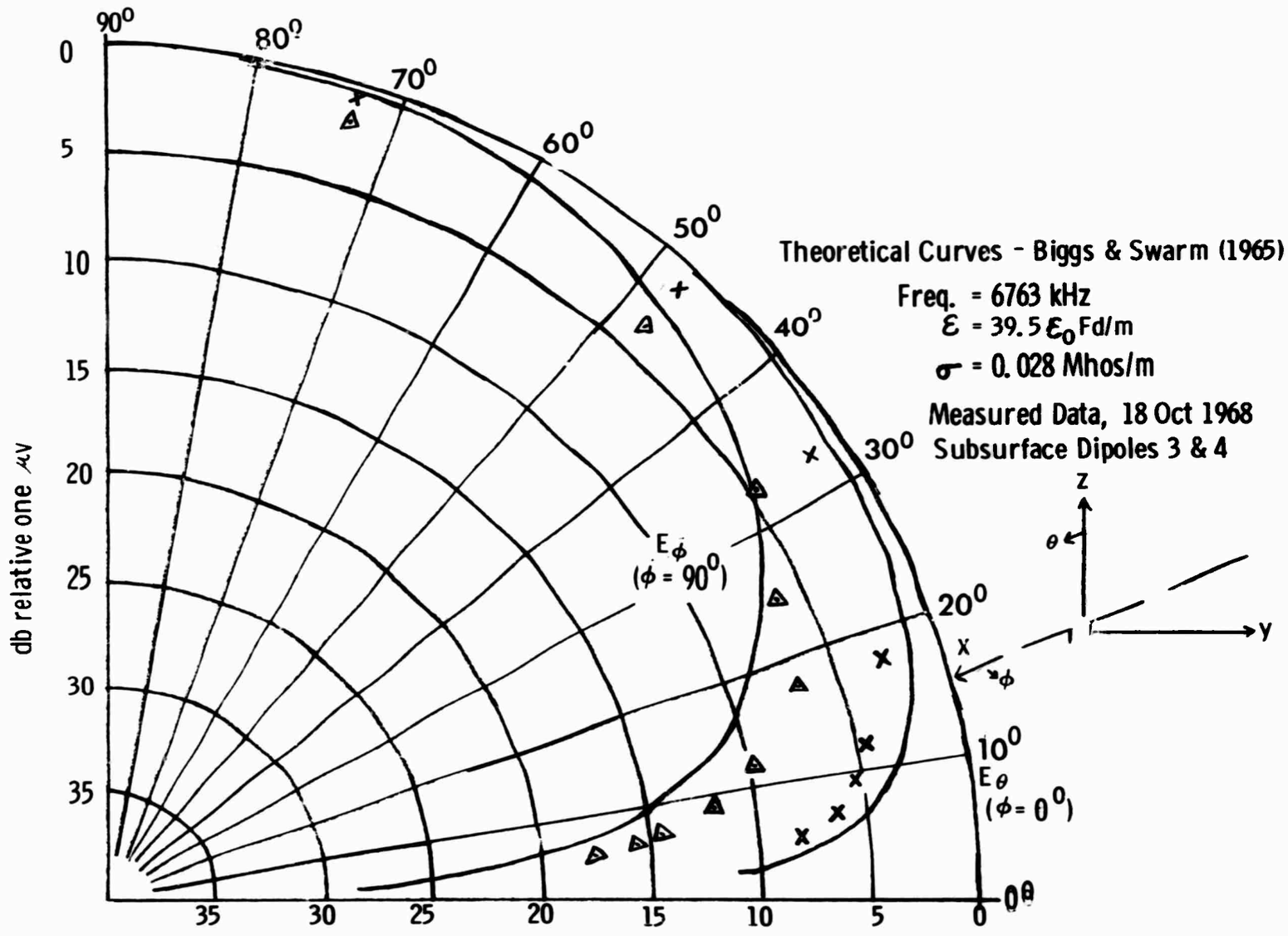

Figure 3-36. Subsurface HF Dipoles Theroretical and Measured Vertical Profiles

decrease directly overhead in order to coincide with the E_ϕ component which is over "good" ground.

The theoretical curves for the subsurface dipole are plots of Equations (2-7) and (2-8) with the measured ground constants of the transmitter site at a frequency of 6.763 MHz. At the low angles (approximately 20° and below) the effect of the other mode of the receiving antenna becomes apparent, however, it is not greater than 3 db. This other mode, of course, does not affect the gain measurements directly overhead.

The subsurface and reference dipoles were oriented orthogonal to each other in order to have similar pattern shapes in the same direction. While it did accomplish that, it complicated the airborne measurements because now the polarizations directly overhead were orthogonal to each other. The relative gain between the two was measured by making closely successive runs over each antenna several times to ensure that equipment calibration and aircraft position did not drift.

Figure 3-37 is the measured relative space wave radiation from all the antennas. This was taken on a heading of 239° which is the direction for maximum radiation from both the reference and horizontal dipoles. Directly overhead, subsurface dipole pair 3 and 4 is approximately -23 db below the reference dipole and subsurface dipole pair 1 and 2 approximately -25.5 db below. For all plots, transmitted

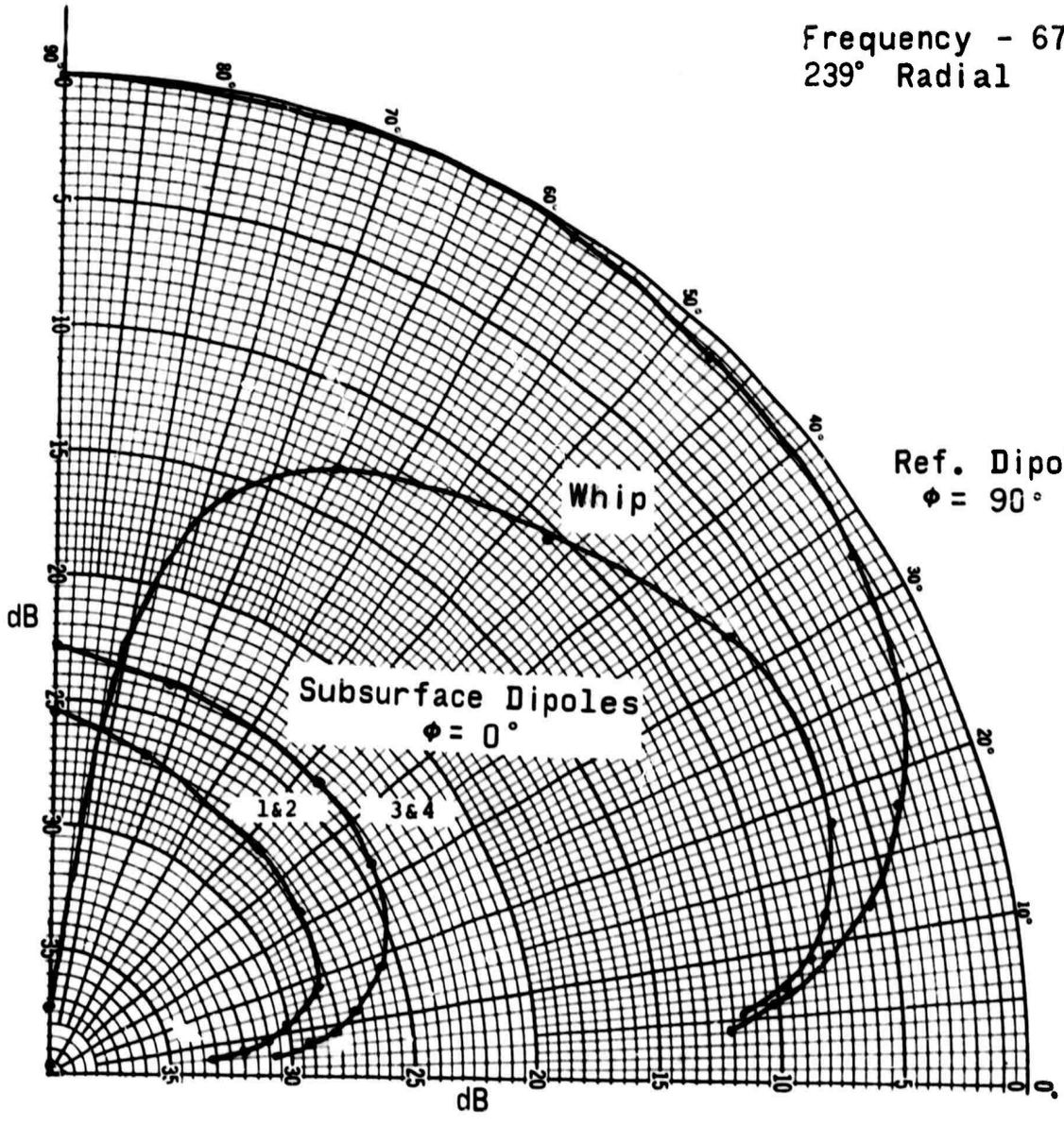

Figure 3-37. Measured Vertical Profiles

power is normalized to the same value. The difference between dipole pairs 1 and 2 and 3 and 4 is somewhat surprising since the field from dipole 3 and 4, being down 3 feet, has approximately 3.8 db more attenuation to the surface than dipoles 1 and 2. The difference is probably due to the smaller dimensions of the RG8 cable for dipoles 1 and 2 compared to the RG19 for dipoles 3 and 4. This affects both losses and current distribution.

Azimuthal pattern measurements at low angles were also made. Figure 3-38 shows measured data from both the reference dipole and subsurface dipole pair three and four as received by the horizontal loop. The input power is normalized and relative field strengths are plotted. The horizontal loop senses the E_ϕ (H_θ) field which is maximum broadside to the dipoles. The slight skewing of the subsurface dipole is attributed to coupling from the stronger E_θ field. Figure 3-39 shows measured azimuthal data for subsurface dipoles 1 and 2 with the long-wire aboard the aircraft used as a receiving antenna. The longwire antenna is sensitive to both the E_θ and E_ϕ polarization and indicates as expected that the E_θ end fire pattern is maximum for the subsurface dipoles.

3. SKYWAVE FIELD STRENGTH VS DISTANCE

In addition to the orbits and short-range radials, extended range radials were made to investigate propagation modes. The results are shown in Figure 3-40. Sky wave, supported by F-layer propagation, becomes the dominant signal at approximately one hundred miles. Calculations based on

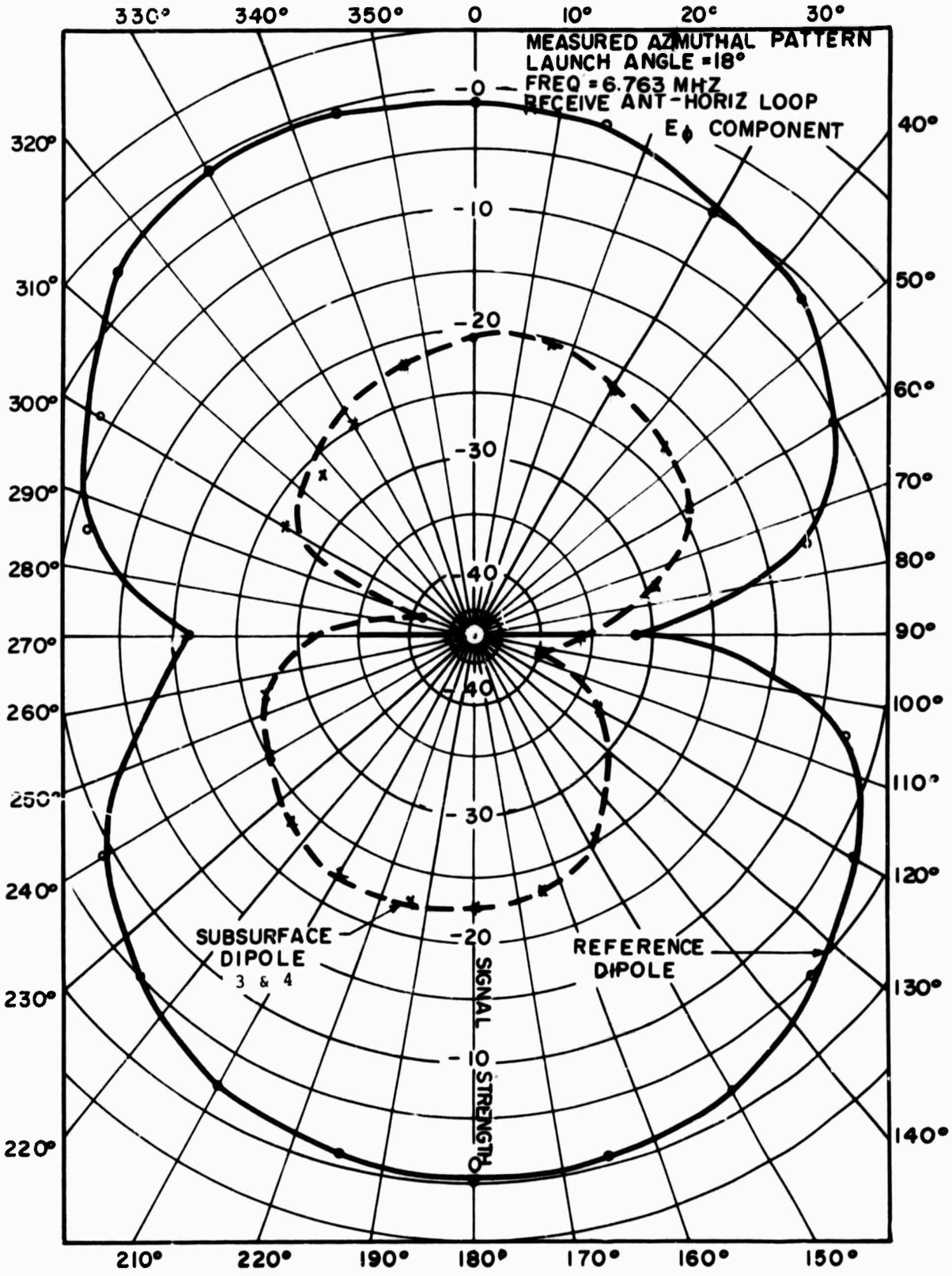

Figure 3-38. Measured Azimuthal Patterns of the Reference and Subsurface Dipoles

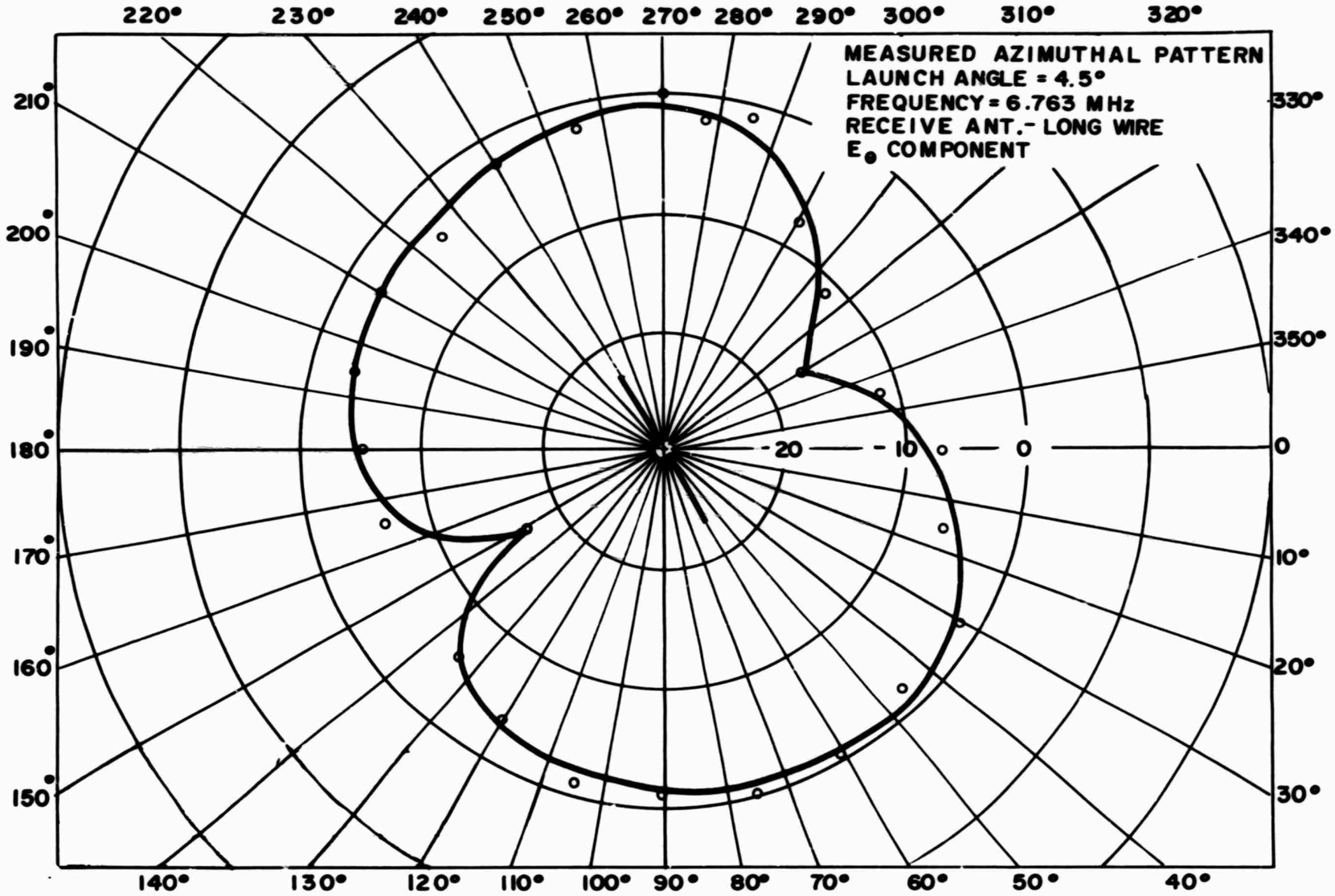

Figure 3-39. Measured Azimuthal Patterns of Subsurface Dipoles 1 and 2

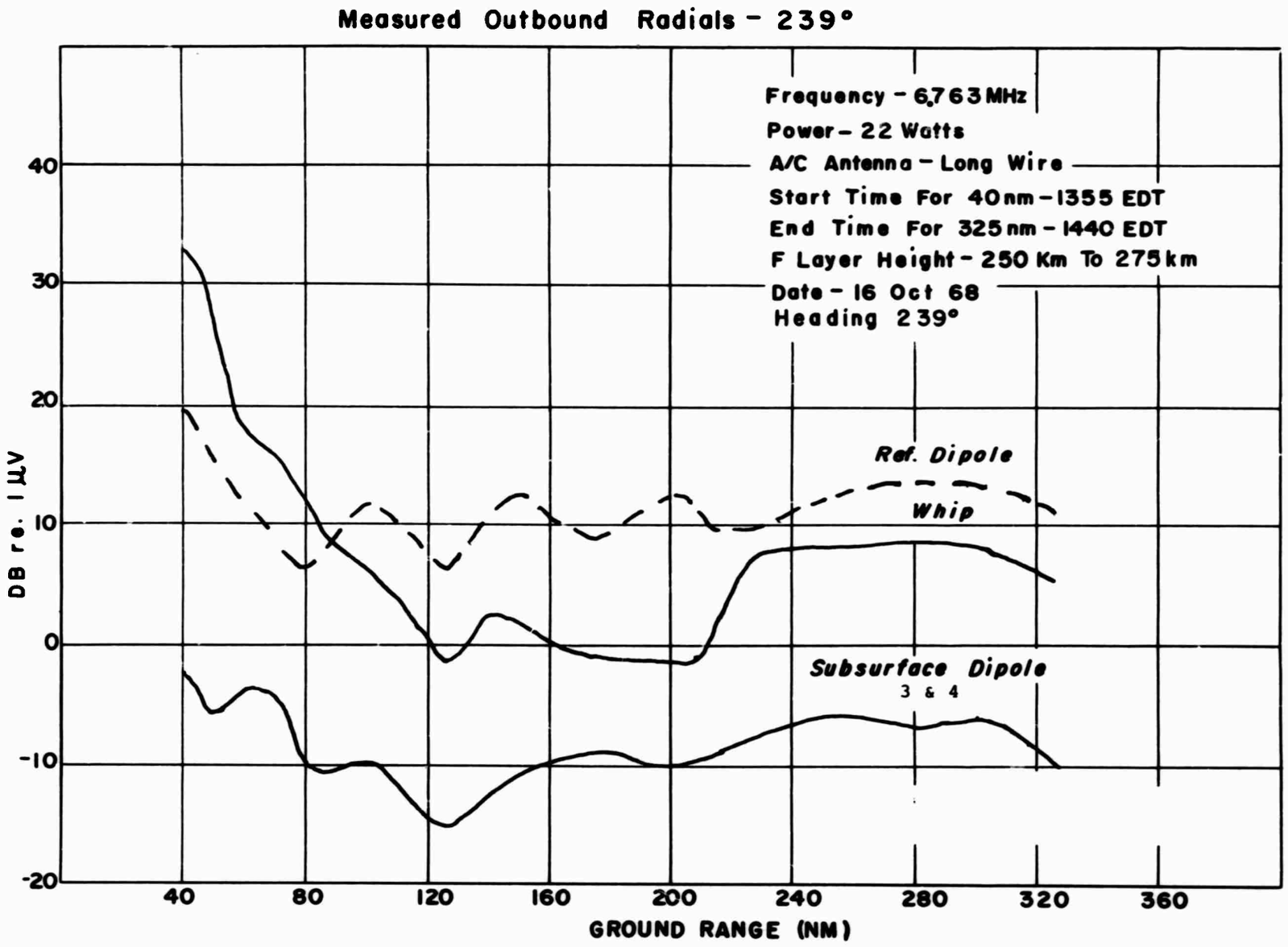

Figure 3-40. Extended Range Signal Strength Measurements

vertical ionospheric sounding data taken during the test period show that E-layer propagation should become evident at approximately 220 miles. Results compared with the sounding predictions are shown in Figures 3-41 and 3-42. The sudden increase of signal strength which is evident in all three curves at approximately 225 miles is due to the E-layer propagation.

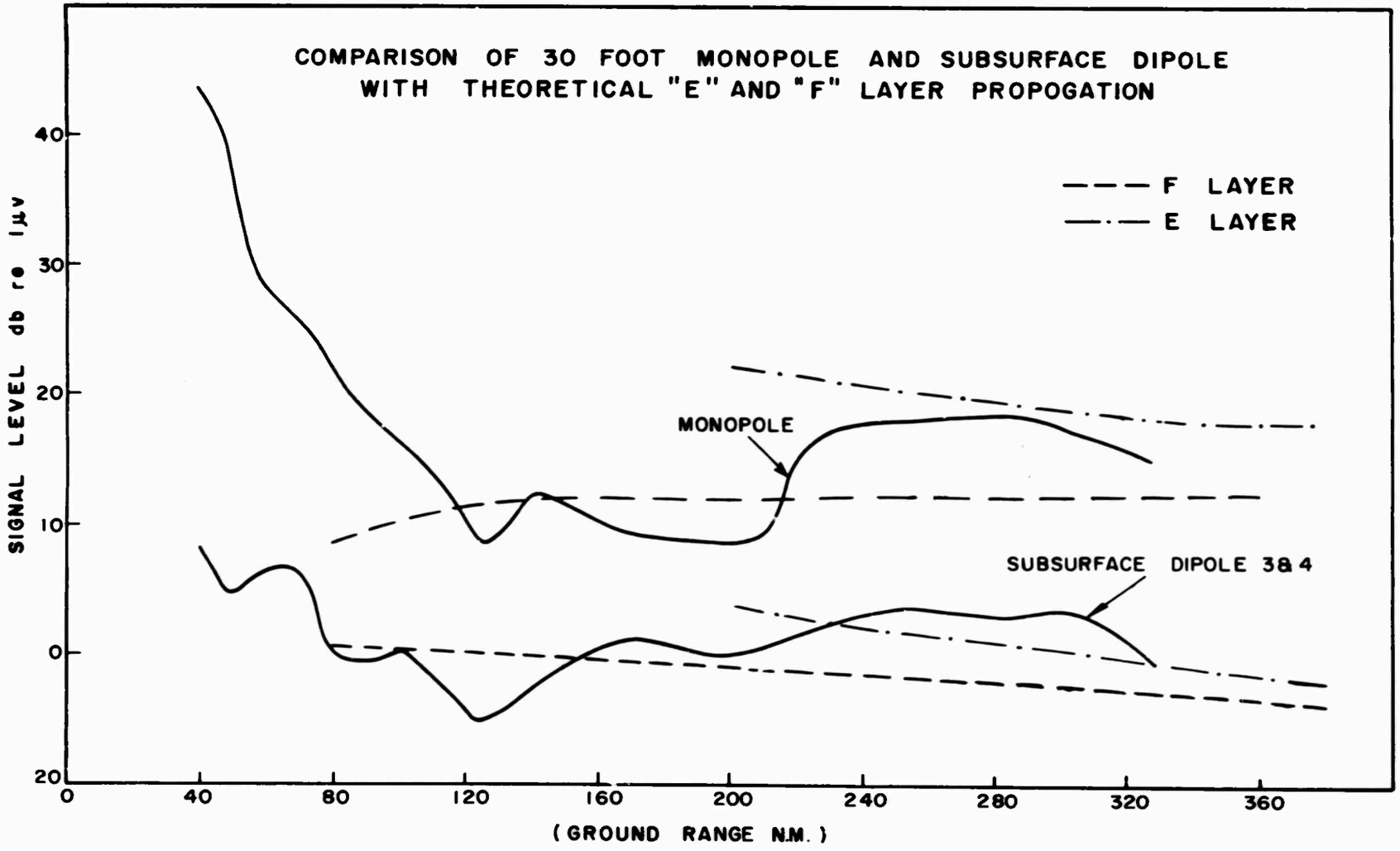
COMPARISON OF 30 FOOT MONOPOLE AND SUBSURFACE DIPOLE
WITH THEORETICAL "E" AND "F" LAYER PROPOGATION
F LAYER
E LAYER
MONOPOLE
SUBSURFACE DIPOLE 3&4
SIGNAL LEVEL db re 1μv
40
30
20
10
0
20
0
40
80
120
160
200
240
280
320
360
(GROUND RANGE N.M.)

FIGURE 3-41.

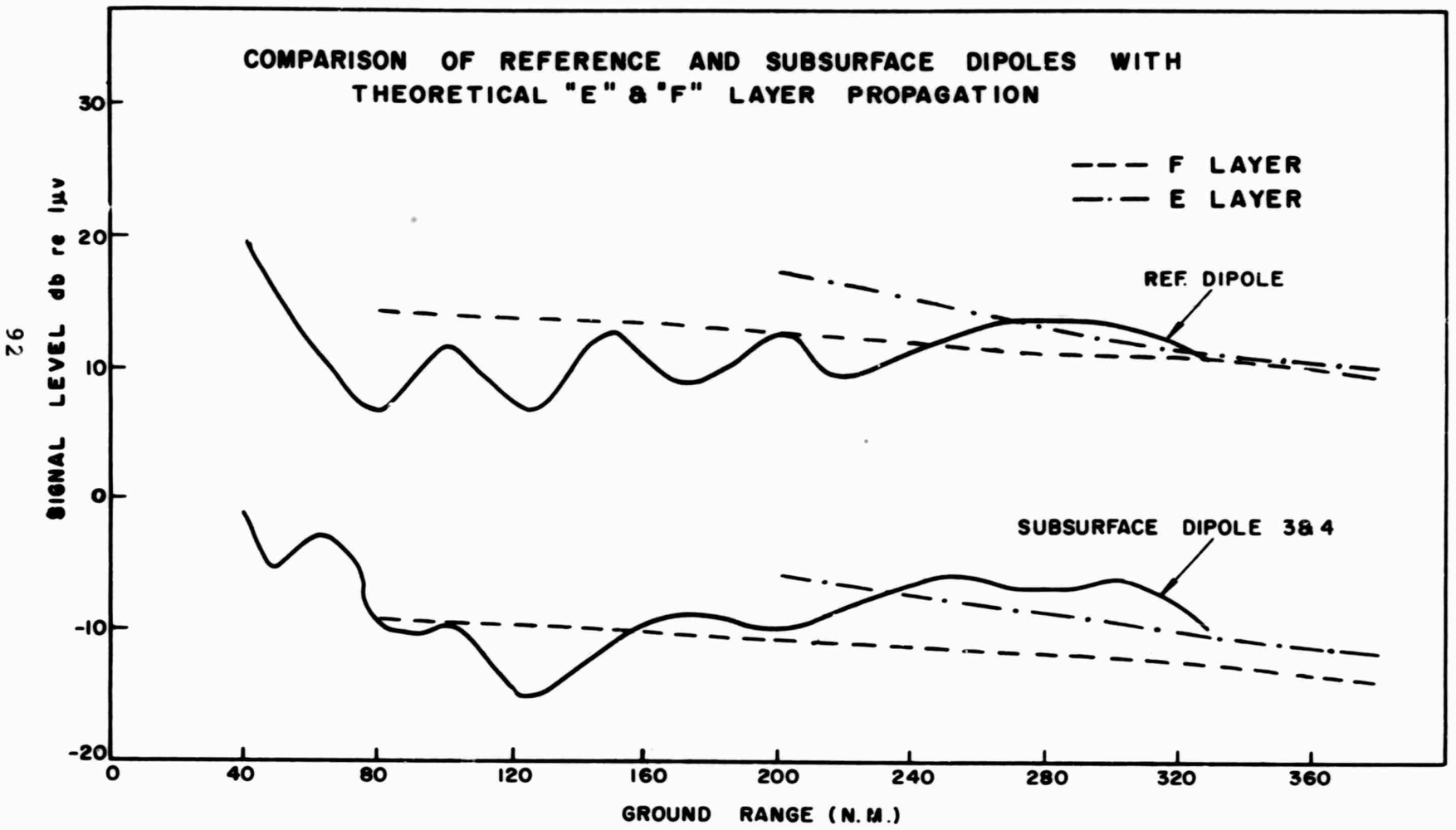
COMPARISON OF REFERENCE AND SUBSURFACE DIPOLES WITH
THEORETICAL "E" & "F" LAYER PROPAGATION
F LAYER
E LAYER
REF. DIPOLE
SUBSURFACE DIPOLE 3&4
SIGNAL LEVEL db re 1μv
30
20
10
0
-10
-20
0
40
80
120
160
200
240
280
320
360
GROUND RANGE (N.M.)

FIGURE 3-42.

E. SURFACE MEASUREMENTS OF RADIATED FIELDS

1. INTRODUCTION

Several measurements were made on the surface of the earth of the subsurface dipoles. The radiation of the subsurface dipoles was compared to that of the reference monopole and dipole. In this section, we will describe experimental measurements performed to resolve the surface and sky wave modes and measure the gain of the surface wave.

2. SURFACE WAVE GAIN

To determine the relative gain of the surface wave launched by the subsurface dipoles, field strength measurements were made at distances ranging from 4.8 miles to 61 miles. To obtain these measurements, a mobile receiving van was driven to various locations in line with the subsurface dipole elements where the surface wave is maximum. Special attention was given to select receiving sites which were free from overhead power lines and other metal obstructions which could affect the field strength readings. The terrain at the different sites varied widely. The receiving van contained equipment necessary to measure and record both pulse and CW signals. The receiving configuration is shown in Figure 3-43. The pulse signals were measured by photographing the IF output of the receiver and then calibrating the receiver system by substituting a calibrated signal source in place of the antenna signal. CW signals were measured by recording the receiver AGC voltage and calibrating the receiver

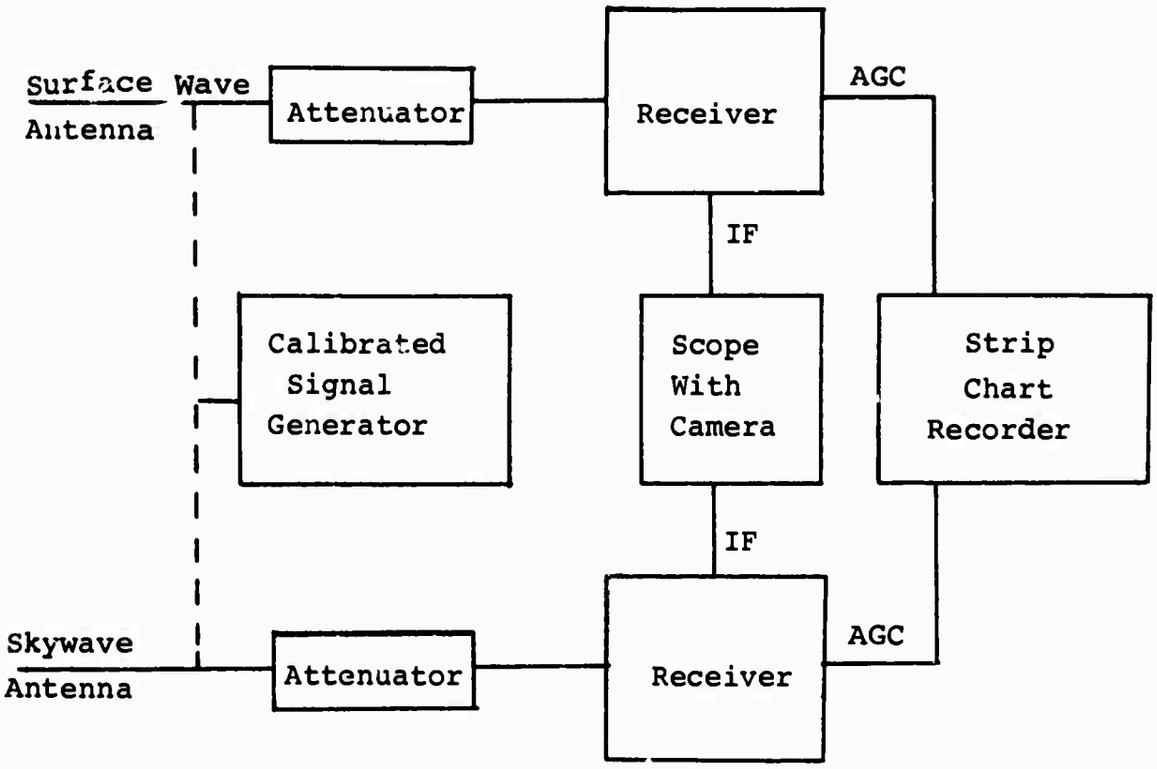

Figure 3-43. Receiving Instrumentation.

gain. Calibrations were made after each 5 to 10 minute recording interval. The surface wave launched from the subsurface dipoles was compared to that radiated from the reference whip antenna. Pulse transmissions were used where it was necessary to discriminate against sky wave propagated energy.

The received power from an antenna is given by

$$P_r = P_t + L_{ct} + L_{lt} + G_t + A + G_r + L_{lr} \qquad (3\text{-}2)$$

where

P_r = Power Received

P_t = Power Transmitted

L_{ct} = Transmitting Antenna Coupler Loss

L_{lt} = Transmitting Transmission Line Loss

G_t = Path Antenna Gain of the Transmitting Antenna

A = Basic Path Loss

G_r = Path Antenna Gain of the Receiving Antenna

L_{lr} = Receiving Transmission Line Loss.

For the surface wave mode the difference between the power received from the subsurface antenna and the monopole is given by:

$$\Delta P = P_r(S) - P_r(R) = (P_t + L_{ct}+L_{lt}+G_t+A+G_r+L_{lr})_S - (P_t+L_{ct}+L_{lt}+G_t+A+G_r+L_{lr})_R. \quad (3\text{-}3)$$

If the power delivered to the antennas is the same and the same antenna is used to receive both transmissions, the difference becomes

$$P_r(S) - P_r(R) = G_t(S) - G_t(R) \quad (3\text{-}4)$$

or $\Delta P = \Delta G$

where

$P_r(S)$ = Power Received from the Subsurface Antenna

$P_r(R)$ = Power Received from the Reference Antenna

$G_t(S)$ = Path Antenna Gain of the Subsurface Antenna

$G_t(R)$ = Path Antenna Gain of the Reference Antenna

and ΔG is the relative gain of the subsurface antenna compared to the reference antenna. The data obtained is shown plotted as a function of range in Figure 3-44. A theoretical curve whose slope is based on measured ground parameters is also shown in this figure for comparison and indicates

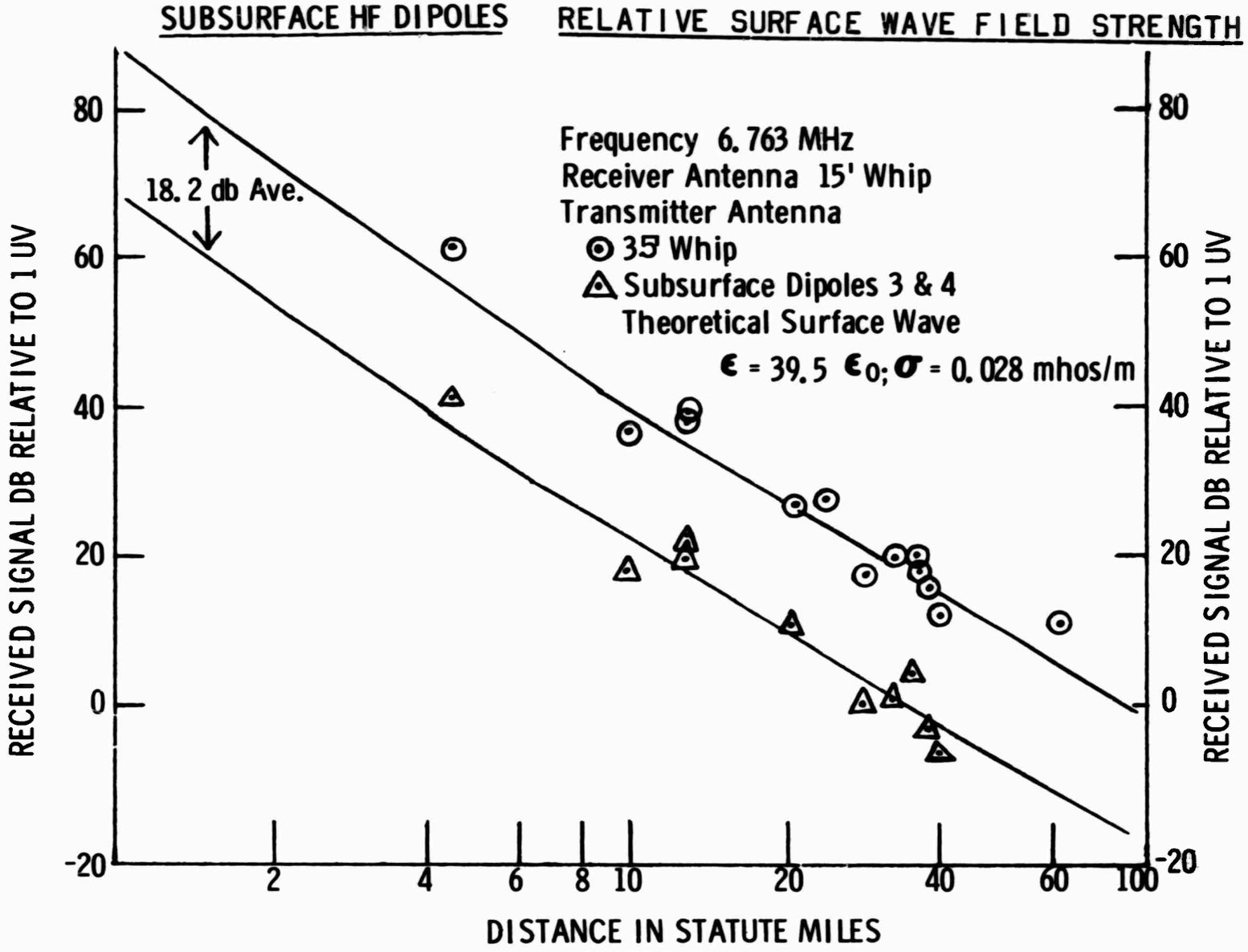
SUBSURFACE HF DIPOLES
RELATIVE SURFACE WAVE FIELD STRENGTH
Frequency 6.763 MHz
Receiver Antenna 15' Whip
Transmitter Antenna
⊙ 35' Whip
△ Subsurface Dipoles 3 & 4
Theoretical Surface Wave
ε = 39.5 ε0; σ = 0.028 mhos/m
18.2 db Ave.
RECEIVED SIGNAL DB RELATIVE TO 1 UV
RECEIVED SIGNAL DB RELATIVE TO 1 UV
80
60
40
20
0
-20
2
4
6
8
10
20
40
60
100
DISTANCE IN STATUTE MILES

FIGURE 3-44.

excellent agreement. The slope for both the reference monopole and the subsurface dipole, between 10 and 60 miles, varies approximately as 40 log r. The average difference (ΔG) between the reference monopole field strength and the field strength of the subsurface dipoles is -18.2 dB. Using this and the estimated efficiency of the reference monopole (-4.2 db) we obtain a gain of -22.4 db referenced to a perfect monopole. This -22.4 db is the gain for a pair of subsurface dipoles. A single dipole is 3 db less or -25.4 db below a perfect monopole.

Figure 3-45 shows samples of data taken at the 36.5 mile and 13 mile stations. The data has been calibrated and normalized to 1 KW input to each antenna. The surface wave signals can be compared directly but the subsurface dipole photograph taken at Station B was not taken when the fading skywave signal was at its peak and therefore, cannot be quantitatively compared to the other which was taken at peak.

Looking at Figure 3-45 one can see that there is approximately 18 db difference between the surface wave signal at the 13-mile station and the 36.5-mile station for both antennas. This is consistent with a 40 log r attenuation of the surface wave. One can also see that there was -18 dB and -17 dB less signal received from the subsurface antenna at these stations than was received from the reference whip.

In addition to obtaining the surface wave data from Figure 3-45, it is interesting to note how the skywave

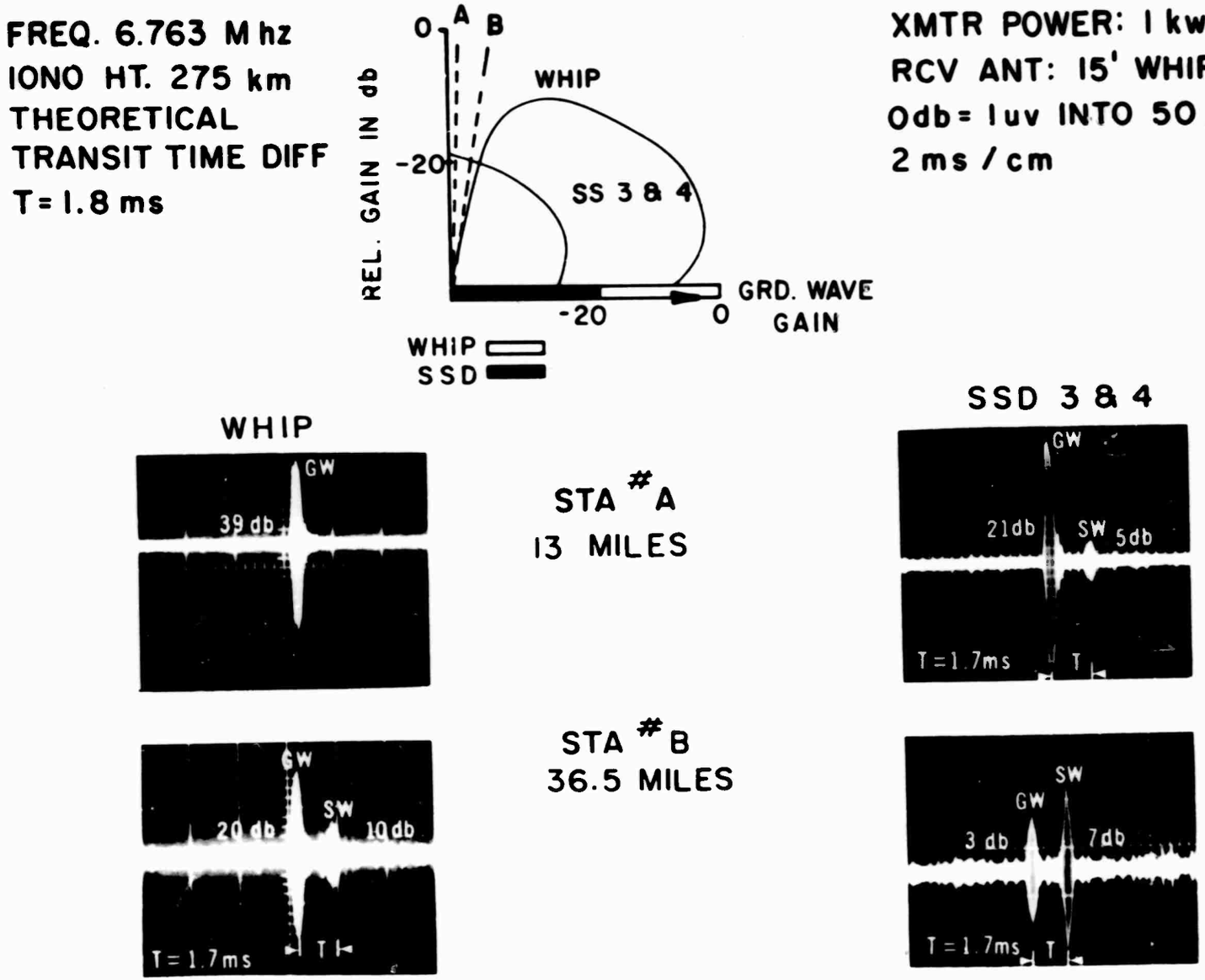

Figure 3-45. Surface Wave Measurements

behaved. There was no observable skywave received from the whip at 13 miles, but there was signal observed at the 36.5-mile station. This is consistent with the deep null found in the whip antenna pattern directly overhead and the rapid rise between the take-off angle of 90° and 80°. In comparison, the data for the subsurface antenna shows skywave at both ranges as one would expect from looking at its space wave pattern.

Proper identification of the modes in these photos is further exemplified by comparing the time delay of the two modes. The theoretical transit time difference, based on measured ionospheric height, between the ground wave and skywave modes is approximately 1.8 ms and the observed value was 1.7 ms.

A test was also conducted to determine the relative surface wave gain of subsurface dipoles 3 and 4 as a function of operating frequency. This was accomplished by measuring the field strength of CW signals transmitted from the reference monopole and subsurface dipoles 3 and 4. An NF-105 Field Intensity Meter with appropriate loop antenna was located 1.2 miles off the 239° end of the dipoles to make these measurements. The gain of subsurface dipoles 3 and 4 relative to the whip is shown in Figure 3-46 as a function of frequency. It is significant to note that the gain is fairly flat (±3 db) from about 2 MHz to 7 MHz and drops off markedly at 9.5 MHz and 19 MHz. An attempt to measure the relative gain in the

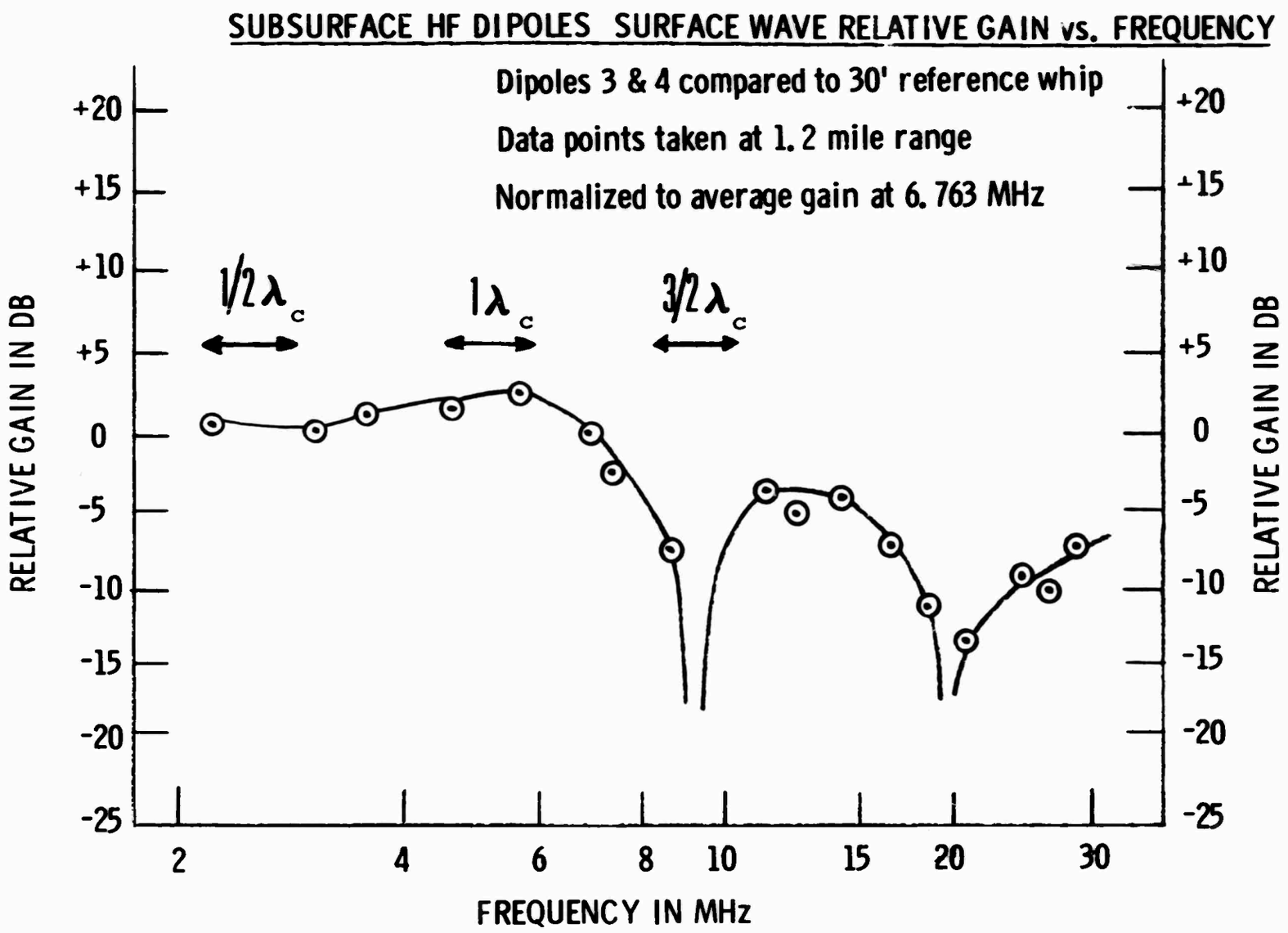
SUBSURFACE HF DIPOLES SURFACE WAVE RELATIVE GAIN vs. FREQUENCY
Dipoles 3 & 4 compared to 30' reference whip
Data points taken at 1.2 mile range
Normalized to average gain at 6.763 MHz
1/2λc
1λc
3/2λc
RELATIVE GAIN IN DB
+20
+15
+10
+5
0
-5
-10
-15
-20
-25
2
4
6
8
10
15
20
30
FREQUENCY IN MHz

FIGURE 3-46.

vicinity of 9.6 MHz failed because the signal level from the subsurface dipole was so low that it was below the noise. Using the noise level as an upper limit, the relative gain of the subsurface dipole had to be less than -20 dB at this frequency.

The data presented so far in this section is for subsurface dipole elements fed in parallel which theoretically should give a 3 dB gain over a single element. To verify this increase in gain over a single element, a comparison was made of the ground wave field strength off the ends of the subsurface dipoles 3 and 4 and subsurface dipole 5. The field strength at 6.763 MHz was 3 dB less for the single element than the two elements, verifying the prediction.

3. SKY WAVE GAIN

The subsurface antenna launches both a surface wave and a space wave and if the operating frequency is below the ionospheric critical frequency for a point-to-point path, both surface wave and skywave propagated modes can be present in the received signal. As a further verification of the space wave gain of the subsurface dipoles as determined by the airborne measurements, tests were conducted to identify and measure the relative gain of these modes on four point-to-point circuits from 5 to 540 miles. The four receiver sites were (1) Rome Air Development Center Stockbridge Test Annex, Griffiss AFB, N.Y.; (2) RADC Ava Test Annex; (3) Seneca Lake Army Depot, Seneca Lake, N.Y.; and

(4) Trabine Test Site, Wright-Patterson AFB, Ohio. The distances and bearings to these sites are: Stockbrige - 8.6 miles, 192°; Ava - 21 miles, 272°; Seneca Lake - 61 miles, 245°; and Trabine - 524 miles, 239°.

Both pulse and CW transmissions were used. All of the receiving stations had the same basic equipment and measuring capability to receive and analyze the pulse and CW transmissions. The receiver configuration is the same as that in the mobile van shown in Figure 3-43.

Where possible, a vertically polarized dipole or monopole type antenna was used to receive the surface wave signal and a horizontally polarized dipole type antenna was used to receive the skywave signals. This was done to maximize the signal-to-noise ratio by taking advantage of the directive gain of these antennas. The Trabine Site was the only exception. Here a vertically polarized monopole array was used for the skywave. This was very satisfactory, however, since its main lobe was oriented along the circuit in both elevation and azimuth.

There are three basic parameters which differentiate the surface wave from the skywave:

(a) the relationship of field strength and range.

(b) the transit time between transmitter and receiver.

(c) the fading characteristics of the received signals.

The structure of pulse transmissions received from a subsurface dipole should look similar to that shown in Figure 3-47.

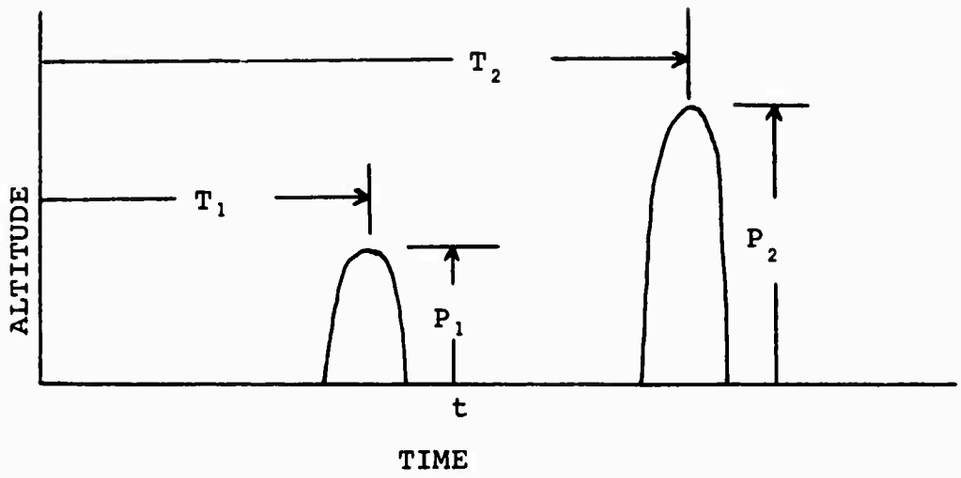

Figure 3-47. Mode Resolution.

The first signal received at T_1 is the surface wave and the second arriving at T_2 is the skywave. The surface wave would have a steady amplitude whereas the skywave would fade because of multipath and Doppler. The power received on each mode would be given by Equation 3-2. By analyzing the fading characteristics, transit times and the power received at various distances from the transmitter test site, we were able to resolve the propagation modes and determine path antenna gain.

We will first discuss mode resolution with reference to the transit time differences between the surface wave and the skywave. Figure 3-48 shows the time delay difference between signals received at the Ava Test Site. There is approximately 1.9 ms delay between the first and second returns and

FREQUENCY: 6.763 Mhz XMTR POWER: 1 kw	RCV. SITE-AVA , N.Y. 21 MILES RCV. ANT - A-VERTICAL DIPOLE ARRAY B-HORIZONTAL DIPOLE
TRANSIT TIME DIFF FOR 290 km IONOSPHERIC HT. T= 1.9 ms	DISPLAY CALIBRATION 0db= 1uv INTO 50 Ω 2 ms / cm

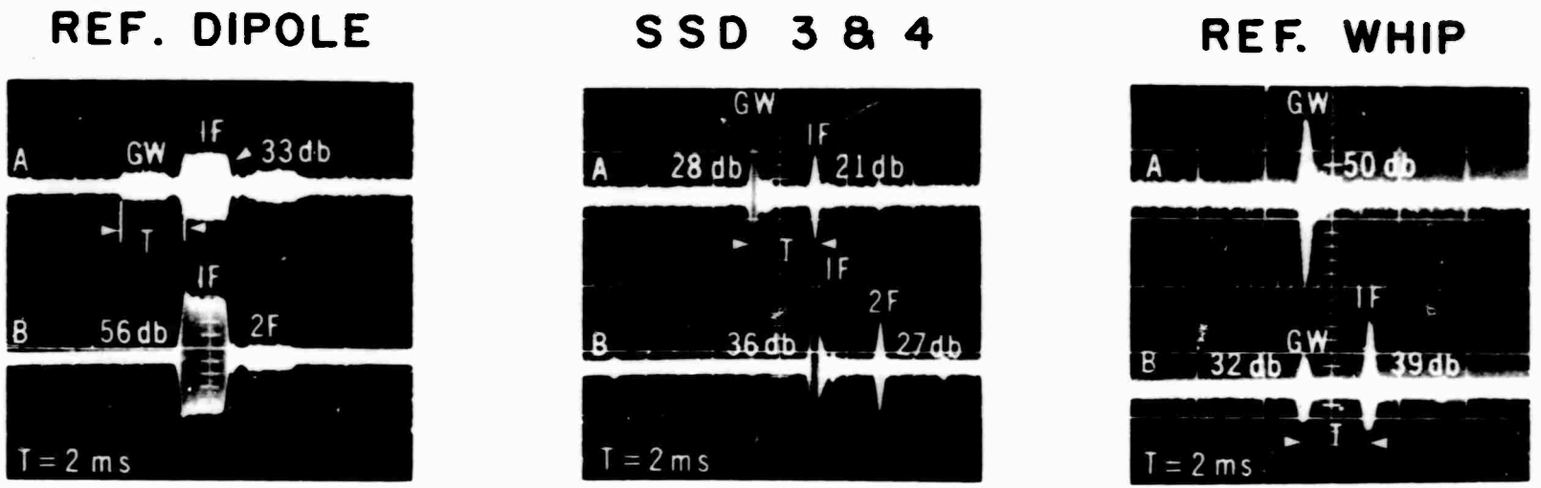

Figure 3-48.
Sky Wave Measurements

2.0 ms between the second and third returns. This correlates with the calculated delay differences based on the measured ionospheric height between the 1 hop F and surface wave modes and between the 2 hop F and 1 hop F skywave modes. Similar results were obtained at the other stations and at other frequencies.

The fading characteristics of the different modes were also observed at these locations and frequencies. When present, the surface wave was very stable in amplitude whereas the skywave mode fluctuated greatly with time. Similar resolution of the surface wave and skywave was obtained by comparing the field strength received from the subsurface dipole with the fields of the reference monopole and horizontal dipole, respectively. From these field strength measurements, ΔP was calculated for the surface wave and skywave modes. Results are tabulated in Tables 3-5 and 3-6. These tables also contain corresponding values of ΔG which are calculated from the measured airborne patterns and average surface wave gain. These values of ΔG are corrected for the azimuth and elevation angle. Correlation between ΔP and ΔG was very good for the surface wave mode and was fair for the skywave mode.

Table 3-5 shows data for the frequency 6.763 MHz taken at four different sites. To illustrate how the data was obtained, we show actual test data in Figure 3-48 which was taken for the first Ava Station measurement listed. From

SKY WAVE DATA

Frequency: 6.763 MHz
Test Antenna: Subsurface Dipoles 3 and 4

Reference Antennas:
Surface Wave - 35' Monopole
Skywave - Horizontal Dipole

SITE	DIST. MILES	SURFACE WAVE			SKYWAVE			
		ΔG	ΔP	ΔG-ΔP	PROP. MODE	ΔG	ΔP	ΔG-ΔP
Stockbridge	8.6	-23.7	-20	-3.7	1F	-	-	-
Ava	21	-21.3	-22	+ .7	1F	-24.7	-20	-4.7
		-	-	-	1F	-24.7	-23	-1.7
Seneca	61	-	*	*	1F	-25.0	-24	-1.0
Trabine	524	-	*	*	1F	-25.2	-22	-3.5
		-	*	*	1F/1E	-25.2	-28	+2.8

* Receiver Sites were beyond surface wave range of the test antenna.

NOTE: ΔG based on average surface measurements and airborne measurements.

TABLE 3-5

SKY WAVE DATA

Test Antenna: Subsurface Dipoles 3 and 4

Reference Antennas:
Ground Wave - 35' Monopole
Skywave - Resonant Dipole

FREQ. MHz	SITE	DIST. MILES	SURFACE WAVE			SKYWAVE (IF)		
			ΔG	ΔP	ΔG-ΔP	ΔG	ΔP	ΔG-ΔP
6.763	Stkb.	8.6	-23.7	-20	-3.7	-	-	-
	Ava	21	-21.3	-22	+0.7	-24.7	-20	-4.7
	Seneca	61	-20.0	*	*	-25.0	-24	-1.0
4.450	Stkb	8.6	-	-25	-	-	-20	-
	Ava	21	-	-23	-	-	-23	-
			-	-	-	-	-23	-
	Seneca	61	-	*	-	-	-30	-
2.232	Seneca	61	-	*	-	-	-24	-

NOTE: ΔG based on average surface measurements and airborne measurements.

TABLE 3-6

Figure 3-48 one can see that the difference between the surface wave amplitude of the reference whip and the subsurface dipole as received on the vertical dipole (antenna A) at Ava is -22 dB. This represents the observed surface wave gain differences of the two antennas. Likewise, the -20 dB difference between the reference dipole and subsurface dipole skywave signal amplitude received on the horizontal dipole (antenna B) approximates the space wave antenna gain difference of the two antennas.

The agreement between the calculated and the observed skywave values in Tables 3-5 and 3-6 is reasonable considering the fact that signals propagated through the ionosphere experience multipath and Doppler which make measurements of this type subject to a large statistical variance. Since the two transmitters were not on simultaneously, errors due to long-term fading (i.e. 5 - 15 mins) affect the data. Another big factor affecting the accuracy of these measurements is that each pulse must be photographed at its peak amplitude to compensate for the short-term fading. In an attempt to do this, the signal was observed over a five-minute period and photographed at its maximum value. Without a continuous recording of the pulse amplitude, errors may be present in assuming that the pulse was photographed at its peak. The fading rate of these signals varied from about 0.1 Hz to 0.5 Hz. Better agreement between ΔG and ΔP would require continuous recording of simultaneous pulse

transmissions radiating from both antennas, and averaging the data over a longer period of time.

The data in Table 3-6 is for three different frequencies (2.232, 4.450 and 6.763) and three different sites (Stockbridge, Ava and Seneca). From it, one can say only that the results at 2.232 and 4.450 are comparable to the more extensive results obtained at 6.763 MHz and that the modes of propagation are the same.

The pulse and CW measurements taken at Trabine are of particular interest since this is approximately the same range at which other investigators reported a super ground wave. (Ref. 1). Figure 3-49 shows samples of the pulse data and Figure 3-50 shows CW data recorded at Trabine. The data in Figure 3-49 was taken at the same time the airborne measurements reported in Section 3-D were taken.

There was no surface wave observable at Trabine as would be predicted by existing theory. The pulses shown in Figure 3-49 are from 1E and 1F skywave modes. The calculated transit time difference between these two modes is 0.5 ms and the observed value was of the same order. The two modes were resolved with the 100 μs pulse of the subsurface antenna and the monopole, but could not be resolved with the 1.4 ms pulse of the reference dipole. The reference dipole signal in Figure 3-49 shows that the 1.4 ms pulse lost most of its original shape because of the interference of the signals

Trabine Site
Wright-Patterson AFB, Ohio

Freq: 6.763 MHz
Date: 16 Oct 68

Rcv. Ant.: Monopole Array
Time: 1610-1640 EDT

Ref Whip

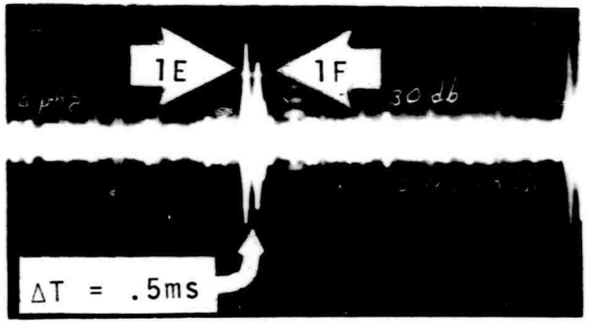

SSD 3&4

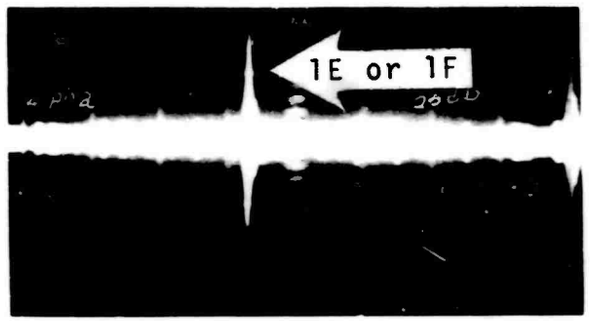

SSD 3&4

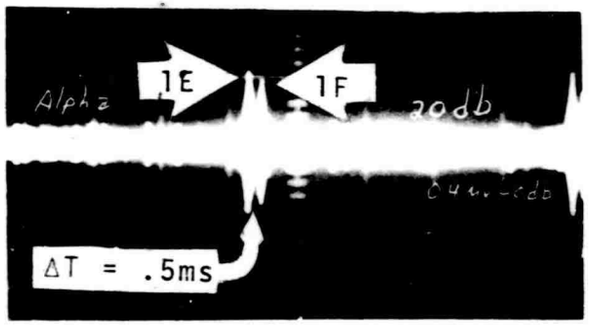

Ref Dipole

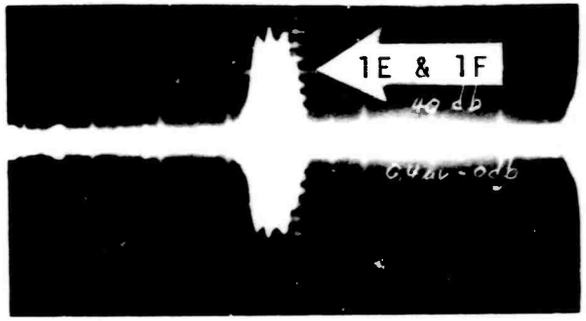

Figure 3-49. Pulse Data

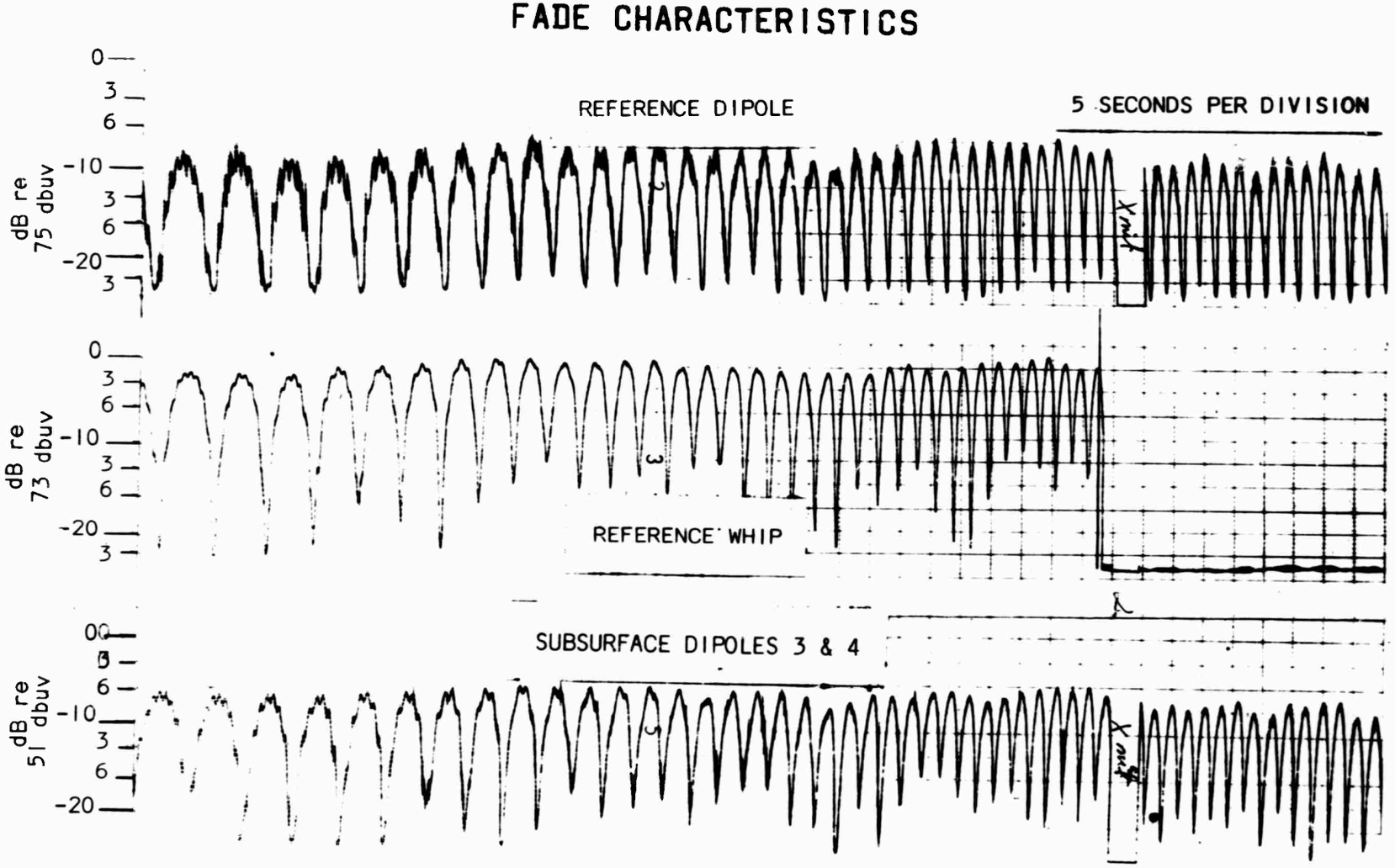

Figure 3-50 CW Data

from the two modes. One can see that accurate ΔP measurements could not be expected under these conditions. Both the 1E and 1F returns faded during this period. One of the modes received from the subsurface dipole in Figure 3-49 had faded out completely in one photo (top right) and reappeared moments later in the second picture (bottom left).

To further substantiate proper identification of modes in the Trabine data, a simple ray tracing was constructed for the circuit and is shown in Figure 3-51. The ray tracing is based on a vertical ionogram which was taken at the Stockbridge Test Site only 8.6 miles from Verona. From the virtual height versus frequency data found on the ionogram (top right corner of Figure 3-51), one can determine the virtual heights and critical take-off angles for 1E and 1F oblique transmission paths by using the Secant Law.

From the ray tracing it is apparent that only F modes would be expected out to a range of 400 km (216 NM) and that both F and E modes would be received beyond this range out to Trabine. The recordings taken by the aircraft, Figures 3-41 and 3-42, Section 3.D, do show an abrupt change in recording signal level at about 220 NM and the data in Figure 3-49 shows 1E and 1F returns being received at Trabine.

Figure 3-50 shows a recording of the amplitude of separate CW transmissions received at Trabine. All three transmitters were on simultaneously at Verona but offset in frequency by 5 KHz. The chart shows the signal amplitude

MODE RESOLUTION

DATE: 16 OCT. 68
TIME: 1600 EDT

STATION: VERONA SITE N.Y.
FREQUENCY: 6.763 MHZ

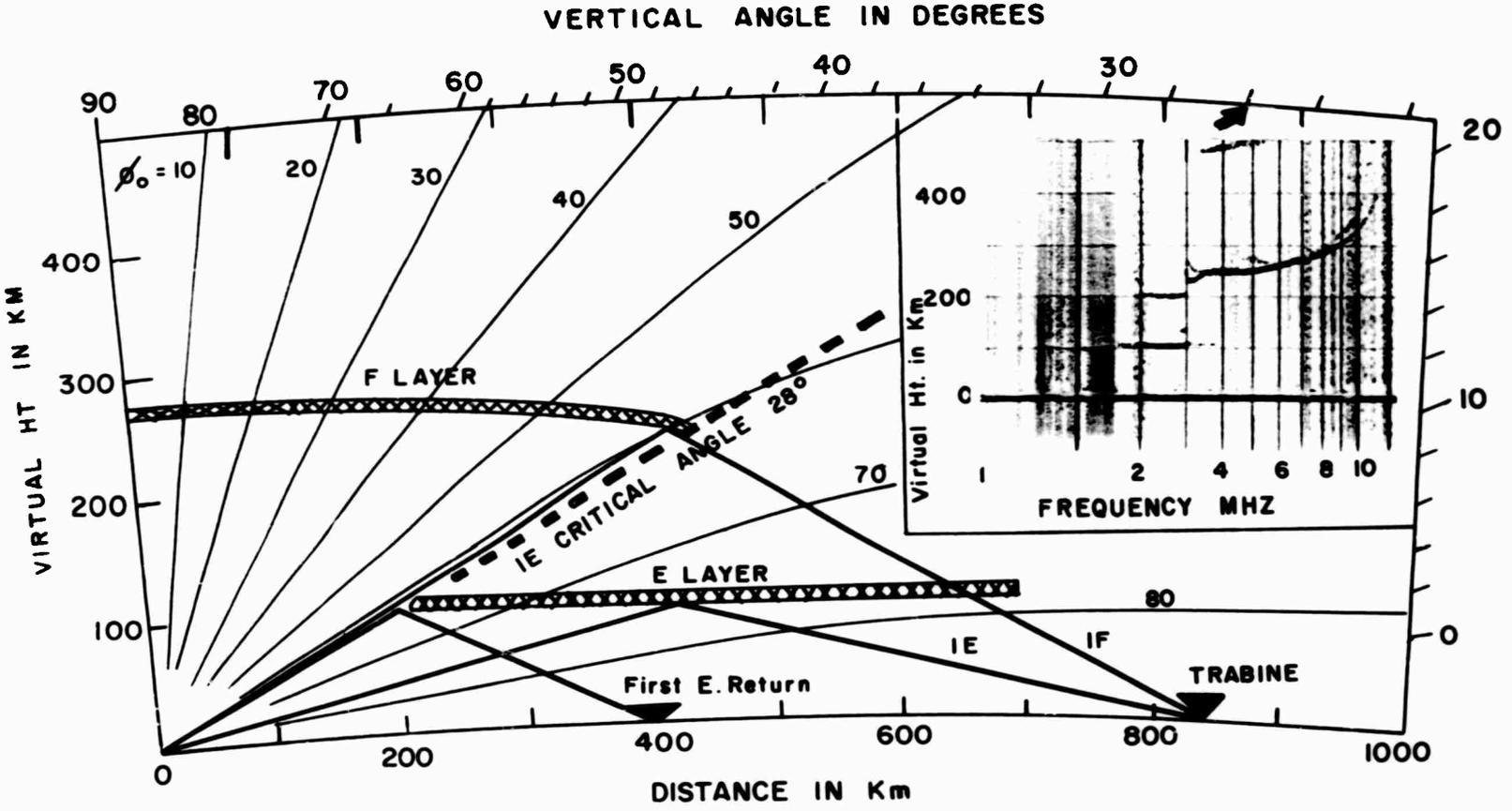

FIGURE 3-51 RAY TRACING

of the three transmissions received on the monopole array. The receivers were operated with a 1 KHz bandwidth to separate the 5 KHz space signals. Successful separation is illustrated by the fact that during the long period the whip transmitter was off for identification in Figure 3-50, there was no observable effect on the other two signals. The small off period observed on the other two traces was caused by the TR switch at the receiver site when communication calls were made from Trabine. This example shows the worst fading encountered during the test but illustrates that all three had the same basic fading rate and fading depths. The calibration at the left of Figure 3-50 is the received signal strength normalized to a 1 kw input to each of the three test antennas. The actual powers transmitted from the reference dipole, reference whip, and subsurface dipoles were 34, 55, and 90 watts, respectively.

In general, the point-to-point data recorded at Ava, Stockbridge, Seneca Lake, and Trabine shows that the subsurface dipoles launched conventional surface and space waves which were subject to normal losses and propagation anomalies.

4. SUMMARY

A. INTRODUCTION

Extensive measurements were made of the electrical and radiation characteristics of subsurface dipoles in the HF band and the purpose of this section is to summarize the measurements and their comparisons with theoretical predictions.

B. ELECTRICAL MEASUREMENTS

A comparison of the measured impedance of a single dipole compared to the theoretical impedance of a dipole having the same dimensions is shown in Figure 3-20. Apparently, the attenuation is slightly greater than calculated but fairly good agreement is obtained as far as the general shape and resonant frequency is concerned.

C. RELATIVE GAIN MEASUREMENTS

The relative surface wave gain of a pair of subsurface dipoles compared to a 35-foot monopole antenna was measured and shown in Figure 3-44. The average gain for a number of measurements was computed as -18.2 db. Table 4-1 illustrates the excellent agreement this gives when compared to that calculated from the theory in Section 2.

The relative space wave gain of a pair of subsurface dipoles was also measured compared to a half-wave dipole which was a quarter wave above ground. Table 4-2 illustrates again the excellent agreement between this measured data and the theory of Section 2. Figure 3-36 shows the good correlation

TABLE 4-1

RELATIVE GAIN OF SURFACE WAVE
FOR SUBSURFACE HF DIPOLE PAIR AT 6.763 MHz

	THEORETICAL (db)	MEASURED (db)
Relative Gain of 1 element Compared to Perfect Monopole @ d=0, L=λ_c Measured Verona Soil - Figure 2-13.	-19.0	- -
Array gain for pair	+ 3.0	+ 3.0
Depth Loss (d=1 meter) (Figure 2-16)	- 6.5	- -
Meas. Rel. Gain of Perfect Monopole Compared to Practical Monopole (Eq 3-1)	+ 4.25	+ 4.25
Total: Rel. Gain. of Element Pair at d=1 m compared to practical monopole.	-18.25	-18.2 (Figure 3-44)

TABLE 4-2

RELATIVE GAIN OF SPACE WAVE
FOR SUBSURFACE HF DIPOLE AT 6.763 MHz

	THEORETICAL (db)	MEASURED (db)
Relative Gain of Surface wave for 1 element compared to perfect monopole, d=0, L=λ_c, measured Verona soil (Figure 2-13)	-19.0	--
Difference of relative gain of surface wave compared to relative gain of space wave over that of a perfect half wave dipole $\lambda_0/4$ above ground. (Eq. 2-38).	- 3.5	--
Array gain for pair	+ 3.0	+ 3.0
Depth loss (d=1 meter) Figure 2-16.	- 6.5	--
Approx. relative gain of perfect half wave dipole compared to practical half wave dipole (Ref. 35, pg 109)	+ 2.0	--
Total: Relative gain of element pair at d=1 m compared to practical half wave dipole at h = $\lambda_0/4$.	-24.0	-23.5 Figure 3-37

between the theoretical and measured pattern shapes of the space wave radiation.

A comparison of the measured and theoretical relative surface wave gain as a function of frequency is shown plotted in Figure 4-1. By noting that the measured conductivity increases with frequency as shown in Figure 3-8, the excellent agreement is apparent.

D. CONCLUSIONS

The characteristics of HF subsurface dipoles can be predicted well within measurement accuracy. The subsurface dipoles radiate a normal surface wave field that attenuates approximately as 40 log r and would be useful for limited ranges. They also radiate a space wave field which attenuates as 20 log r, with a pattern similar to that of an above ground dipole. This space wave pattern would provide direct line of sight communication to aircraft and when the signal is reflected from the ionosphere would provide conventional ionospheric hop communications to large distances. It is apparent from Figures 2-19 and 2-20 that economical and relatively small arrays of HF dipoles in average soil can have gains of approximately -9 to -13 db compared to practical above ground antennas as shown in Figure 4-2. Section 2 provides the necessary design information to enable system engineering of such arrays and accurate predictions of their performance.

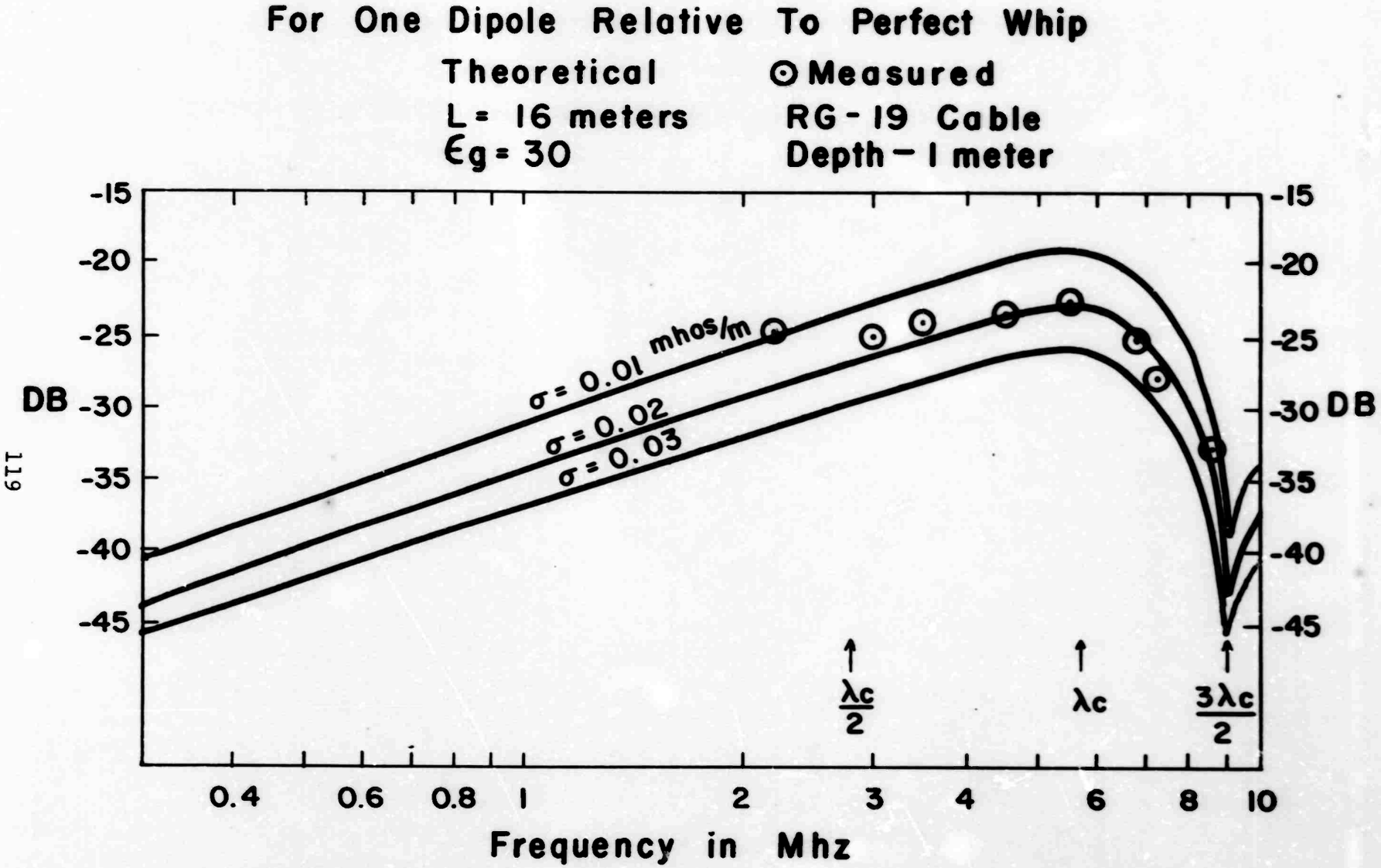

Figure 4-1. Subsurface Dipole Antenna Surface Wave Gain Vs. Frequency

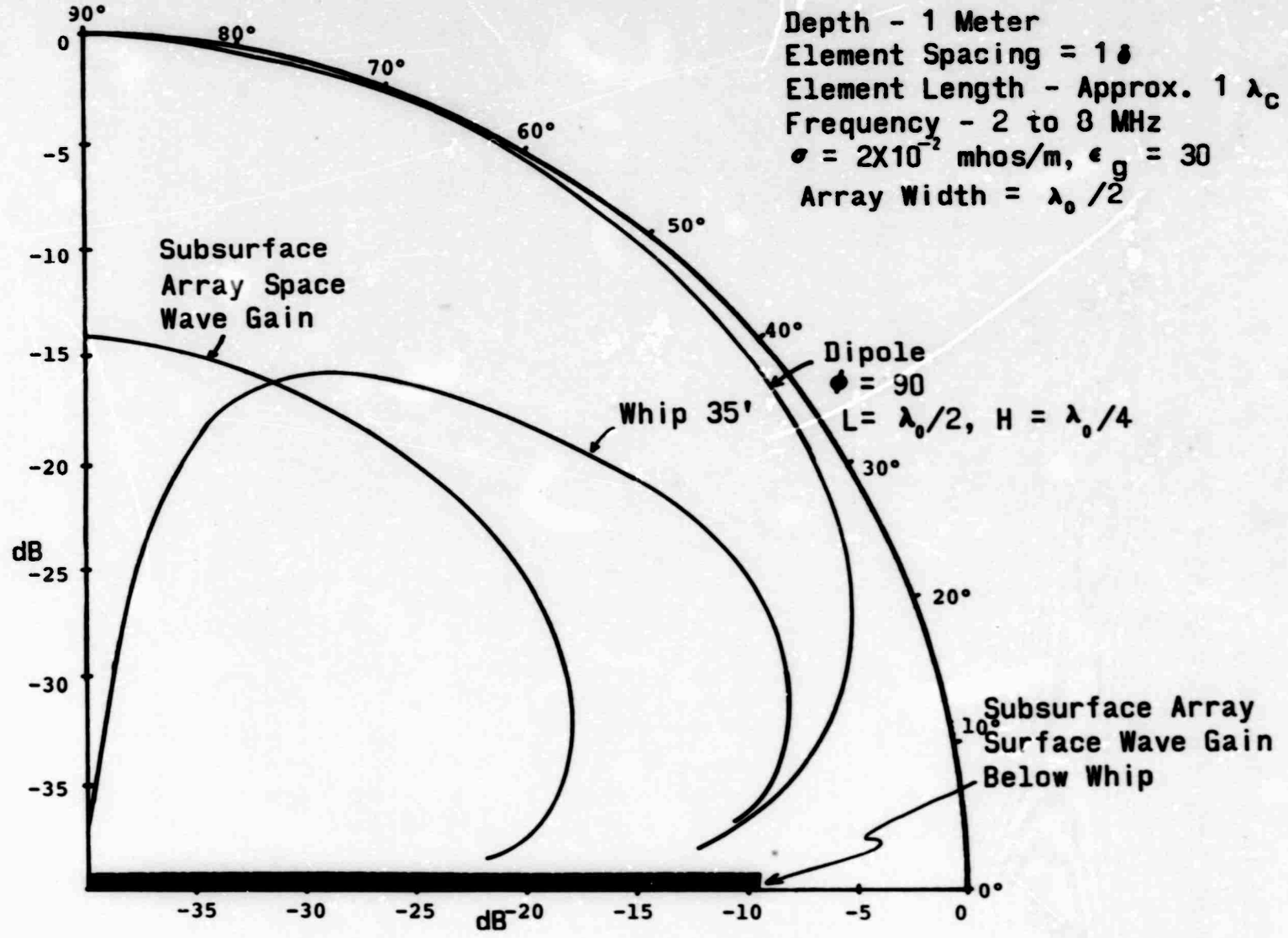

Figure 4-2. Approximate Gain of Subsurface Array Compared to Typical Antennas

Typical performance estimates of such an array are shown in Figures 4-3 to 4-5 with an input power of 10 KW and operating in soil with a conductivity of 20 milli-mhos/meter and a dielectric constant of 30.

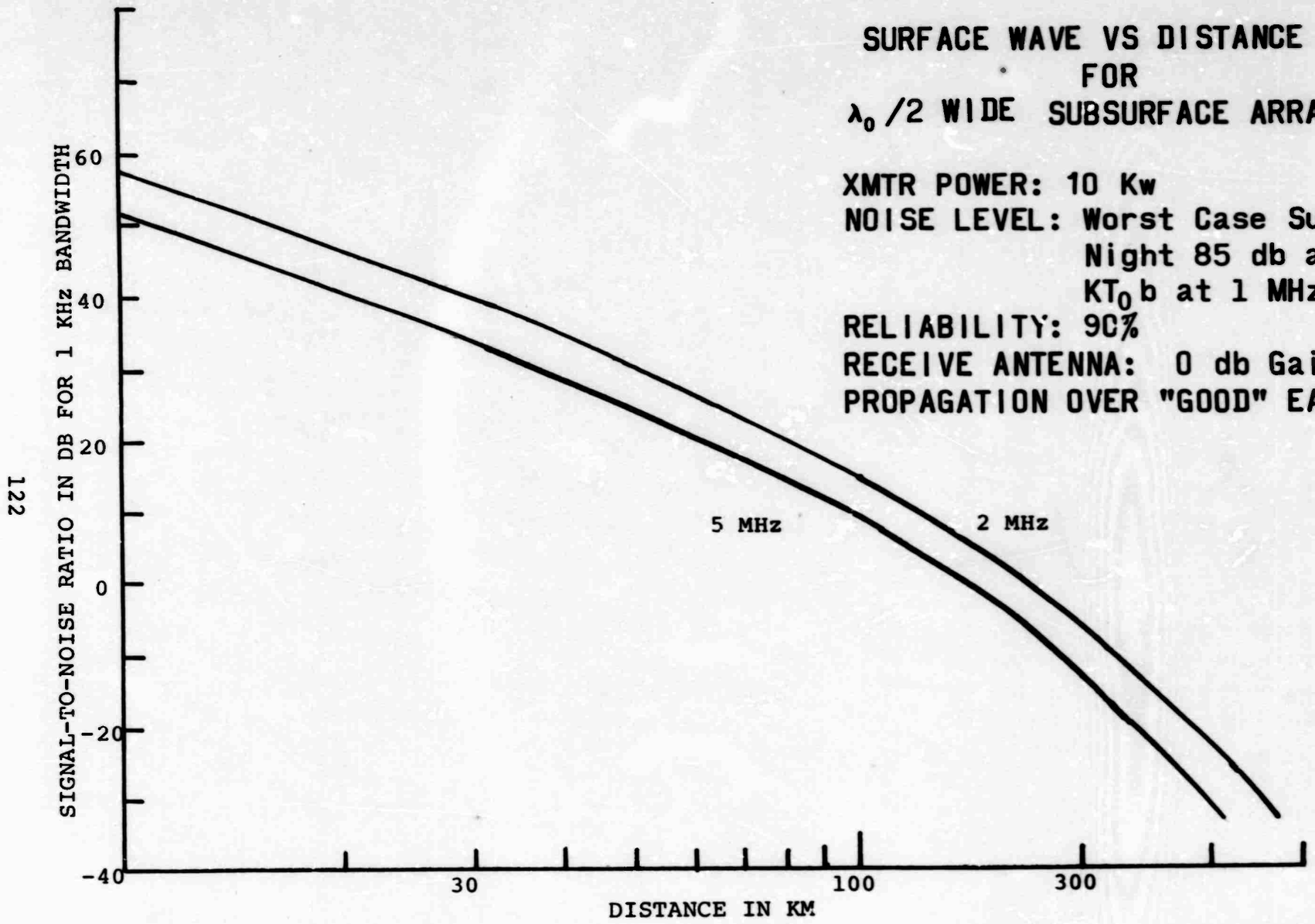
SURFACE WAVE VS DISTANCE
FOR
λ_0/2 WIDE SUBSURFACE ARRAY
XMTR POWER: 10 Kw
NOISE LEVEL: Worst Case Summer Night 85 db above KT_0b at 1 MHz
RELIABILITY: 90%
RECEIVE ANTENNA: 0 db Gain
PROPAGATION OVER "GOOD" EARTH
SIGNAL-TO-NOISE RATIO IN DB FOR 1 KHz BANDWIDTH
60
40
20
0
-20
-40
5 MHz
2 MHz
30
100
300
DISTANCE IN KM

FIGURE 4-3.

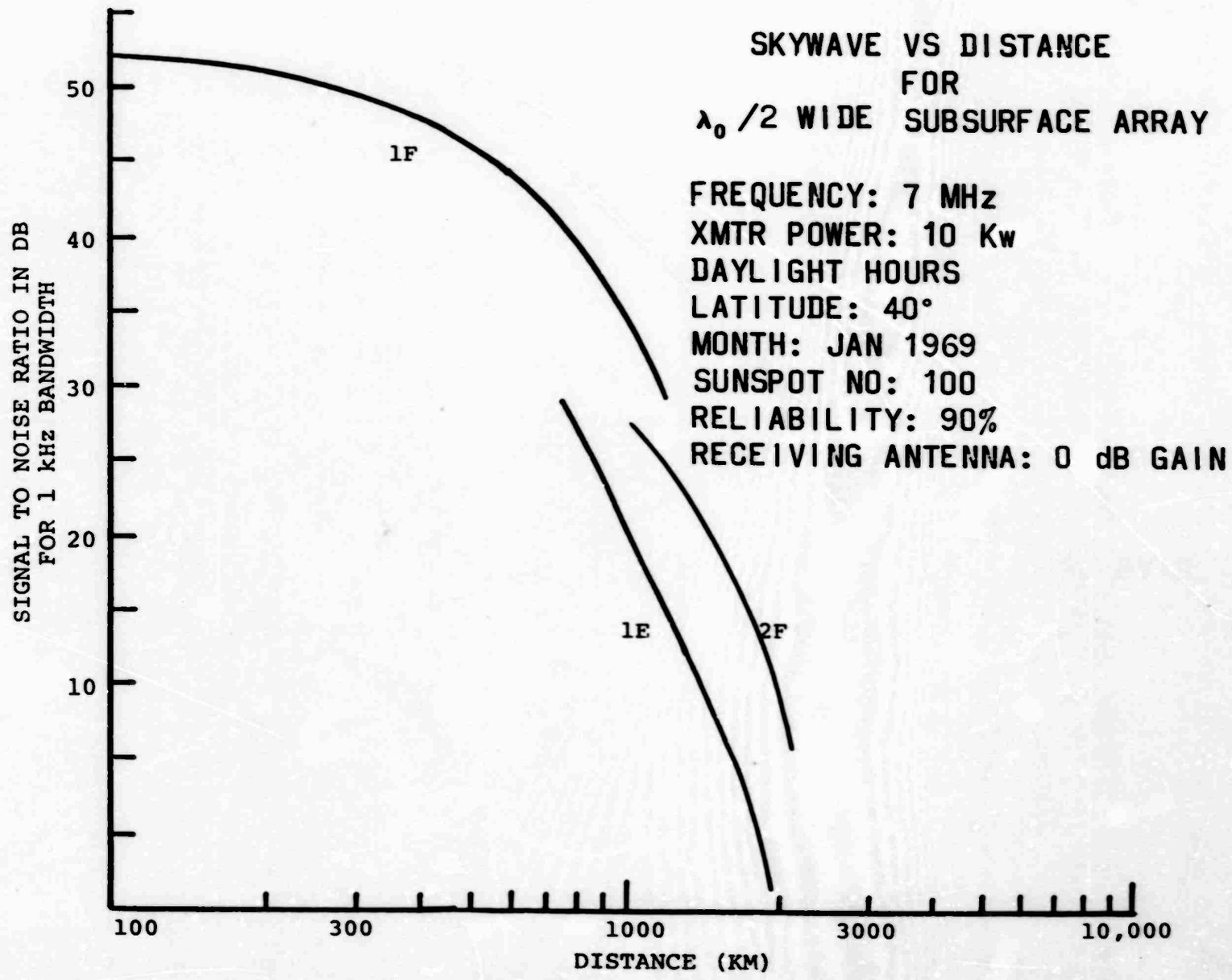
SKYWAVE VS DISTANCE
FOR
$\lambda_0/2$ WIDE SUBSURFACE ARRAY
FREQUENCY: 7 MHz
XMTR POWER: 10 Kw
DAYLIGHT HOURS
LATITUDE: 40°
MONTH: JAN 1969
SUNSPOT NO: 100
RELIABILITY: 90%
RECEIVING ANTENNA: 0 dB GAIN
SIGNAL TO NOISE RATIO IN DB
FOR 1 kHz BANDWIDTH
50
40
30
20
10
1F
1E
2F
100
300
1000
3000
10,000
DISTANCE (KM)

FIGURE 4-4.

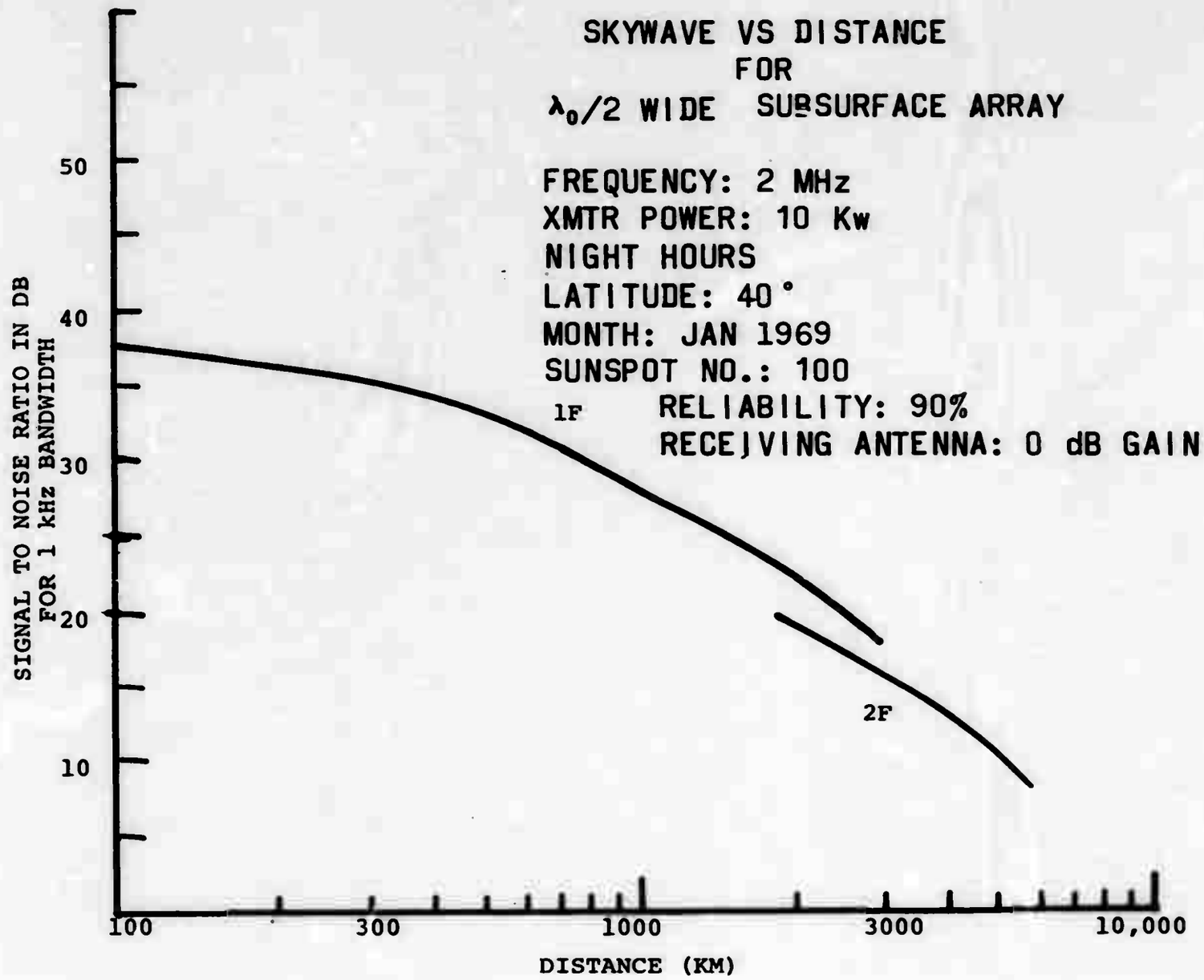
SKYWAVE VS DISTANCE
FOR
$\lambda_0/2$ WIDE SUBSURFACE ARRAY
FREQUENCY: 2 MHz
XMTR POWER: 10 Kw
NIGHT HOURS
LATITUDE: 40°
MONTH: JAN 1969
SUNSPOT NO.: 100
RELIABILITY: 90%
RECEIVING ANTENNA: 0 dB GAIN
1F
2F
SIGNAL TO NOISE RATIO IN DB
FOR 1 kHz BANDWIDTH
50
40
30
20
10
100
300
1000
3000
10,000
DISTANCE (KM)

FIGURE 4-5.

REFERENCES

1. Mussett, R.D.G., and Jenkins, J.A., Analysis of Buried Antennae, Report No. EWP(P)(68)2, British Ministry of Defense, (1968).

2. Hansen, R.C., "Radiation and Reception with Buried Antennas," IEEE Trans. Antennas and Propagation, Vol. AP-11, No. 3 (May 1963).

3. Brock-Nannestad, L., Bibliography - Electromagnetic Phenomena with Special Reference to ELF (1-3000 cps), NATO SACLANT ASW Research Center, Tech. Rpt. 10 (Sep 62), AD-291 179, and Tech. Rpt. 25 (Oct 64) (new edition of Sep 62 report).

4. US LIBRARY OF CONGRESS, AEROSPACE INFORMATION DIVISION, Underground Communications - Annotated Bibliography of Soviet-Bloc Literature for Period 1960-1962, (Preliminary), AID Rpt. No. B-63-99 (26 July 1963).

5. Entzminger, J.N., and Huss, J.P., A Summary Report on Tri-Service ELF Communications, Vol. II - Bibliography, RADC-TR-65-233, Rome Air Development Center (Sep 65) (AD 474 516).

6. Moore, R.K., The Theory of Radio Communication Between Submerged Submarines, A Thesis: Presented to the Faculty of the Graduate School of Cornell University for the Degree of Doctor of Philosophy, microfilm, Cornell Univ. Library (Jun 51).

7. Moore, R.K., and Blair, W.E., "Dipole Radiation in a Conducting Half Space," J. Res. Nat. Bur. Stand., Vol. 65D, No. 6, pp. 547-563 (Nov-Dec 1961). Phys. Abstr. 5478/1962.

8. Lein, R.H., "Radiation from a Horizontal Dipole in a Semi-Infinite Dissipative Medium," J. Appl. Phys., Vol. 24, No. 1 (Jan 53).

9. Baños, A., Jr., and Wesley, J.P., The Horizontal Electric Dipole in a Conducting Half-Space, Scripps Inst. Oceanography, La Jolla, California, Part I, SIO Reference 53-33 (Sep 53) and Part II, SIO Reference 54-31 (Aug 54).

10. Wait, J.R., "The Electromagnetic Fields of a Horizontal Dipole in the Presence of a Conducting Half-Space," Can. J. Phys., Vol. 39, pp. 1017-1028 (Jul 61).

11. Guy, A.W., and Hasserjian, G., Design Criteria for Buried Antennas, Preliminary Rpt, D2-7760, Boeing Aircraft Co., (Jan 61).

12. Guy, A.W., Experimental Data on Buried Antennas, Preliminary Rpt D2-11190, Boeing Aircraft Co.

13. Hasserjian, G., and Guy, A.W., "Low-Frequency Subsurface Antennas," IEEE Trans. Antennas and Propagation, Vol. AP-11, No. 3 (May 63).

14. Guy, A.W., and Hasserjian, G., "Impedance Properties of Large Subsurface Antenna Arrays," IEEE Trans. Antenna and Propagation, Vol. AP-11, No. 3 (May 63).

15. Rommel, T.A., Underground Antenna Systems Design Handbook, Boeing Co. Rpt. No. D2-13588, Control No. AF04(647)-289 (Jun 62).

16. Biggs, A.W., "Radiation Fields from a Horizontal Electric Dipole in a Semi-Infinite Conducting Medium," IRE Trans. Antennas and Propagation, Vol. AP-10, pp. 358-362 (Jul 62).

17. Biggs, A.W., and Swarm, H.M. "Radiation Fields of an Inclined Electric Dipole Immersed in a Semi-Infinite Conducting Medium," IEEE Trans. Antennas and Propagation, Vol. AP-11, No. 3 (May 63).

18. Biggs, A.W., and Swarm, H.M., Analytical Study of the Radiation Fields from an Electric Dipole in Stratified and Inhomogeneous Terrain, Tech Rpt No. 98, Univ. of Washington, College of Engineering (Sep 65).

19. Lavrov, G.A., and Knyazev, A.S., Near Earth and Buried Antennas, Sovetskoye Radio, 1965. Translation: JPRS 41, 131 (May 67) and JPRS 47075, Bibliography (Dec 68).

20. Staiman, D., and Tamir, T., "Nature and Optimization of the Ground (Lateral) Wave Excited by Submerged Antennas," Proc. IEE, Vol. 113, No. 8, (Aug 66).

21. Norton, K.A., "The Propagation of Radio Waves Over the Surface of the Earth and in the Upper Atmosphere," Part II, Proc. IRE, Vol. 25, pp. 1203-1236 (Sep 37).

22. Jordan, E.C., Electromagnetic Waves and Radiating Systems, Englewood Cliffs, New Jersey, Prentice-Hall, Inc. (1950).

23. The Boeing Co., Missile and Information Systems Division, Final Tech Rpt, Survivable Antenna Task - Project 672A , Boeing Rpt No. 125789-1, Contract AF04(694)-67-C-0116, Space and Missile Systems Organization (17 Jun 68).

24. Private correspondence with Ted Johnson, The Boeing Co., Missile and Information Systems Division, Seattle, Wash (Mar 69).

25. Kraus, J.D., Antennas, McGraw Hill, New York, NY (1950).

26. Blair, W.E., "Experimental Verification of Dipole Radiation in a Conducting Half-Space," IEEE Trans. Antennas and Propagation, Vol. AP-11, No. 3 (May 63).

27. Blair, W.E., A Modeling Technique for Experimental Verification of Dipole Radiation in a Conducting Half-Space, New Mexico University Engineering Experiment Station, Albuquerque, New Mexico, Tech Rpt EE-59, P. 24 (Jul 62).

28. Fenwick, R.C., and Weeks, W.L., "Submerged Antenna Characteristics," IEEE Trans. Antennas and Propagation, Vol. AP-11, No. 3 (May 63).

29. Hughes Aircraft Co., Feasibility Demonstration of a Ground Wave Hardened HF Communications System, Rpt No. 60H-11022/6325-001 (Oct 60) (Proprietary).

30. Northrop Nortronics, Report on Tests of a Survivable Earth-Embedded Antenna, Rpt No. MED 65-1 (Jan 65) (Proprietary).

31. Defense Communications Agency (Code 931), Technical Evaluation of HF Transmission with Deep-Buried Antennas, Final Rpt (Apr 66) (Proprietary).

32. Page Communications Engineers, Inc., Report on Tests of Page Survivable Earth-Embedded Antenna Model PCE-SEEA-2, Rpt No. PCE-R-1152-0119 (Jul 67) (Proprietary).

33. Northrup-Nortronics and Page Communications Engineers, Survivable High Frequency Antenna System, Final Rpt No. PCE-R-4063-0001, Contract DA 18-049-SCC-1068 for US Army Joint Support Command (Jul 67) (Classified).

34. Moore, J.D., et al, Soil Conductivity Measurement Techniques, Final Rpt RADC-TR-67-659, Contract AF30(602)-67-C-0114, Southwest Research Institute (May 68) (AD 833 890).

35. Berry, L.A., and Chrisman, M.E., Linear High Frequency Antennas Over a Finitely Conducting Spherical Earth, Rpt No. IER 8-ITSA-8 Institute for Environmental Research (Sep 66) (AD 809 305).

36. Corson, D.R., and Lorrain, P., Introduction to Electromagnetic Fields and Waves, W.H. Freeman and Co., San Francisco, Calif (1962).

UNCLASSIFIED
Security Classification

DOCUMENT CONTROL DATA - R & D

(Security classification of title, body of abstract and indexing annotation must be entered when the overall report is classified)

1. ORIGINATING ACTIVITY (Corporate author)	2a. REPORT SECURITY CLASSIFICATION
Rome Air Development Center (EMCAH) Griffiss Air Force Base, New York 13440	UNCLASSIFIED
	2b. GROUP N/A

3. REPORT TITLE

MEASURED PERFORMANCE OF HF SUBSURFACE DIPOLES

4. DESCRIPTIVE NOTES (Type of report and inclusive dates)
In-House

5. AUTHOR(S) (First name, middle initial, last name)
John N. Entzminger, Jr.
Thomas F. Treadway
Stuart H. Talbot

6. REPORT DATE	7a. TOTAL NO. OF PAGES	7b. NO. OF REFS
June 1969	127	36

8a. CONTRACT OR GRANT NO.	9a. ORIGINATOR'S REPORT NUMBER(S)
N/A b. PROJECT NO. 6523 c. d.	RADC-TR-69-221 9b. OTHER REPORT NO(S) (Any other numbers that may be assigned this report)

10. DISTRIBUTION STATEMENT
This document has been approved for public release and sale; its distribution is unlimited.

11. SUPPLEMENTARY NOTES	12. SPONSORING MILITARY ACTIVITY
	Rome Air Development Center (EMCAH) Griffiss Air Force Base, New York 13440

13. ABSTRACT

Theoretical analysis and measured data are presented for determining the characteristics of High Frequency (HF) subsurface dipole antennas. The agreement between theory and experimental data is shown to be excellent. It is shown that HF subsurface dipoles radiate a surface wave having the same characteristics as that launched by an above ground vertical monopole and also radiate a space wave which has a pattern identical to that of a half wave horizontal dipole located a quarter wavelength or less above ground. The subsurface dipole length is shortened to about one-third to two-thirds of its above ground equivalent.

Engineering curves are presented which enable the system engineer to design a small, physically hard, relatively cheap HF antenna array having a gain of approximately -10 db below that of simple above ground antennas, and having the radiation characteristics of both above ground whip and horizontal dipole antennas.

DD FORM 1 NOV 65 1473

UNCLASSIFIED
Security Classification

UNCLASSIFIED
Security Classification

14. KEY WORDS	LINK A		LINK B		LINK C	
	ROLE	WT	ROLE	WT	ROLE	WT
Subsurface Dipoles						
Subsurface Antennas						
Buried Dipoles						
Buried Antennas						
HF Antennas						
HF Dipoles						
HF Communications						
Hardened Antennas						
Hardened Communications						

UNCLASSIFIED
Security Classification

AFLC—Griffiss AFB NY 9 Jul 69-180